From the
Physiological Genomics – Biomedical Center (BMC)
of the Ludwig-Maximilians-Universität München
Director: Prof. Dr. Magdalena Götz

Overexpression of Transmembrane-Agrin in the Murine Central Nervous System

---

Dissertation zum Erwerb des Doktorgrades der
Naturwissenschaften
an der Medizinischen Fakultät der
Ludwig-Maximilians-Universität zu München

Submitted by

Anna Schick

from München

2017

With the permission of the Medical Faculty of the
Ludwig-Maximilians-Universität München

Supervisor: Prof. Dr. Stephan Kröger

Second evaluator: Prof. Dr. Michael Kiebler

Dean: Prof. Dr. med. dent. Reinhard Hickel

Date of oral defence: 17.05.2018

For Johnny and Niklas

Eidesstattliche Versicherung / Affidavit

Hiermit versichere ich an Eides statt, dass ich die vorliegende Dissertation **"Overexpression of Transmembrane-Agrin in the Murine Central Nervous System"** selbstständig angefertigt habe, mich außer der angegebenen keiner weiteren Hilfsmittel bedient und alle Erkenntnisse, die aus dem Schrifttum ganz oder annähernd übernommen sind, als solche kenntlich gemacht und nach ihrer Herkunft unter Bezeichnung der Fundstelle einzeln nachgewiesen habe.

I hereby confirm that the dissertation **"Overexpression of Transmembrane-Agrin in the Murine Central Nervous System"** is the result of my own work and that I have only used sources or materials listed and specified in the dissertation.

Anna Schick

München, den 25.07.2018/ Unterschrift / Signature

Munich, Date 25.07.2018

Summary

New synapses are generated throughout life to enable memory formation and retrieval. The efficacy of synaptic transmission must be precisely regulated for the immense neuronal network of the nervous system to function properly. Synaptogenesis during postnatal development and in adult organisms is a poorly understood process. Many synaptic organizers and synaptogenic proteins have been found but their precise function and their physiological role often remains unknown. One of them is the heparan sulfate proteoglycan agrin. Agrin is necessary for the formation and maintenance as well as the regeneration of the neuromuscular junction, the synapse between a motoneuron terminal and its target muscle fiber. There is evidence for the transmembrane form of agrin (TM-agrin) being involved in synaptogenesis in the CNS. For instance, TM-agrin overexpression in various cell culture systems, including neurons, causes the cells to produce filopodia, which are hypothesized to constitute the precursors for dendritic spine synapses. Moreover, mice depleted for agrin in the CNS show a reduction in the number of dendritic spines and synapses as well as fewer dendritic branches and impaired excitatory synaptic transmission. This can be explained by TM-agrin playing a role in synaptogenesis and/or in synaptic plasticity.

The aim of this thesis was to investigate the role of TM-agrin in the formation of synapses. Specifically I wanted to address the following questions:

1. Does the overexpression of TM-agrin induce filopodia-like processes *in vivo*?

2. Does overexpression of TM-agrin in glutamatergic neurons affect their existing synapses in the adult?

To this end, I generated a mouse line, which overexpresses TM-agrin conditionally under the spatiotemporal control of the inducible forebrain-specific CamKIICreERT2 promoter. Analysis of the mice overexpressing TM-agrin in adult glutamatergic neurons showed that they are viable and fertile and the total number of synaptic PSD95-positive and bassoon-positive puncta is not apparently affected. However, I discovered that the PSDs of glutamatergic synapses are larger and show more intense immunofluorescence staining of the PSD95 scaffolding protein compared to those from littermate controls. In addition, on basal dendrites of pyramidal neurons of cortex layer 2-3, the total spine head size and the thin spine head size showed an increase in TM-agrin overexpressing mice compared to control. Basal dendrites of hippocampus CA1 pyramidal neurons showed an increase in stubby spines accompanied with a decrease in mushroom spines on their basal dendrites. The gene expression profile revealed that genes relating to glutamatergic synapse function were upregulated, while gene expression relating to GABAergic synapse function was downregulated. Thus, apparently TM-agrin affects excitatory and inhibitory synapses in a directly opposing manner. These results are discussed by concluding that agrin strengthens synapses when present in a stoichiometric ratio on both synaptic membranes.

Contents

1. Introduction

Before 1888, it was widely believed that the nervous system was made up of one continuous network of tubular structures, despite mounting evidence that all organisms and tissues consist of cells. This made the nervous system the only exception from the 'cell theory', which was originally proposed by Matthias Schleiden and Theodor Schwann in 1838 and still holds true, stating that all organisms are composed of organs and that cells constitute the smallest independent units of organs (Schleyden & Schwann, 1847).

However, Santiago Ramon Y Cajal discovered in 1888 that individual nerve cells are responsible for the transduction of signals through what we call the nervous system and he was the first researcher to describe the 'neuron doctrine' (reviewed in translation: Lopez-Munoz et al., 2006). Today we know that the neuron doctrine holds true. Neurons of the nervous system are the smallest functional units and they communicate with each other using chemical synapses rather than forming a continuous tubular network. At synapses, nerve impulses are transmitted via a chemical neurotransmitter between individual neurons. This facilitates communication between a wide range of different cell types making up the functional units of the entire central and peripheral nervous system (CNS and PNS).

Throughout the life of an organism, synapses are formed, pruned and removed. This so-called synaptic plasticity generates and modulates memories, allowing adaptation to changing environments. The efficacy of synaptic communication needs to be regulated precisely for this immense neuronal network to function properly and to enable memory formation and

retrieval. The cerebral cortex of an adult human, for instance, harbours on average 10 billion neurons, which communicate through 60 trillion synapses (Tang et al., 2001). Thus, the formation of synapses as well as their changes during adult plasticity is a central question of developmental neuroscience. Synaptogenesis, the formation of new synapses, which for the largest part occurs during early postnatal development, is defined as the process of a presynaptic membrane of one neuron forming a chemical synapse with the postsynaptic membrane of the neuron receiving the chemical signal. During this process, both pre- and postsynaptic specializations form in response to trans-synaptic interactions, mainly of trans-synaptic adhesion proteins across the emerging synaptic cleft (for recent review see de Wit & Ghosh, 2016). As a result, the presynaptic terminal forms an active zone where the vesicles carrying neurotransmitter dock and release the transmitter into the synaptic cleft. In addition, the postsynaptic density forms, incorporating scaffolding proteins such as PSD95 and neurotransmitter receptors, such as NMDA and AMPA receptors in glutamatergic postsynapses.

Both during synaptogenesis and after the pre- and postsynaptic specializations are established, synapses are strengthened by synaptic activity, the postsynaptic density grows in size and incorporates a larger amount of neurotransmitter receptors (Matsuo et al., 2008). Molecular mechanisms that guide synaptogenesis during development are very likely similar to those mechanisms that are responsible for synaptic plasticity in the adult.

Despite a vast amount of research on the formation and function of synapses and despite the identification of many synapse organizers, we so far

have no comprehensive model of how a particular synapse is formed at a particular time point and at a particular position in the CNS. In contrast to the complex situation in the CNS, a particular synapse in the PNS is fairly well understood. This synapse is the contact site between a motoneuron and its target muscle fiber. In 1987, the key regulator of the NMJ was discovered, that is essential for the formation of postsynaptic specializations at the motor endplate: the heparan sulfate proteoglycan agrin (Nitkin et al., 1987). Since then, many independent lines of evidence have shown that agrin is involved in synaptogenesis in the CNS as well (for review see: Kröger & Pfister, 2009). However, the precise mechanism of action of agrin in the CNS and how it affects synaptic structure and development are unknown.

1.1. Synaptic organization in the forebrain

In order to understand how synaptic organizers might function it is important to consider the structure of synapses in the CNS. George Gray first described cortical synapses in detail in the rat visual cortex in 1959. Using electron microscopy he characterized two different types of synapses (Gray, 1959a and Gray, 1959b). Type I synapses form on dendritic spines and are asymmetric, showing a thicker postsynaptic- than presynaptic density. The presence of glutamate-immunoreactivity in electron micrographs later confirmed that these synapses use the neurotransmitter glutamate (Clements et al., 1990). Type II synapses form directly on the soma or on the dendritic shaft and the pre- and postsynaptic densities are symmetric and less dense than the ones of type I synapses. Symmetric type II synapses were later

shown to be mainly inhibitory, the presynaptic terminal often releasing the neurotransmitter γ-aminobutyric acid (GABA, Chase et al., 1976).

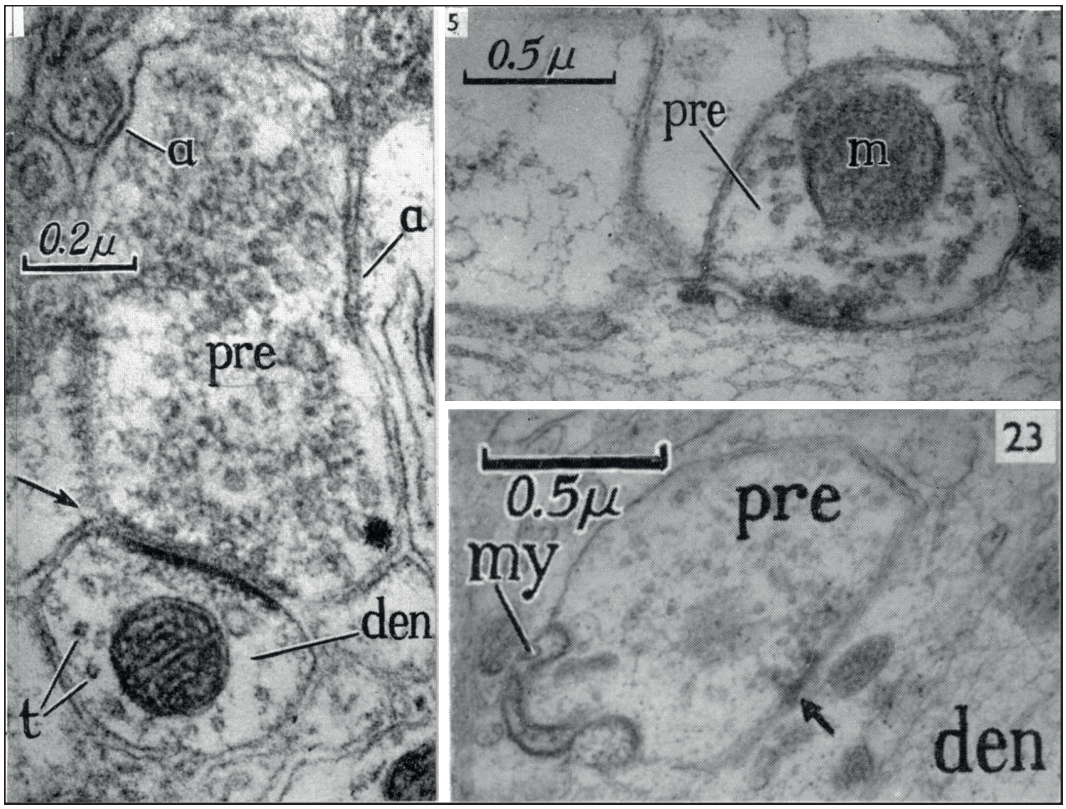

Figure 1: Type I (left) and type II (top and bottom right) synapses in electron micrographs of the cortex of adult rats. Type I synapses exhibit the typical postsynaptic thickening. Reproduced from Gray, 1959a with the publisher's permission. a: Non-thickened membranes; t: dendrite tubules; den: dendrite; pre: pre-synaptic process; m: mitochondria; my: myelin sheath.

Neurotransmitters other than GABA and glutamate also use asymmetric type I and symmetric type II synapses. Serotonergic synapses can form asymmetric type I synapses as well as symmetric type II synapses (Van Bockstaele et al., 1994), while noradrenergic synapses have been found to form symmetric type II synapses in the cat spinal dorsal horn (Doyle & Maxwell, 1991). Axonal projections of dopaminergic neurons were found to form small symmetric synapses with dendritic spines of their target neurons in the rat neostriatum (Groves et al., 1994). Also cholinergic synapses in the central nervous system have been found to be mainly symmetric, although

some variability among the synapse types can be observed depending on brain region (Houser, 1990).

Additionally, dually innervated spines have been observed on neocortical pyramidal neurons of rats that receive excitatory as well as inhibitory input (Kubota et al., 2007). Another exception to the classification according to Gray is the discovery of inhibitory chandelier cells forming axo-axonic synapses transmitting GABA (Howard et al., 2005). While the classification of synapse types according to Gray is still useful today, the above additions and exceptions observed since the first discovery of asymmetric and symmetric synapses show that synapse classification is more complex.

On a molecular level, synapse formation and organization in the CNS is a complex process with many protein families involved (Collins et al., 2006; Sugiyama et al., 2005). So far, no single gene has been found whose loss-of-function allele will completely obliterate synapse formation in CNS neurons, indicating that the processes are rather abundant and that the molecules involved exhibit partial functional redundancy. The following Figure 2 and Table 1 aim at giving an overview of synaptic organizers.

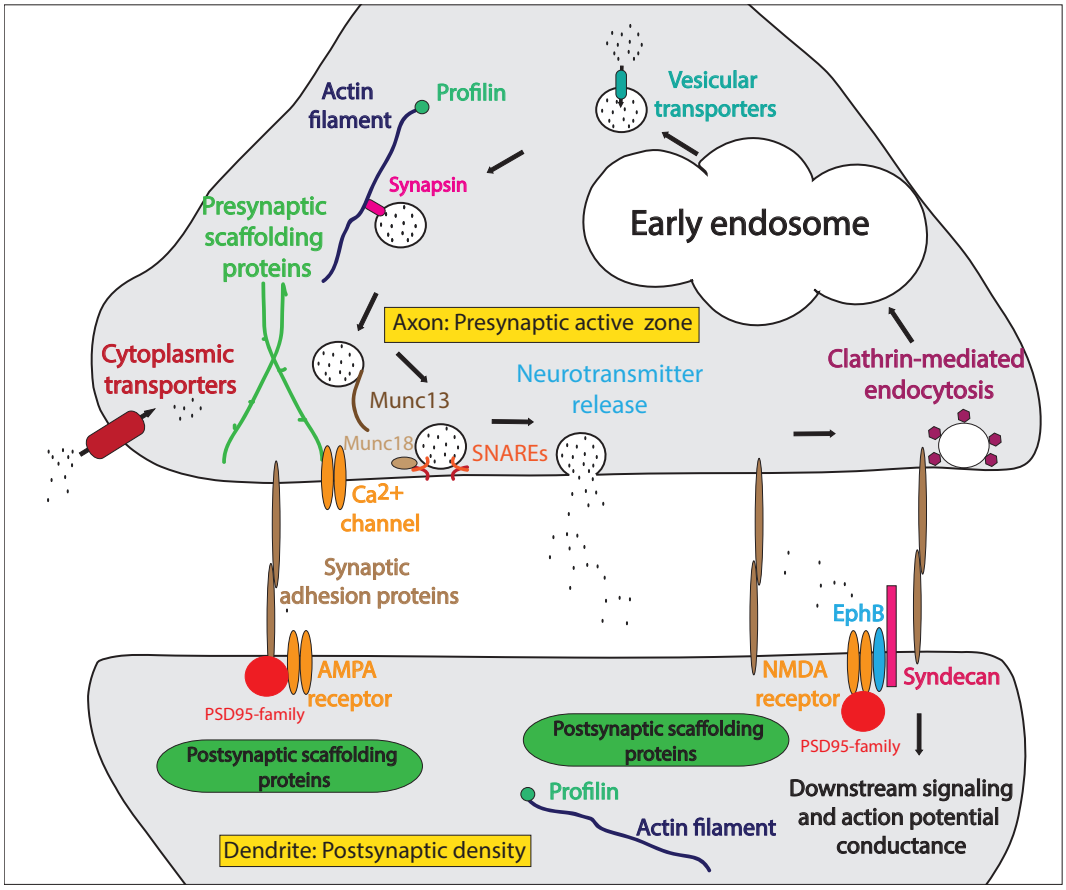

Figure 2: Simplified schematic representation of the molecular organization of an excitatory synapse. The presynaptic active zone is depicted with proteins involved in vesicle docking, release and recycling. Cytoplasmic and vesicular transporters fill the vesicles with the appropriate neurotransmitter, scaffolding proteins and vesicle-bound SNAREs together mediate precise docking and release of primed vesicles. Vesicles are released in response to Ca^{2+}-influx, which is triggered by an incoming action potential. Plasma membrane is recycled by clathrin-mediated endocytosis and fusion of recycled vesicles with the early endosome. Adhesion molecules connect the presynaptic terminal to the postsynaptic density (see text for examples). Postsynaptic scaffolding proteins (for example PSD95) cluster and lock neurotransmitter receptors in the postsynaptic plasma membrane. Neurotransmitter receptors generate an excitatory postsynaptic potential upon binding the neurotransmitter, which might lead (after spatial and temporal summation) to the formation of an action potential at the axon hillock.

Presynaptic	Function	Synapse type	References
Neurexins	Adhesion to neuroligins and LRRTMs	Excitatory and inhibitory	Reissner et al., 2008; de Wit et al., 2009
Glypican 1, 2, 3, 4, 5	Adhesion to LRRTM4, synaptogenic	Excitatory	de Wit et al., 2013; Siddiqui et al., 2013
Postsynaptic			
Neuroligins	Adhesion to neurexins	1,3: excitatory 2,4: inhibitory	Reissner et al., 2008
LRRTM4	Adhesion to glypican 1	Excitatory	de Wit et al., 2013; Siddiqui et al., 2013
LRP4	Unknown	Excitatory	Gomez et al., 2014; Tian et al., 2006; Karakatsani et al., 2016, manuscript submitted
Pre- and postsynaptic			
Agrin	Unknown	Possibly excitatory and inhibitory	Ksiazek et al., 2007; McCroskery et al., 2006
Cadherins	Adhesion, stability, synaptic vesicle recruitment	N-cadherin: excitatory E-cadherin: inhibitory	Yamagata et al., 1995; Benson and Tanaka, 1998; Fiederling et al., 2011
Integrins	Synaptic strength, plasticity	Excitatory and inhibitory	Yamagata et al., 1995; Kawaguchi and Hirano, 2006
Syndecan 2	Adhesion to LRRTM4, synaptogenic Spine maturation through EphB	Excitatory	Siddiqui et al., 2013; Ethell et al., 2001; Ethell and Yamaguchi, 1999
ephrinB	Synapse formation by binding to EphB receptor, presynaptic differentiation	Excitatory	Dalva et al., 2000; Klein, 2009; Grunwald et al., 2004
EphB	Synaptogenesis and plasticity,	Excitatory	Dalva et al., 2000; Klein, 2009; Grunwald et al., 2004
Astrocyte-secreted			
Thrombospondins	Synaptogenic	Excitatory	Christopherson et al., 2005
Hevin	Synaptogenic	Excitatory	Kucukdereli et al., 2011
Sparc	Anti-synaptogenic	Excitatory	Kucukdereli et al., 2011
Glypican 4 and 6	Synaptogenic	Excitatory	Allen et al., 2012

Table 1: Proteins involved in synaptogenesis and synapse stability. This table summarizes some of the known synapse organizers and is not exhausting.

1.2. Dendritic spine morphology and maturation

Most glutamatergic synapses form on spines decorating the dendrite. Dendritic spines were first observed as small protrusions on dendrites of cortical neurons in the early works of Ramon Y Cajal in 1888, using the silver

impregnation technique introduced by Camillo Golgi (for translations of original observations see Ramon Y Cajal, 1995 and Golgi, 1989).

Dendritic spines can be divided into three different main types based on their morphology: Filopodia, stubby spines and mushroom spines (Jones & Powell, 1969). Additionally, synapses can form directly on the dendrite shaft (shaft synapses). A detailed electron microscopic study of serial sections of the developing rat hippocampus CA1 region revealed that the percentages of different types of synapses change dramatically in the first two weeks after birth, the period during development when most synapses are being formed (Fiala et al., 1998). Between postnatal day 1 and postnatal day 12, the percentage of filopodia carrying synapses decreases from 22% to 7% while synapses on dendritic spines increase from 5% to 37%. The number of synapses on the dendrite shaft decreases from 53% to 32% during this time. These observations confirmed the hypothesis that synapse development starts with filopodia which mature to mushroom-like dendritic spines (Papa et al., 1995, Dailey and Smith, 1996, for review on excitatory synapse structure see Harris and Weinberg, 2012).

Dendritic spines not only increase the membrane surface of a neuron but also create a locally restricted area for protein synthesis and degradation (Bourne and Harris, 2008). Moreover, the size of the spine neck represents a strong barrier for postsynaptic electrical currents, suggesting that spine morphology influences the efficacy of synaptic transmission. Long-term potentiation (LTP), the most extensively studied form of synaptic plasticity, is a phenomenon observed at glutamatergic synapses. It describes the long-lasting increase in synaptic efficacy (determined by the amplitude of the

excitatory postsynaptic potential) in response to high frequency NMDA (N-methyl-D-aspartate) receptor activation (Bliss and Lomo, 1973). LTP is widely regarded as the cellular basis for memory formation, since it describes a use-dependent change in transmission and is accompanied by changes in synaptic structure, such as dendritic spine enlargement (for review see Blundon and Zakharenko, 2008 and van Bommel & Mikhaylova, 2016). Local protein synthesis has been linked to long-lasting synaptic plasticity after LTP induction (Pierce et al., 2000; Deller et al., 2003).

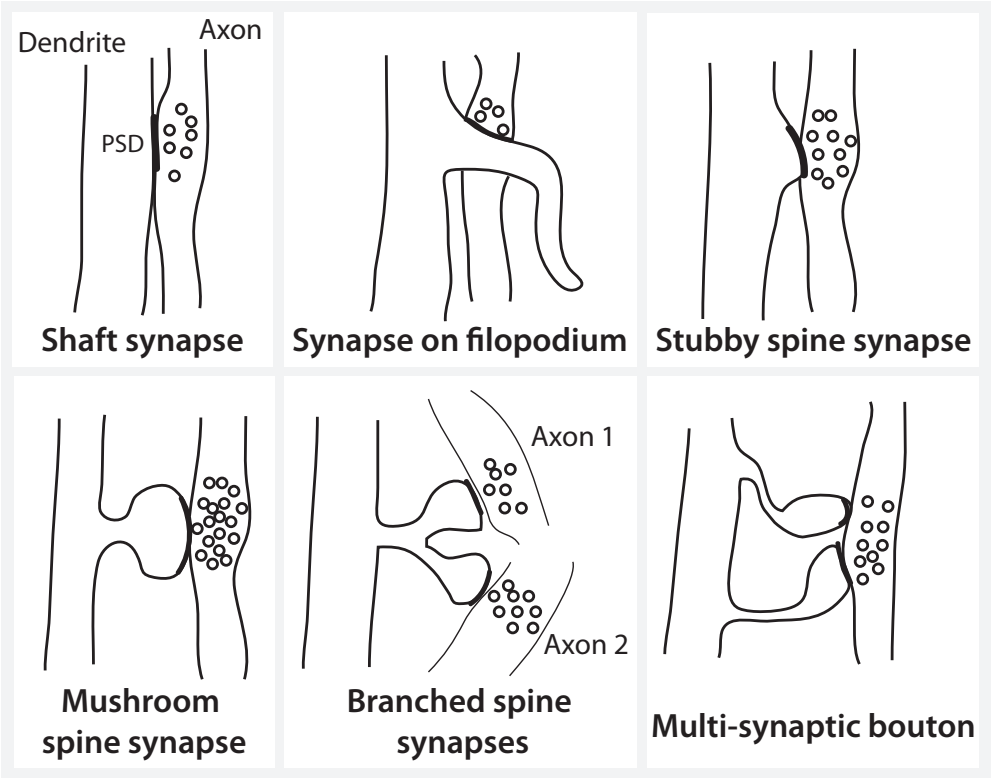

Figure 3: Model of different synapses forming on filopodia, spines or dendritic shaft. Branched spines can contact more than one axon. Adapted from Fiala et al., 1998 and Harris et al., 1992 and extensively modified.

1.3. Agrin at the neuromuscular junction

Heparan sulfate proteoglycans (HSPGs) such as agrin are large extracellular matrix proteins, which are post-translationally modified by covalently bound heparan sulfate groups (Neill et al., 2015). While these proteins are present in many tissues and often involved in basal lamina integrity, many HSPGs, such as syndecan, glypican and agrin have been shown to be important in CNS function and specifically synaptic organization (Sarrazin et al., 2011).

Agrin was first discovered as a key organizer of the neuromuscular junction (NMJ; Nitkin et al., 1987; McMahan, 1990; Tintignac et al., 2015). The vertebrate neuromuscular junction is a cholinergic synapse, the innervation of a single muscle fiber by a motoneuron axon terminal, translating an action potential via a chemical signal into muscle force (for review on NMJ structure and development see Sanes and Lichtman, 2001). This specialized synapse has long been a useful model for studying synaptogenesis due to its easy accessibility, its size and its capability to regenerate and represents the best-characterized synapse in the entire nervous system. The postsynaptic specializations of the NMJ consist of an intricate network of scaffolding proteins such as rapsyn and Dok-7 responsible for holding acetylcholine receptor (AChR) aggregates in place. Furthermore, deletion of the E3-ligase domain of rapsyn has been recently shown to result in the abolishment of the formation of postsynaptic specializations, showing that rapsyns enzyme activity is required for AChR-clustering (Li et al., 2016). The chain of events from agrin secretion by the growth cone to the formation of the postsynaptic specializations has been thoroughly characterized (for review see Wu et al., 2010). Figure 4 shows a schematic representation of NMJ development.

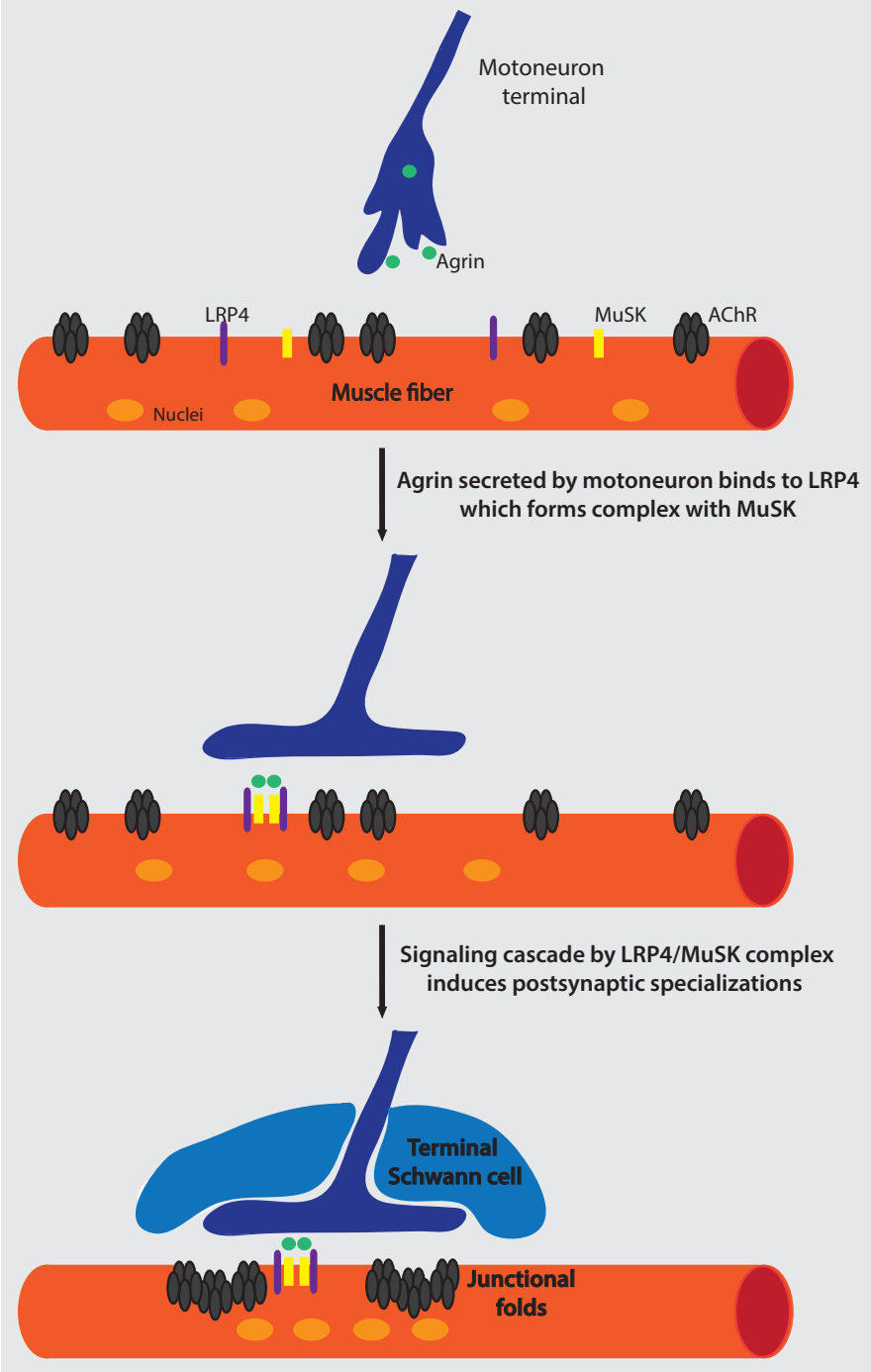

Figure 4: Schematic representation of neuromuscular junction development. The approaching motoneuron growth cone secretes agrin, which binds to LRP4 in the muscle fiber membrane. LRP4 forms a complex with MuSK, leading to MuSK kinase activation and downstream signaling events. These result in AChR aggregation and the formation of junctional folds in the muscle fiber basement membrane. Nuclei producing synapse-specific mRNA for NMJ development accumulate close to the synaptic specializations. MuSK: muscle specific kinase; AChR: acetylcholine receptor; LRP4: low-density lipoprotein receptor-related protein 4.

Agrin was initially purified in soluble form from the electric organ of the marine ray *Torpedo californica.* Soluble agrin is sufficient to induce AChR

aggregates on cultured myotubes (Nitkin et al., 1987; Wallace, 1989). Moreover, the addition of anti-agrin antibodies, which inhibit agrin activity, to co-cultures of motoneurons and myotubes reversibly inhibits the clustering of AChRs on the myotubes (Reist et al., 1992). These results provide strong evidence for agrin being the chemical messenger secreted by the approaching motoneuron growth cone that induces the postsynaptic specializations as originally proposed by the 'agrin hypothesis' (McMahan, 1990; Nitkin et al., 1987; Campagna et al., 1995; Wallace, 1988).

Secreted soluble agrin binds to the γ-chain of laminin, which immobilizes agrin in the basal lamina of the synaptic cleft (Denzer et al., 1997; Kammerer et al., 1999). Conditional deletion of agrin from motoneurons in adult mice leads to the loss of postsynaptic specializations, demonstrating agrin's essential role not only in the formation, but also in the maintenance of the neuromuscular junction (Samuel et al., 2012). The search for a receptor of agrin at the muscle membrane lead to the finding that myotubes lacking MuSK (muscle-specific kinase) fail to exhibit AChR clusters in response to addition of soluble agrin, providing evidence for the kinase being necessary for agrin signalling (Glass et al., 1996). Another protein, LRP4, was shown to bind directly to agrin and inhibition of expression or loss-of-function mutation of LRP4 results in a decrease of MuSK activation and AChR clustering in muscle cells, providing evidence for LRP4 as co-receptor for agrin (Zhang et al., 2008; Kim et al., 2008). MuSK phosphorylation, which is necessary for its activity, is abolished in the absence of functional LRP4 (Kim & Martin, 2015). In addition, null mutations in any of these three genes, agrin, MuSK and LRP4, result in perinatal

lethality due to respiratory muscle insufficiency (Gautam et al., 1996; DeChiara et al., 1996; Weatherbee et al., 2006). When analysed in detail, the neuromuscular junctions of agrin-deficient mice appear disorganized and smaller in size in several different muscle types compared to the heterozygous control mice. The absence of postsynaptic organizations on agrin-deficient myotubes from these mutant mice can be rescued *ex vivo* by adding recombinant agrin, resulting in the formation of AChR-aggregates. This evidence shows that the formation of the neuromuscular junction is in fact agrin-dependent (Gautam et al., 1996). Most of the motor nerve terminals contained very few neurotransmitter-bearing vesicles compared to heterozygous control mice, showing that even presynaptic specializations are aberrant in agrin-deficient mice (Gautam et al., 1996).

Summarizing this evidence, the complex of LRP4 and MuSK is thought to be activated by agrin binding to the extracellular domain of LRP4, which in turn triggers MuSK kinase activity and starts an intracellular cascade leading to clustering of AChRs and implementation of pre- and postsynaptic specializations necessary for neuromuscular synapse function. In addition to its well-studied function in the organization of the neuromuscular junction, additional roles of agrin have been documented, noteworthy being the development of sympathetic ganglia, another cholinergic synapse (Gingras et al., 2002). The sympathetic ganglions of agrin-deficient mouse embryos show a decrease in the alignment of pre- and postsynapses by around 40% in addition to defects in synaptic transmission potentiation. This suggests that agrin is also essential for the function of interneuronal cholinergic synapses (Gingras et al., 2002).

1.4. Domain structure and expression pattern of agrin

Since the first discovery of agrin in 1987 (Nitkin et al., 1987), several homologues have been found in different species, including chick, rat, mouse, zebrafish and human, and the sequences are highly conserved (Tsen et al., 1995; Tsim et al., 1992; Rupp et al., 1991; Burgess et al., 2000; Groffen et al., 1998).

The agrin gene is transcribed into an mRNA of app. 9 kb that is subjected to extensive posttranscriptional modifications, giving rise to several alternatively spliced isoforms. Additionally, alternative first exon usage creates a transmembrane (TM) N-terminus or a small, globular N-terminal (NtA) domain (Burgess et al., 2000; Neumann et al., 2001). This results in two different agrin proteins, one membrane-integrated and one secreted form. Motoneurons and epithelial cells express the NtA-isoform predominantly, where the secreted protein integrates into the adjacent basal lamina by binding to the γ1 subunit of the laminin heterotrimers (Denzer et al., 1997; Mascarenhas et al., 2005). The TM-isoform integrates into plasma membranes as a type-II transmembrane protein in an N_{cyto}/C_{exo} orientation and is primarily expressed by neurons of the central nervous system (Neumann et al., 2001;). The different N-termini are followed by identical protein sequences, consisting of different structural domains, such as follistatin-like domains and laminin-EGF-like domains. The core protein carries the glycosaminoglycan (GAG) side chain attachment sites on the extracellular domains (Winzen et al., 2003). The C-terminus consists of three globular laminin-G like domains, which harbour two alternative splicing sites (named y and z in rodents). Splicing at these sites generates different agrin

isoforms, which have a tissue-specific distribution. Only the isoforms containing an insert of 8, 11 or 19 amino acids at the z-site are synaptogenic at the NMJ (Ferns et al., 1993; Ruegg et al., 1992). For details on agrin domain structure and the splice sites see Figure 5.

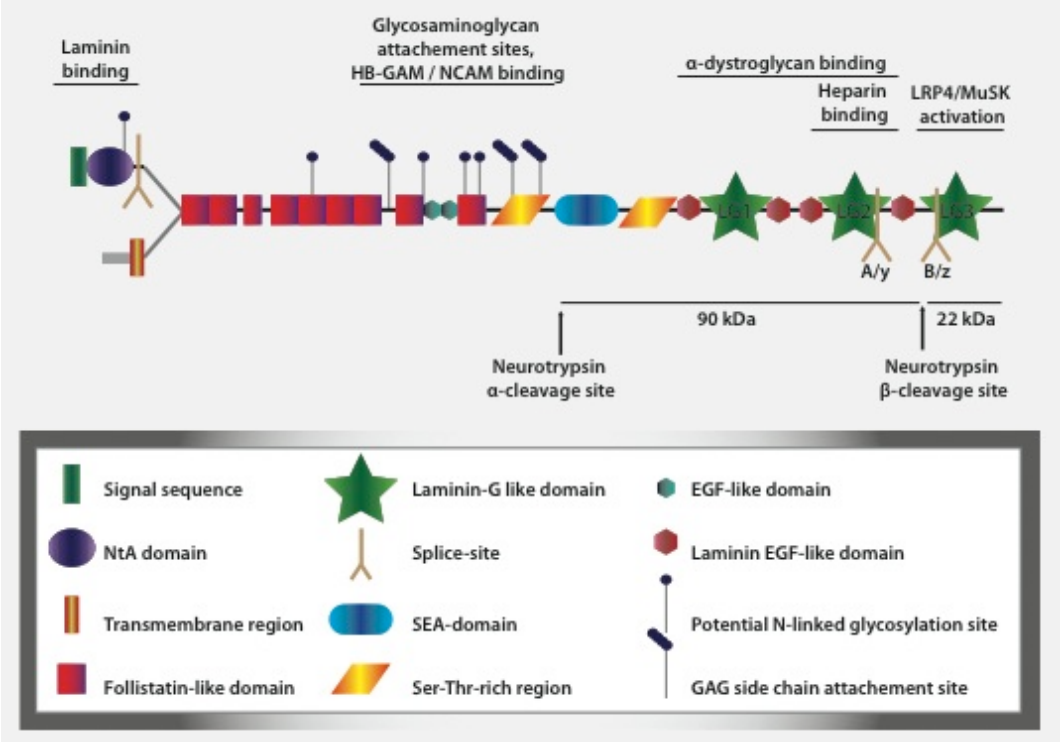

Figure 5: Schematic representation of the agrin protein indicating the different isoforms and conserved domains. The structural domains and regions involved in interactions with other proteins in different tissues are indicated. Alternative first exon usage generates two different N-termini: The NtA-isoform is functionally important for NMJ development, while the TM-isoform is expressed in the CNS. Alternative splicing at two major splice-sites (A and B in chick, y and z in mammals) generates several different C-termini with different synaptogenic activity at the NMJ. Proteolytic processing of agrin by neurotrypsin in the CNS generates two soluble fragments (cleavage sites are indicated). HB-GAM: heparin binding growth-associated molecule (pleiotrophin); NCAM: Neural cell adhesion molecule; LRP4: low-density-lipoprotein-receptor-related protein 4; SEA-domain: Sea urchin sperm protein-enterokinase-agrin domain. Adapted and modified from Kröger and Pfister, 2009.

1.5. Transmembrane agrin in the central nervous system

NtA-agrin is essential for the formation, maintenance and regeneration of the neuromuscular junction (Samuel et al., 2012; Werle and VanSaun, 2003; Gautam et al., 1996; for review see Tintignac et al., 2015). The structural and

functional similarities between the NMJ and synapses in the CNS let us assume that agrin may play a similar role in the central nervous system during interneuronal synapse formation. Neurons of the CNS primarily express the transmembrane isoforms of agrin (Neumann et al., 2001). One of the first milestones in the investigation of agrin's role in CNS synaptogenesis was the observation that neurons of the developing chick retina express agrin isoforms during the period of synaptogenesis, after which expression is downregulated (Kröger et al., 1996). Furthermore, neuronal isoforms of agrin have been detected in the synaptic cleft between neurons of the chick retina by electron microscopy (Koulen et al., 1999; for reviews on agrin's involvement in CNS synaptogenesis see Daniels, 2012 and Kröger and Schroder, 2002).

Another line of evidence was provided by *in vitro* studies of mammalian cells, which show a formation of numerous filopodia-like processes in response to clustering of agrin by polyclonal antibodies raised against the C-terminus (Annies et al., 2006). Since filopodia can be the precursors of dendritic spines (Papa et al., 1995, Dailey and Smith, 1996), it was hypothesized that these protrusions might be involved in spine synapse formation (Annies et al., 2006). Likewise, overexpression of the transmembrane isoform, but not of the secreted isoform results in the formation of similar filopodia in neurons as well as non-neuronal cells (McCroskery et al., 2006; Ramseger et al., 2009). This indicates that the basic mechanism leading to filopodia formation in response to TM-agrin signalling is conserved between species and cell types. Similar gain-of-function phenotypes have been observed in response to overexpression of other

known synaptic proteins, such as syndecan-2 (Granes et al., 1999), Gpm6a (Alfonso et al., 2005), synaptotagmin (Johnsson and Karlsson, 2012) and ASIC1a (acid-sensing ion channel 1a; Zha et al., 2006).

The signalling cascade leading to filopodia formation by TM-agrin was determined and the site of TM-agrin responsible for filopodia induction was mapped in neurons and non-neuronal cells (Porten et al., 2010). The region within the agrin protein, which is responsible for filopodia induction, was mapped to the 7th follistatin-like domain by extensive deletion studies (Porten et al.,), demonstrating that separate domains within the agrin protein mediate AChR aggregation and filopodia induction. Filopodia formation was demonstrated to be reduced after treatment with the lipid raft destabilizing agent methyl-β-cyclodextrin in a dose-dependent manner. In addition, the addition of MAP-kinase (mitogen-activated protein kinase) phosphorylation inhibitors to cultured retinal ganglion cells results in a dose-dependent decrease in the number of processes induced by TM-agrin clustering. These experiments show that filopodia formation involves the formation of lipid rafts and the activation of MAP-kinases (Ramseger et al., 2009).

Further evidence in favour of the hypothesis that agrin is important for CNS synapse formation was provided by a study knocking down all agrin isoforms in neuronal culture. These cells showed a 43% decrease in the number of neuronal filopodia compared to mock-control infected cells. In addition, siRNA infected cells showed a 52% decrease in the number of PSD95- and synaptotagmin-immunoreactivity positive puncta. This demonstrates that not only filopodia but also synapses are markedly reduced in the absence of TM-agrin in mature neurons (McCroskery et al., 2006).

In vivo studies of agrin loss-of-function are complicated by the fact that agrin knock-out mice exhibit perinatal lethality due to respiratory muscle insufficiency (Gautam et al., 1996). A creative *in vivo* approach rescuing perinatal lethality by re-expressing agrin in motoneurons circumvented this technical issue, allowing the analysis of agrin-deficient brains. These agrin-deficient brains show a decrease in the number of synaptic protein clusters in the cortex, a reduced number of spines, a change in dendritic morphology as well as a decrease in the frequency of spontaneous postsynaptic currents at glutamatergic synapses (Ksiazek et al., 2007). All of these alterations suggest a reduced number of specifically glutamatergic synapses. Thus, these results clearly indicate a function for agrin during glutamatergic synapse formation in the CNS. However, the mechanism how agrin regulates CNS synaptogenesis remains unknown.

Additional evidence for agrin's involvement in CNS synaptogenesis is provided by the observation that agrin is most highly expressed during periods of synaptogenesis, which in mice and rats occurs around the first three postnatal weeks (Li et al., 1997; O'Connor et al., 1994). After this period, agrin expression is downregulated and only remains high in regions of synaptic plasticity such as the hippocampus and the olfactory bulb. In the adult brain, agrin mRNA levels increase if synapse rearrangements are taking place, such as after traumatic brain injury, or after induction of synaptic seizures (O'Connor et al., 1995; Falo et al., 2008). *In vitro* cell cultures of cortical neurons were also analysed for the agrin expression timeline and a high correlation between agrin upregulation and the emergence of postsynaptic potentials was observed. Interestingly, the isoform profile

differs from that detected at the NMJ, in that all z-splice site isoforms are expressed, z0, z8, z11 and z19 (Li et al., 1997). The z0 isoform, which exhibits no synaptogenic potential at the NMJ, was found to be as abundant as z19, albeit with different expression timelines. In agreement with this observation, the gain-of-function phenotype of agrin, filopodia production in hippocampal neuron cultures, was shown to be independent of y- and z-splice site isoforms (McCroskery et al., 2006; Porten et al., 2010). In more detail, a highly conserved asparagine residue within the 7th follistatin domain of TM-agrin was shown to be essential for the initiation of filopodia production (Porten et al., 2010). This indicates that the mechanism by which agrin regulates synapse development in the CNS and at the NMJ might involve different protein domains, and in conclusion also different receptors.

Recently, a set of experiments investigated agrin's function during synaptogenesis in adult-born neurons (Burk et al., 2012). This study made use of the observation that neuronal precursors from the subventricular zone (SVZ) migrate along the rostral migratory stream (RMS) to the olfactory bulb (OB), differentiating along the way and finally integrating into the granule cell layer or periglomerular layer of the OB as GABAergic interneurons (Altman, 1969; for review: Ming and Song, 2011). After injecting genetically labelled embryonically derived agrin-deficient or WT control neurons into the SVZ of adult mice, the investigators followed their fate during migration to and integration into the OB. While agrin-deficient neuroblasts migrated correctly to the OB, they failed to integrate into the neuronal network and died between 30 and 60 days after the injection (Burk et al., 2012). Moreover, the agrin-deficient neurons never developed dendritic spines and had a much

less complex dendritic structure. Since the formation of synapses is essential for neuronal survival this evidence suggests that agrin signalling is necessary for integration and survival of new interneurons in the OB. Since none of the analysed agrin-deficient neurons survived in the OB after 60 days, the study shows the absolute necessity of agrin signalling in CNS neurons, similar to the neuromuscular junction.

It is unknown how agrin mediates its effect on synaptogenesis in the CNS. Several candidate receptors need to be considered. They should be concentrated at CNS synapses, and therefore include LRP4 (Tian et al., 2006; Ksiazek et al., 2007). LRP4 is especially interesting as a co-player in synapse organization in the CNS, since it has been shown to be necessary for LTP induction in the hippocampus, and mice lacking LRP4 in the CNS exhibit spatial learning and memory deficits in the Morris water maze test (Gomez et al., 2014). Additionally, knocking down LRP4 in embryonically derived hippocampal and cortical cultures at day three *in vitro* results in a significant decrease in the number of primary dendrites as well as a decrease in the number of dendritic spines and synaptic specializations visualized by immunostaining of presynaptic proteins bassoon and synaptobrevin-2 (Karakatsani et al., 2016, manuscript submitted). Overexpression of LRP4 at day three *in vitro* conversely results in a significant increase in the number of primary dendrites, dendritic spines and immunostaining of the presynaptic markers (Karakatsani et al., 2016, manuscript submitted). This line of experiments performed in our lab shows a necessity for LRP4 in normal dendritic arbour and synapse formation.

Knock-out mice lacking LRP4 expression in glial cells and neurons in the brain show a significant decrease in miniature and spontaneous excitatory postsynaptic currents and impairment of LTP in the hippocampus CA1 region (Sun et al., 2016). In addition, astrocyte-specific knock-out mice show impaired glutamate release while the number of dendritic spines does not appear to be altered (Sun et al., 2016). These studies taken together show that different mechanisms involving neuronal and astrocytic LRP4 exist that are controlling dendrite and spine number and electrophysiological synaptic activity.

1.6. Aim of this study

There is ample evidence for agrin being important for synapse formation and/or function in the CNS. However, the precise mechanism of action is entirely unknown. This study was designed to shed light on the mechanism by which TM-agrin influences synapses formation and function in the CNS. Ksiazek et al. conclusively showed a 30% decrease in glutamatergic synapses in the cortex of agrin-deficient brains (Ksiazek et al., 2007). This observation can either be explained by endogenous agrin having a synapse-inducing or a synapse-strengthening effect. In addition, overexpression of the transmembrane isoform of agrin results in the formation of filopodia in neurons as well as non-neuronal cells (McCroskery et al., 2006; Ramseger et al., 2009). To analyse whether TM-agrin overexpression induces the formation of filopodia *in vivo* as well and to try to understand how agrin influences CNS synapses, I designed a TM-agrin overexpressing mouse

model. Specifically, I aimed at addressing the following unanswered questions:

1. Does the overexpression of TM-agrin induce filopodia-like processes *in vivo*?

2. Does overexpression of TM-agrin in glutamatergic neurons affect their existing synapses in the adult?

I chose the CreERT2-system of inducible gene expression, since this approach ensures precise tissue-specific induction of expression at a flexible time point chosen by the researcher. The majority of neurons in the cortex and hippocampus, the CNS regions most extensively studied for TM-agrin expression and function, are glutamatergic pyramidal neurons. Therefore, the CamKIIα-promoter was chosen to drive Cre expression, since its activity is restricted to glutamatergic pyramidal neurons of the forebrain (Dittgen et al., 2004; Erdmann et al., 2007).

2. Materials and Methods

2.1. Strategy for generation of the TM-agrin x CamKIICreERT2 mouse line

To date, full-length TM-agrin had only been cloned into an expression vector from chick cDNA (Neumann et al., 2001). In order to exclude any artificial phenotype caused by the overexpression of a species-foreign protein, I cloned mouse TM-agrin (msTMagrin). The msTMagrin cDNA was recombined in four pieces originating from mouse head mRNA into a transient expression vector taking advantage of the yeast (*Saccharomyces cerevisiae*) homologous recombination system (Suzuki et al., 1983). Homologous recombination in yeast has two significant advantages over traditional cloning. One, yeast can combine several pieces of double-stranded DNA in one recombination step. Two, recombination cloning is dependent on stretches of 30 to 40 base pairs of direct homology within the linear DNA, rather than exact restriction sites. Thus, it is more flexible for the researcher, and more efficient than traditional cloning using restriction enzymes and ligases.

2.2. Cloning and assembly of mouse transmembrane agrin cDNA

The 5' region of the agrin cDNA coding for the N-terminal transmembrane domain as well as the 3' exons coding for the C-terminal domains were amplified from embryonic mouse head cDNA (strain Bl6N, 12.5 days postnatal). The RNA was purified from two different mouse heads by Susi

Pfeiffer (Helmholtz Zentrum, Neuherberg, Germany) with Trizol and Phenol/Chloroform extraction, followed by Ethanol precipitation and resuspension in ddH_2O. The RNA was transcribed into cDNA using the iscript kit (Bio-Rad, Hercules, USA). The 5' region of the agrin cDNA coding for the transmembrane part of agrin were amplified using primers prAS31 and prAS26 (for primer sequences and PCR protocols see Table 2). The 3' part of agrin was amplified in two pieces using primer pairs prAS27/prAS28 and prAS29/prAS32, respectively. All PCR products were purified by agarose gel electrophoresis using the PCR Clean-up kit (Macherey-Nagel, Düren, Germany) according to the manufacturer's instructions, and eluted in 25µl ddH_2O.

The remaining exons coding for the middle domains of the protein were obtained by restriction digest of the pCR-XL-TOPO-BC150703.1-Agrin clone (Figure 6, Imagene Source Bioscience, Nottingham, UK) using restriction enzymes SfiI and ApaLI (New England Biolabs, Ipswich, USA). Since SfiI restriction sites are partially blocked by methylation, the source vector was first transformed into a dcm^- dam^- *E.coli* strain (New England Biolabs) and re-purified. The bacterial transformation was performed as follows: The plasmid DNA (1µg in 5µl) was incubated on ice for 40min with 10µl of the competent bacteria, followed by heat-shock at 42˚C for 30s. After incubation at 37˚C for 60min, the cells were selected overnight on agar plates containing kanamycin. Plasmid DNA from kanamycin-resistant colonies was purified using the Zyppy Plasmid miniprep Kit (Zymoresearch, Irvine, USA) following the manufacturer's instructions. The plasmid was then digested using 200ng DNA, 6 units SfiI and 3 units ApaLI in NEB4 buffer supplemented with BSA at

a final concentration of 100µg/ml. The 4029 bp restriction fragment containing the middle exons of the agrin cDNA was excised from a 0.8% agarose-ethidium bromide gel on a blue light table, purified using the NucleoSpin® Gel and PCR Clean-up kit (Macherey-Nagel) according to the manufacturer's instructions, and eluted in 30µl ddH_2O.

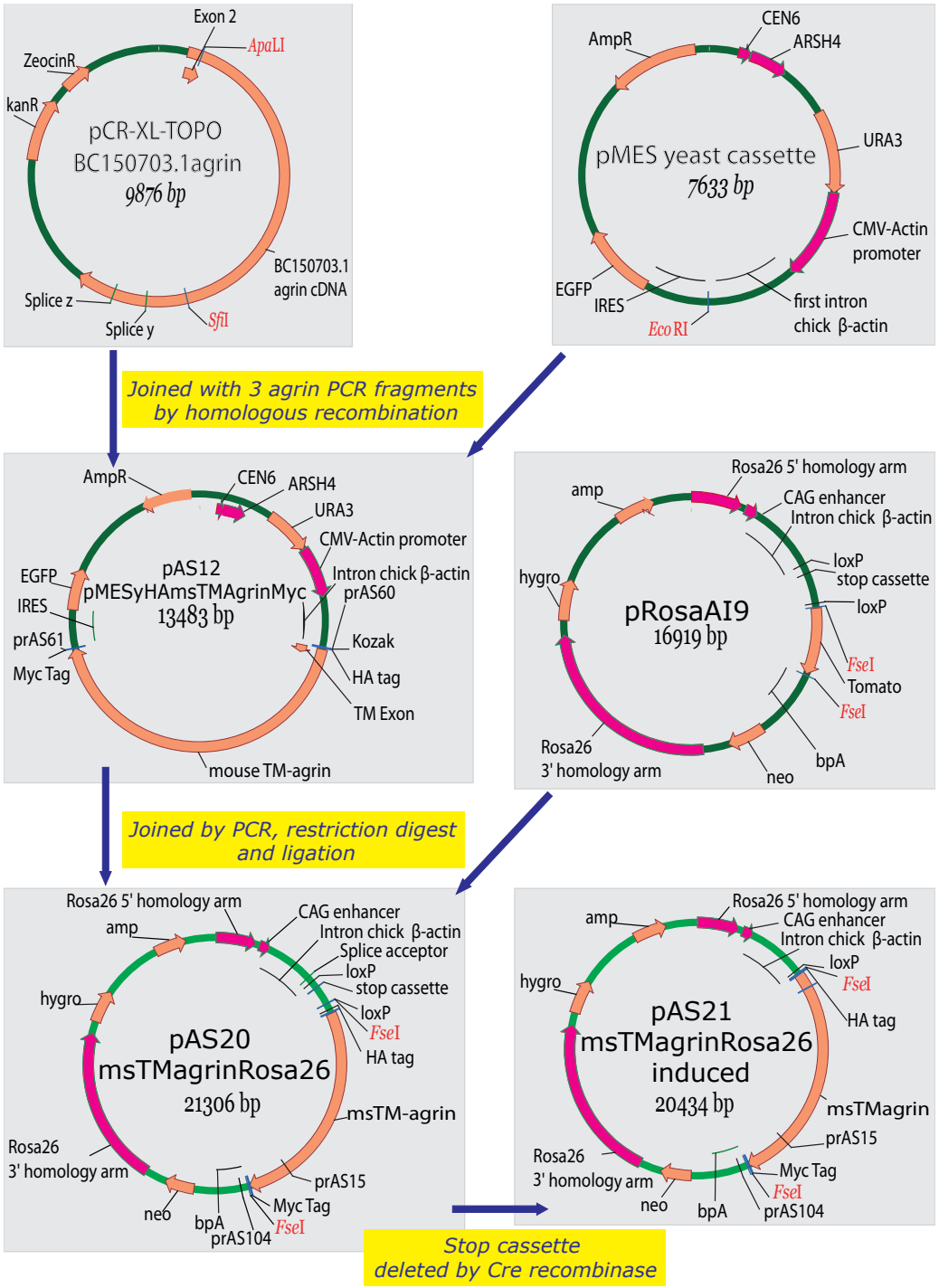

Figure 6: Vector maps of the plasmids used for cloning in this study. The middle piece of the TM-agrin cDNA was obtained by restriction digest from PCR-XL-TOPO BC150703.1 and joined with 3 agrin cDNA PCR fragments and the pMESyeastcassette backbone to yield pAS12. The TM-agrin cDNA was amplified from pAS12 and cloned into the pRosaAI9 backbone by ligation to yield the targeting vector pAS20. Cre recombinase activity excises the stop cassette in pAS20 and activates the CAG promoter. Relevant restriction sites are annotated. ZeocinR: Zeocin resistance; kanR: Kanamycin resistance; amp: Ampicillin resistance; CEN6: yeast centromer region; ARSH4: yeast autonomous replication sequence; URA3: uracil auxotrophy; IRES: internal ribosome entry site; hygro: Hygromycin resistance; neo: Neomycin resistance; bpA: SV40 late polyadenylation signal.

Amplification of agrin 5' region from mouse cDNA (510 bp)

prAS31	CGTGCTGGTTGTTGTGCTGTCTCATCATTTTGGCACCATGGGCTATCCATATGACGTTCCAGATTACGCTCCTCCTCTGCCACTGGAACACAGACC						
prAS26	CAGGTCACATTGGCACAGGGGTCC						
Pipetting	Template 1µl	Primers each 1µl	Buffer 5µl	dNTPs 2µl	Taq polymerase 0.25µl	DeepVent 0.25µl	H_2O 39.8µl
Cycling	94˚C 30s	65˚C -57˚C touchdown 45s			72˚C 1min	25 cycles after touchdown	

Amplification of first agrin 3' region piece from mouse cDNA (655 bp)

prAS27	GCTGTGGTTCAAAGCTCTGGTGTGG						
prAS28	CCTTGCGGGATTTCGGAGATTCC						
Pipetting	Template 1µl	Primers each 1µl	Buffer 5µl	dNTPs 2µl	Taq polymerase 0.25µl	DeepVent polymerase 0.25µl	H_2O 39.8µl
Cycling	94˚C 30s	65˚C - 57˚C touchdown 45s			72˚C 1min	25 cycles after touchdown	

Amplification of second agrin 3' region from mouse cDNA (965 bp)

prAS29	GAATCTCCGAAATCCCGCAAGGTCC						
prAS32	GATCCCGGGCCCGCGGTACCGTCGACTGCATCACAGATCCTCTTCTGAGATGAGTTTTTGTTCGAGAGTGGGGCAGGGTCTTAGCTCTG						
Pipetting	Template 1µl	Primers each 1µl	Buffer 5µl	dNTPs2 µl	Taq polymerase 0.25µl	DeepVent polymerase 0.25µl	H_2O 39.8µl
Cycling	94˚C 30s	65˚C -57˚C touchdown 45s			72˚C 1min	25 cycles after touchdown	

Amplification of agrin cDNA from pAS12 with FseI sites (18167 bp)

prAS60	CTAGATCGAATTCGGCCGGCCGCCACCATGGGCTATCCATATGACGTTCCAGAT
prAS61	CGAATTCCTGCAGGGCCGGCCTCACAGATCCTCTTCTGAGATGAGTTTTTGT

Sequencing primers

prAS45	CTGGTTGTTGTGCTGTCTCA	Sequencing pAS12 forward
prAS46	CCGTCGACTGCATCACAGAT	Sequencing pAS12 reverse
prAS47	TTGGACATCAACAACCAGC	Sequencing pAS12 internal
prAS48	ACACCGGCCTTATTCCAAGC	Sequencing pAS12 internal

Table 2: Sequences and protocols for DNA oligonucleotides used for cloning and sequencing. The part of the sequence homologous to the template is highlighted in red, added sequences (linkers, restrictions sites) are highlighted in blue. All PCR protocols included an initial denaturation step at 94˚C for 1min and a final elongation step at 72˚C for 10min. Concentrations of primer stock solutions (Invitrogen Thermo Fisher Scientific, Waltham, USA): 100µM. Mouse head cDNA concentration of stock solution: 1.2µg/µl. Concentration of dNTP stock solution (New England Biolabs): 10mM. Concentration of DeepVent® polymerase (New England Bioloabs): 2000 units/ml. Concentration of Taq polymerase (New England Biolabs): 5000 units/ml. PCR cycler: C1000 Touch Thermal Cycler (Bio-Rad). The total volume per vial for cloning PCR protocols was 50µl.

The pMES vector (Swartz et al., 2001) was chosen as backbone for testing overexpression of the agrin construct *in vitro*, since it also includes IRES-GFP,

which facilitates the assessment of transfection efficiency (Figure 6 vector map). For the vector to be used for yeast recombination cloning, a yeast cassette including the following contents was added (for vector map see Figure 6): ARSH4 (yeast autonomous replication sequence), URA3 (ORF encoding the enzyme necessary for making uracil, used for selection on medium lacking uracil) and CEN6 (yeast centromere, which ensures proper distribution of the centromeric plasmid during the cell cycle). The pMES-yeast-cassette plasmid was linearized using EcoRI (2.8µg DNA, 3 units EcoRI, in NEB4 buffer, incubation for 1h at 37˚C), and the restriction sites blunted with Klenow polymerase (New England Biolabs) using 20 units Klenow polymerase and 33.3µM dNTPs (New England Biolabs) in NEB2 buffer. The blunting reaction was stopped after 15min incubation at 25˚C by addition of EDTA (250mM in 50% glycerol) and incubation at 75˚C for 20min.

For homologous recombination cloning, the yeast strain CAY29 (MATa, ura3-52) was prepared for transformation using the Lithium-Acetate (LiOAc) protocol (Gietz & Woods, 2002). In short, a yeast colony from an YPD-agar plate (peptone 20g/L, glucose 20g/L, yeast extract 10g/L, agar 20g/L) was inoculated in 2ml of two times concentrated YPD media (peptone 40g/L, glucose 40g/L, yeast extract 20g/L) media and grown overnight at 30˚C with moderate shaking. This saturated culture was then diluted in fresh, two times concentrated YPD media to OD_{600} = 0.15 and grown for three generations to log phase (OD_{600} = 1.0 - 1.2). The cells were harvested by centrifugation at 2500 x g for 2min at RT and washed once with 10ml ddH_2O and once with 5ml LiOAc (100mM, pH8) using the same centrifugation parameters. Finally, the cell pellet was resuspended in 50µl LiOAc (100mM, pH8), and the linear

DNA fragments to be recombined were added to the cells (20µl for each of the four agrin fragments and 0.7µg in 10µl vector DNA) together with 10µl carrier DNA (10mg/ml salmon sperm DNA) and 300µl 39% PEG 4000 in LiOAc (100mM, pH8). After 1min of vortexing, the transformation mixture was incubated at 42˚C for 40min. The cell suspension was plated onto SC plates (synthetic complete medium, Formedium, Norfolk, United Kingdom) lacking uracil for selection of cells containing the plasmid. A vector-only control transformation was performed on the side, showing a 100-fold higher efficiency of recombination when the inserts were included in the transformation.

Plasmids that have recombined in yeast need to be re-transformed into *E.coli* in order to produce the plasmid in high enough quantity to make testing of the colonies possible. For recovery of the plasmid from the yeast cells, I took advantage of a modified plasmid prep protocol using the buffers and filter columns contained in a plasmid miniprep kit (Qiagen, Hilden, Germany). To this end, all the yeast colonies from one plate were resuspended in 10ml TE pH8 buffer. This suspension was washed once with 10ml TE pH8 buffer by centrifugation (as above) and 1ml was transferred to an Eppendorf tube and pelleted again by centrifugation. The cells were re-suspended in 200µl P1 buffer (Miniprep kit, Qiagen), 100µl lyticase solution (5U/µl in TE pH8, Sigma-Aldrich, Gallen, Switzerland) was added and the mixture was incubated at 37˚C to digest the yeast cell wall. After a 2h incubation, 300µl P2 buffer was added and the mixture was incubated at RT for 10min, after which 420µl N3 buffer was added and the debris from the lysed cells was pelleted at 20,000 x g at 4˚C for 10min. The supernatant

containing the plasmid and the genomic DNA were transferred to a column inside a collection tube, centrifuged at 20,000 x g, and washed with 500µl PB buffer and 700µl PE buffer by centrifugation for 1min at 20,000 x g each time. The column was dried with another centrifugation and the DNA was eluted with 30µl EB buffer by heating the tube to 65˚C for 5min.

After the plasmid was recovered from yeast, it was transformed into *E.coli* and 10 colonies were screened with restriction digests, the positive clones tested by restriction digest and confirmed by sequencing (sequencing primers prAS45-prAS48, Table 2).

2.3. Validation and expression of mouse TM-agrin in cell culture

HEK293T cells (human embryonic kidney, Graham et al., 1977) were chosen for validation of transient expression, since these cells show high expression rates. For Western blot analysis of the expressed protein, one T25 flask of HEK293T cells was grown overnight to about 90% confluence, and transfected with 5µg of plasmid DNA using the Superfect transfection reagent (Qiagen) according to the manufacturer's instructions. 24 hours later, the cells were harvested in 1ml of lysis buffer (20mM HEPES pH7.5, 150mM NaCl, 10% glycerol, 1% NP-40, 1mM PMSF, 1 protease inhibitor tablet (cOmplete Tablets, Mini EDTA-free, EASYpack, Roche, Basel, Switzerland) per 10ml) by scraping, incubation on ice for 10min and centrifugation for 15min at 21,000 x g and 4˚C. The cell lysates were subjected to electrophoresis in polyacrylamide gels (Miniprotean TGX 4-15% gradient, Bio-Rad) at 120V and transferred to nitrocellulose membranes (Protran, Schleicher & Schuell, Sigma-Aldrich). The membranes were then blocked overnight in 10% skim

milk powder in TBS-T (100mM Tris-HCl pH8, 8.8g/L NaCl, 0.1% Tween-20) and incubated with primary antibody diluted in TBS-T containing 5% skim milk powder (rabbit anti-mouse agrin, rat anti-HA, Table 5) for 1h, washed 3 times for 10min with TBS-T, and incubated 1h with horseradish peroxidase-coupled secondary anti-rabbit or anti-rat antibody.

The membranes were washed three times with TBS-T for 10min and then incubated with horseradish peroxidase substrate (Luminol Enhancer Solution and Stable Peroxide Solution in equal parts, PIERCE, Thermo Fisher Scientific, Waltham, USA) and the luminescence signal captured on film.

In order to confirm correct expression and insertion of TM agrin in the cell membrane, and to confirm the filopodia-inducing phenotype of TM-agrin overexpression, the cells were transfected with the full-length msTM-agrin overexpression construct in the pMES vector and stained with antibodies for immunofluorescent microscopy. The cells were plated in 6-well plates and transfected as above. After 24 hours, the cells were washed with PBS and fixed with 100µl 2% formaldehyde for 10min. After washing with PBS, the cells were blocked in staining solution containing 5% BSA, 0.3% Triton X-100 and 10% sheep serum in PBS for 1h. The cells were incubated overnight with primary antibody diluted in staining solution (rabbit anti-mouse agrin, rat anti-HA, mouse anti-c-myc, Table 5) and with secondary antibody for 1h after two washes. After 50min, 2mg/ml DAPI was added. After two additional washes, the cells were embedded on glass slides with Mowiol solution (to 31ml 240mM Tris-HCl pH 8.5 add 6g Mowiol 4-88 and 18.9g Glycerol). Epifluorescent microscopic analysis of the immunostained cells was performed with an Axio Imager M2 (Zeiss, Oberkochen, Germany).

2.4. Cloning of targeting construct for knock-in mouse

After validation of the expression of TM-agrin *in vitro*, the cDNA was transferred to the targeting vector pAI9 (Madisen et al., 2010) by restriction digest and subsequent ligation. To this end, the agrin cDNA was amplified from pAS12 by long-range PCR (Table 2 for primer sequences), adding FseI restriction sites in the primer overhang sequences. The PCR product and the pAI9 vector were digested with FseI (New England Biolabs): 3.5µg PCR product with 7 units FseI and 100µg/ml BSA in NEB buffer 4; 2µg vector with 6 units FseI and 100µg/ml in NEB buffer 4; incubation at 37˚C for 1h and inactivation at 65˚C for 20min. After the restriction digest, the vector was de-phosphorylated with 5 units of antarctic phosphatase (New England Biolabs) by incubation at 37˚C for 30min and subsequent inactivation at 65˚C for 10min. Both the vector and the PCR product insert were purified by agarose gel electrophoresis using the PCR Clean-up kit (Macherey-Nagel) according to the manufacturer's instructions, and each eluted with 30µl ddH_2O.

Ligation of insert and vector was performed at an estimated ratio of twice the molar amount of insert to vector using the Quick-Ligation Kit (New England Biolabs) following the manufacturer's instructions. After incubation at room temperature for 5min, chemically competent TOP10 *E.coli* were transformed with 5µl of the ligation reaction mixture by incubation on ice for 15min, heat shock (42˚C) for 90s, incubation on ice for 5min, recovery at 37˚C for 1h, and plating on agar plates containing ampicillin for selection.

Plasmid DNA from ampicillin-resistant colonies was purified using the Zyppy Plasmid miniprep Kit (Zymoresearch) following the manufacturer's instructions. Positive clones were verified by restriction digest using FseI (1

unit for 200ng plasmid DNA in NEB buffer 4 supplemented with 100µg/ml BSA, New England Biolabs) to cut out the insert or SacI (1 unit for 200ng plasmid DNA in SacI buffer, New England Biolabs), which cuts several times inside the insert. Correct amplification and orientation was confirmed with sequencing using primers prAS28 and prAS26 for forward and reverse sequencing including the tags, and prAS15, prAS16 and prAS104 for coverage of a large part of the internal sequence. This cloning step resulted in the targeting vector pAS20 (Figure 6).

2.5. Validation and expression of targeting construct in cell culture

The generation of a knock-in mouse is a time-consuming process. This includes electroporation into embryonic stem (ES) cells, genotyping, validation of expression of the integrated construct, and injection of the ES cells into foster mouse females. Therefore, it is advisable to thoroughly validate any construct to be used in the generation of knock-in mouse lines. To ensure that the cDNA will be correctly expressed only after Cre recombinase activation, the targeting construct activation was validated both in the test tube and in HEK293T cell culture.

The TM-agrin targeting construct pAS20 was activated by excision of the stop-cassette with Cre recombinase (New England Biolabs) using 3 units on 200ng plasmid DNA in the supplied Cre buffer by incubation at 37˚C for 30min, followed by inactivation at 70˚C for 10min. Chemically competent *E.coli* were transformed with 5µl of the reaction mixture (transformation protocol page 30) and incubated overnight at 37˚C on agar plates containing ampicillin. The resulting plasmid pAS21 clones were purified using the

Qiagen Miniprep kit (Qiagen) following the manufacturer's instructions and verified by restriction digests with MfeI (New England Biolabs). Digestion with MfeI resulted in the expected band of 20,434 bp versus four bands of 14,898 bp, 5900 bp and two times 252 bp for the control plasmid pAS20, which was not incubated with the Cre recombinase.

The conditional targeting construct was co-transfected into HEK293T cells with and without pNLSCre (expressing Cre recombinase with a nuclear localization signal, pPGK-Cre-bpA; Gu et al., 1993) to test the baseline expression and the expression after Cre activity *in vitro*. To this end, 6 x 10^6 cells on PDL-coated coverslips were transfected with the following combinations of plasmids (0.8µg) in a 24-well format:

1) pAS20 (TM-agrin in pAI9 targeting vector) alone
2) pAS20 and pNLSCre,
3) pAI9 (empty targeting vector) and pNLSCre
4) pAS12 (TM-agrin in pMES vector)
5) pMES (empty vector for transient expression)

Lipofectamine (2µl per well, Invitrogen Thermo Fisher Scientific) was used to transfect HEK293T cells according to the manufacturer's instructions. After 24 hours of expression, the cells were washed with PBS and fixed with 100µl 2% formaldehyde in PBS for 10min. After washing twice with PBS, to reduce unspecific immunoreactive signals, unspecific binding sites on the cells were blocked using staining solution containing 5% BSA, 0.3% Triton X-100 and 10% sheep serum in PBS for 1h. The cells were incubated overnight with primary antibody diluted in staining solution (rabbit anti-mouse agrin, rat anti-HA, mouse anti-c-myc, Table 5 for dilutions and sources) and with

secondary antibody for 1h. After 50min incubation, 2mg/ml DAPI was added to the antibody solution. After two more washes, the cells were embedded on glass slides with Mowiol and epifluorescent microscopic analysis of the immunostained cells was performed on an Axio Imager M2 (Zeiss).

2.6. Generation of knock-in mice, breeding of mice, and genotyping

Electroporation of the linearized targeting construct pAS20 into E14 mouse embryonic stem cells, verification of correctly targeted clones by PCR and injection of the ES cells carrying the TM-agrin knock-in into mouse blastocysts was performed by Susanne Pfeiffer in collaboration with Dr. Joel Schick's laboratory at the Helmholtz Zentrum Munich.

Female mice that were implanted with the injected blastocysts from BDF-1 donor females (black coat, Charles River) were bred to BL6J males and chimeras showing at least 70% chimerism (estimated by brown coat colour showing E14 stem cell transmission) were picked for breeding to test germline transmission. The TM-agrin knock-in mice were bred to a CamKIICreERT2 transgenic line (Erdmann et al., 2007), in which Cre recombinase activity can be conditionally switched on by tamoxifen administration. All the mice analysed in this study were bred to BL6J mice for at least 3 generations. Agrn//CamKIICre/WT mutant mice and WT/WT//CamKIICre/WT control siblings were given 3 injections in week 5 (Monday-Wednesday-Friday) with 2mg tamoxifen (Sigma-Aldrich) in 100µl Mygliol (Caelo, Hilden, Germany) and analysed between week 7 and week 11. For Western blot analysis of protein levels and qPCR, the mice were fed a diet containing 400mg/kg tamoxifen (LASCRdiet™ CreActive TAM400, LasVendi,

Soest, Germany) for 2 weeks, during which their growth rate, weight and behaviour was monitored, and then had access to regular food for 3 weeks for recovery and expression.

The tails of the mouse litters were clipped 3 weeks after birth and the mouse tail tips were lysed using 100µl 50mM NaOH by incubation at 99˚C for 30min and neutralization by addition of 30µl 1M Tris-HCl pH 7.5. The CamKIICreERT2 allele was analysed with primers prAS116 and pRAS118 and the TM-agrin allele was analysed using primers prAS15 and prAS104 (Table 3). The genotyping of all mice used in experiments was confirmed at the time of tissue preparation.

Genotyping of TM-agrin knock-in allele (product: 1376 bp)

prAS15	TACTCCTCTACAATGGGCAG					
prAS104	GCCACAACTCCTCATAAAGA					
Pipetting	Template 1µl	Primers each 0.1µl	Buffer 2.5µl	dNTPs 0.7µl	Taq polymerase 0.3µl	H_2O 20.3µl
Cycling	95˚C 15s	57˚C 45s	72˚C 90s	40 cycles		

Genotyping of CamKIICreERT2 transgene allele (product: 375 bp)

prAS116	GGTTCTCCGTTTGCACTCAGGA					
prAS118	GCTTGCAGGTACAGGAGGTAGT					
Pipetting	Template 1µl	Primers each 0.1µl	Buffer 2.5µl	dNTPs 0.5µl	Taq polymerase 0.2µl	H_2O 20.6µl
Cycling	95˚C 15s	62˚C 45s	72˚C 45s	35 cycles		

Table 3: Sequences and protocols for DNA oligonucleotides used in genotyping. PCR protocols included an initial denaturation step at 95˚C for 3min and a final elongation step at 72˚C for 10min. Concentration of dNTP stock solution (New England Biolabs): 10mM. Concentration of Taq polymerase (New England Biolabs): 5000 units/ml. PCR cycler: C1000 Tough Thermal Cycler (Bio-Rad).

2.7. Quantitative Western blot analysis of protein levels

The mice were anaesthetized with carbon dioxide and killed by cervical dislocation. The extracted brains were snap-frozen in liquid nitrogen and lysed for initial determination of agrin levels. For detailed analysis of protein levels in the cortex and hippocampus, brains were further dissected and the

subregions separately snap-frozen. The tissue was homogenized by homogenization in lysis buffer on ice (10mM Tris-HCl pH7.5, 10mM EDTA, 0.5mM PMSF one cOmplete tablet, Roche, per 50ml) using a glass pistil homogenizer (Figure 7). The lysate was centrifuged at 2500 x g and 4˚C for 30min and the pellet containing cell debris and nuclei was discarded.

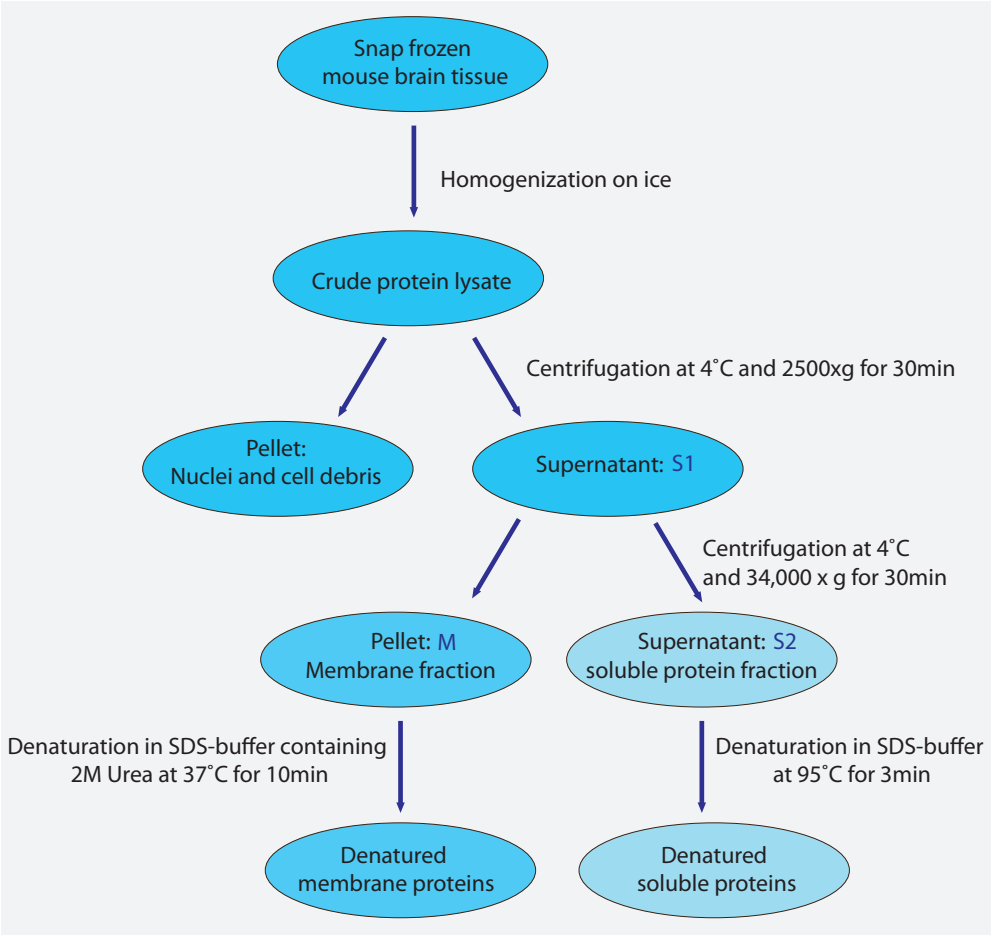

Figure 7: Flow chart of tissue fractionation for Western blot analysis.

The supernatant (S1 fraction) was subjected to another centrifugation step at 34,000 x g and 4˚C for 30min to yield the soluble fraction (supernatant, S2) and the membrane fraction (pellet, M). The proteins in the S2 fraction were denatured by adding one part 4 x SDS sample buffer (5mM Tris-HCl pH8.5, 1% SDS, 25% glycerol, 8% 2-mercaptoethanol, 0.25% Bromphenolblue in H_2O) to three parts lysate and heating of the sample at 95˚C for 3min. The

membrane fraction was denatured by adding 8M urea to the SDS sample buffer and the sample was heated at 37˚C for 10min.

The proteins were separated in 10% polyacrylamide gels by electrophoresis in running buffer (25mM Tris base, 192mM Glycine, 0.1% SDS) at constant 80V and transferred onto nitrocellulose membranes (Protran, Schleicher & Schuell, Thermo Fisher Scientific) at constant 140mA for 2h. The membranes were blocked in 10% skim milk powder TBS (100mM Tril-HCl pH8, 8.8g/L NaCl) overnight and incubated with primary antibody (for antibodies used in quantitative Western blotting, see Table 5) diluted in 5% horse serum TBS-T (100mM Tril-HCl pH8, 8.8g/L NaCl, 0.1% Tween-20) for 3h. After three 10min washing steps with TBS-T, the membranes were incubated with secondary anti-rabbit or anti-mouse antibody for 1h, and again washed 3 x 10min. For antibodies used in quantitative Western blotting, see Table 5. For quantitative analysis of protein levels, the Odyssey infrared scanner system (Licor, Lincoln, USA) was used for imaging of the protein bands and the integrated pixel density of each band was quantified using ImageJ software (National Institute of Health, Bethesda, USA).

2.8. Nissl histology

Mice were intracardially perfused with 4% paraformaldehyde in PBS for 20min after anaesthetization with CO_2 and cervical dislocation. Whole brains were removed and post-fixed in 4% paraformaldehyde overnight. Fixed brains were washed once with PBS and then cryoprotected with 30% sucrose in H_2O for 48 hours. To ensure proper alignment of the sagittal sections, the brains were cut at the midline and both hemispheres were embedded

separately in O.C.T. compound (Tissue-Tek, Sakura, Torrance, USA) with the cut surface facing down. Starting at the midline section, 50µm sections were cut using a cryostat (Leica Microsystems, Wetzlar, Germany). Sections were cut precisely parallel to the midsagittal plane and every section was counted.

The sections were stained with Cresyl Violet following the Cold Spring Harbour protocol for Nissl stains (Paul et al., 2008). After imbedding with Permount mounting medium (Thermo Fisher Scientific), the sections were imaged using bright field microscopy.

2.9. Golgi histology

Mice were killed by cervical dislocation after anaesthetization by CO_2 and the brains were removed. The brains were stained using the FD Rapid Golgi stain kit (FD Neurotechnologies, Columbia, USA) following the manufacturer's instructions. After 3 week incubation with solutions A, B and C, the brains were snap-frozen in isopentane. After 1min the specimen were mounted directly on tissue holders using distilled water on dry ice and cut into 200µm sections. Staining of the sections was done according to the FD Rapid Golgi stain kit manual. After imbedding with Permount mounting medium, brightfield microscopic analysis was performed on an Axio Imager M2 (Zeiss).

2.10. Immunohistochemistry

Agrn/Cre and WT/Cre mice were injected with tamoxifen in week 5 and perfused with 4% PFA in week 8. Whole brains were removed and post-fixed

in 4% paraformaldehyde overnight. Fixed brains were washed once with PBS and then cryoprotected using 30% sucrose in H_2O for 48 hours. Whole brains were embedded in Tissue-Tek (Tissue-Tek, Sakura) and cut sagittally on a cryostat into 20µm thick sections. The sections were mounted onto gelatine/chromealumn-coated glass slides and dried for 30min.

The dry sections were surrounded by Roti®-Liquid Barrier (Carl Roth, Karlsruhe, Germany), washed once with PBS, and treated with proteinase K (20µg/ml in 10mM Tris-HCl pH7.5 1mM EDTA) at 37˚C for 10min to ensure accessibility of the synaptic antigens. After this pre-treatment, the sections were blocked and stained as previously described (Tsen et al., 1995) with antibodies raised against PSD95 and bassoon. Confocal microscopic analysis of the immunostained mouse brain sections was performed on laser scanning confocal microscope (Imager Z1, LSM710 Axio, Zeiss) and the images were analysed using ImageJ (National Institute of Health). Perfusion, cryosectioning, staining and imaging of the mutant and control littermate mice were done blind and side-by-side using identical parameters and settings.

To determine if a correlation between TM-agrin overexpression and density and size of individual synaptic puncta exists, the confocal images were analysed blind using identical settings of the microscope and processed using the ImageJ software (National Institute of Health). The images were processed as follows: the look-up-tables were changed to grey scale and inverted, then an identical threshold was applied across the entire set of images, chosen to show the high intensity as well as the low intensity staining (compare image analysis method: Pribiag et al., 2014).

The threshold binary images were used for fraction area quantification. To measure the area fraction covered by synaptic staining, a threshold between the Agrn/Cre and WT/Cre staining was set for the entire experiment, and the fraction area covered by threshold staining was measured with ImageJ software (National Institute of Health, Bethesda, USA). Fraction area measurements were collected from three mice per genotype in 12 to 36 images per mouse. All parameters, including scanning laser intensity, were identical across experiments.

2.11. RNA extraction and quantitative PCR

For detailed analysis of expression levels in the cortex and hippocampus, mouse brains were prepared as described in section 2.6. and further dissected in PBS using a stereo binocular microscope (Leica MZ6, Leica Microsystems). The brain subregions were separately snap-frozen in liquid nitrogen.

To extract and preserve total RNA, 30mg of tissue were ground with pestles fitting microtubes (Eppendorf micropestles, Sigma-Aldrich) in liquid nitrogen and RNA was extracted using the SV Total RNA Isolation System (Promega, Madison, USA). The RNA was eluted with 100µl nuclease-free H_2O and the quality was assessed using a Nanodrop spectrophotometer. To test the integrity of the total extracted RNA by agarose gel electrophoresis, the samples were prepared as follows: 8µl RNA, 4µl nuclease free H_2O, 10µl formamide, 3.2µl 37% formaldehyde 8µl of 4.5% ethidium bromide, 6µl DNA sample buffer (NEB), heated at 65˚C for 10min and electrophoresed on an agarose gel containing 1% agarose and 6.7% Formaldehyde in MOPS buffer

(20mM MOPS, 5mM Na acetate, 1mM EDTA). After the quality of the RNA was confirmed, the RNA was reverse transcribed into cDNA using the Quantitect Reverse Transcription Kit (Qiagen) following the manufacturer's instructions.

For assessing expression levels of genes possibly affected by transmembrane agrin overexpression, the following intron-spanning primers were designed using the online Universal ProbeLibrary Assay Design Center (Roche and Diagnostics, 2009).

Genes	Primers	Product
Agrn (agrin)	5': GCTACTTCTACGTTGGGCTTTG 3': TGCAGAGTGCCAATGATCTC	114 nt
Bsn (bassoon)	5': TTTAACCCAACACCGCATCT 3': GCCGCTTAGTTTGGCAGTT	67 nt
Dlg3 (SAP-102)	5': AACCGGGACTGGTATGAGC 3': TGCCATTCACCGATAGGC	85 nt
Gria1 (AMPA receptor subunit 1)	5': AGGGATCGACATCCAGAGAG 3' : TGCACATTTCCTGTCAAACC	63 nt
Grin1 (NMDA receptor subunit 1)	5': GCTGGAGGAGCGTGAGTC 3' : AGCAGAGCCGTCACATTCTT	66 nt
Vamp2 (Synaptobrevin)	5': CCAAGCTCAAGCGCAAAT 3' : GGGATTTAAGTGCTGAAGTAAACG	112 nt
Syp (Synaptophysin)	5': CAAGGCTACGGCCAACAG 3' : TCGTGGGCTTCACTGACC	72 nt
Gabra1 ($GABA_A$ receptor, subunit α)	5': GCCCACTAAAATTCGGAAGC 3' : CTTCTGCTACAACCACTGAACG	83 nt
Gphn (Gephyrin)	5': TGGTCTCATCAGTTATTCCCATC 3' : CGAGAAATGATGGAGTCTGGA	72 nt
Unc13a (Munc13-1)	5': CAATGCCTTGGCAGATGATA 3' : GGGTCTTCAAAGGAACACTGG	96 nt
Unc13b (Munc13-2)	5': TGCCTTGGCAGATGATAATG 3' : AGCCCAAATAGGTCCAGTGA	86 nt
Hprt (HPRT)	5': TCCTCCTCAGACCGCTTTT 3': CCTGGTTCATCATCGCTAATC	90 nt
Unc13c (Munc13-3)	5': TCTGACACCAAGACAATGTGC 3': CCTCCTGCATGAAAATATTGCT	72 nt
Dlg4 (PSD95)	5': ACTCCTGCTCCAGCTTCGT 3': GCTCCCTGGAGAATGTGCTA	93 nt
Dag1 (Dystroglycan)	5': CTGCTGCTGCTCCCTTTC 3': CCAGGCAGTGTTGAAAACCT	99 nt
Syt1 (Synaptotagmin-1)	5': ACCTTACTCAACTGGCATTTGTT 3': AGACTGCGGATGTTGGTTGT	92 nt
Nlgn2 (Neuroligin-2)	5': CCTACGTGCAGAACCAGAGC 3': TCGCCTCGTCACGTTTTT	93 nt
Pipetting	cDNA (10ng/µl): 6µl Primers (2.5µM): 2µl each	
Quantification **Melting curve**	95°C 5min 95°C 5min	

Table 4: qPCR primers and specifications. Primers were designed intron-spanning in all cases. All primers were purchased from Thermo Fisher Scientific. nt: nucleotides.

Quantitative PCR analysis was performed on a Light Cycler 480 (Roche), using Sybr green dye (SensiMix SYBR No-ROX Mastermix, Bioline, London, UK) in a 96-well format with a volume of 20µl per well, adding 10µl of SensiMix per reaction (primer sequences: Table 4). To ensure primer

binding specificity and efficiency, a melting curve assay was performed on the product after each round of acquisition. The data was only further analysed when the corresponding PCR product showed one melting point peak, indicating specific binding and generation of only one specific product. In addition, the samples were analysed on a 3% agarose gel to visualize the DNA bands. The analyses were performed in triplicates.

2.12. Antibody specifications

The following antibodies were use in this study, for immunocytochemistry, immunohistochemistry and Western blot:

Primary antibodies	**Source**	**Species**	**Dilution**
anti-mouse agrin (204)	Eusebio et al., 2003	Rabbit	1:2000 WB, 1:500 IF
anti-HA (3F10)	Roche	Rat	1:3000 WB, 1:250 IF
anti-c-myc (9E10)	Dr. Elisabeth Kremmer	Mouse	1:10 WB
anti-PSD95 (MA1-045)	Thermo Fisher Scientific	Mouse	1:500 IF
anti-bassoon (SAP7f)	Jastrow et al., 2006	Rabbit	1:1000 IF
anti-cre (ab137240)	Abcam, Cambridge, UK	Rabbit	1:50 IF
Secondary antibodies			
anti-rabbit-IgG (HRP)	Invitrogen Thermo Fisher Scientific	Goat	1:3000 WB
anti-rat-IgG (HRP)	Abcam	Donkey	1:2000 WB
anti-mouse-IgG (HRP)	Invitrogen Thermo Fisher Scientific	Goat	1:3000 WB
anti-mouse-IgG (IRDye680)	Li-Cor, Cambridge, UK	Donkey	1:20,000 WB
anti-rabbit-IgG (IR800CW)	Li-Cor	Donkey	1:20,000 WB
anti-rabbit-IgG (Alexa488)	Invitrogen Thermo Fisher Scientific	Goat	1:1000 IF
anti-mouse IgG (Cy3)	Jackson, West Grove, USA	Goat	1:1000 IF

Table 5: Antibodies used in this study. HRP: horseradish peroxidase; ms: mouse; WB: Western blot; IF: immunofluorescence. For simplicity and since concentrations of polyclonal antibodies often are not known, dilution is given.

3. Results

3.1. Expression of mouse transmembrane agrin *in vitro*

To investigate if the cDNA construct coding for mouse TM-agrin elicits the same *in vitro* phenotype as chick TM-agrin I validated it *in vitro* by overexpressing the cDNA in HEK293T cells. The primers designed for the C-terminal part of agrin amplified the isoform containing the y4 splice insert and missing the z- splice insert (TM-agrin$_{0,4,0}$). Since the *in vitro* phenotype of filopodia production by TM-agrin overexpression has been shown to be independent of the z-splice insert (McCroskery et al., 2006), this cDNA was used for further analysis. The pMES transient expression vector was chosen, since it contains an IRES-GFP sequence, which allows easy distinction of transfected cells.

Figure 8 shows Western blot analysis using antibodies raised against the C-terminal extracellular domain of mouse agrin (Eusebio et al., 2003) and anti-HA-tag antibodies.

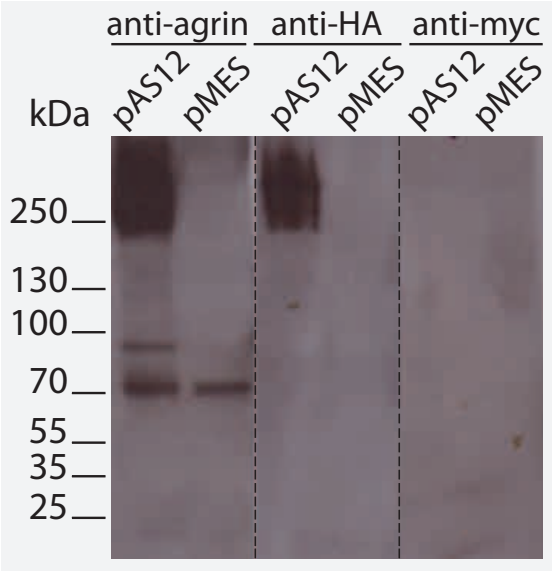

Figure 8: Western blot showing agrin immunoreactivity in HEK293T cell lysates. HEK293T cells were transfected with pAS12 plasmid coding for HAmsTM-agrinMyc or the empty vector pMES. Both the HA and agrin antibodies detected the expected high molecular smear above 250kDa. The mouse agrin antibody detected an unspecific band at 70kDa and an agrin-specific cleavage product around 90kDa. The anti-myc antibody did not recognize the agrin fusion construct.

Both antibodies reveal a broad smear with a molecular mass of approximately 500 kDa, representing the staining pattern previously described for chick agrin (Kroger & Mann, 1996).

HEK293T cells transfected with the mouse TM-agrin$_{0,4,0}$ construct demonstrated that this cDNA obtained from total mouse brain tissue elicited similar filopodia-like protrusion, as the chick TM-agrin cDNA *in vitro* (Figure 9). This demonstrated the suitability of the mouse cDNA for analysis of TM-agrin function i*n vivo*.

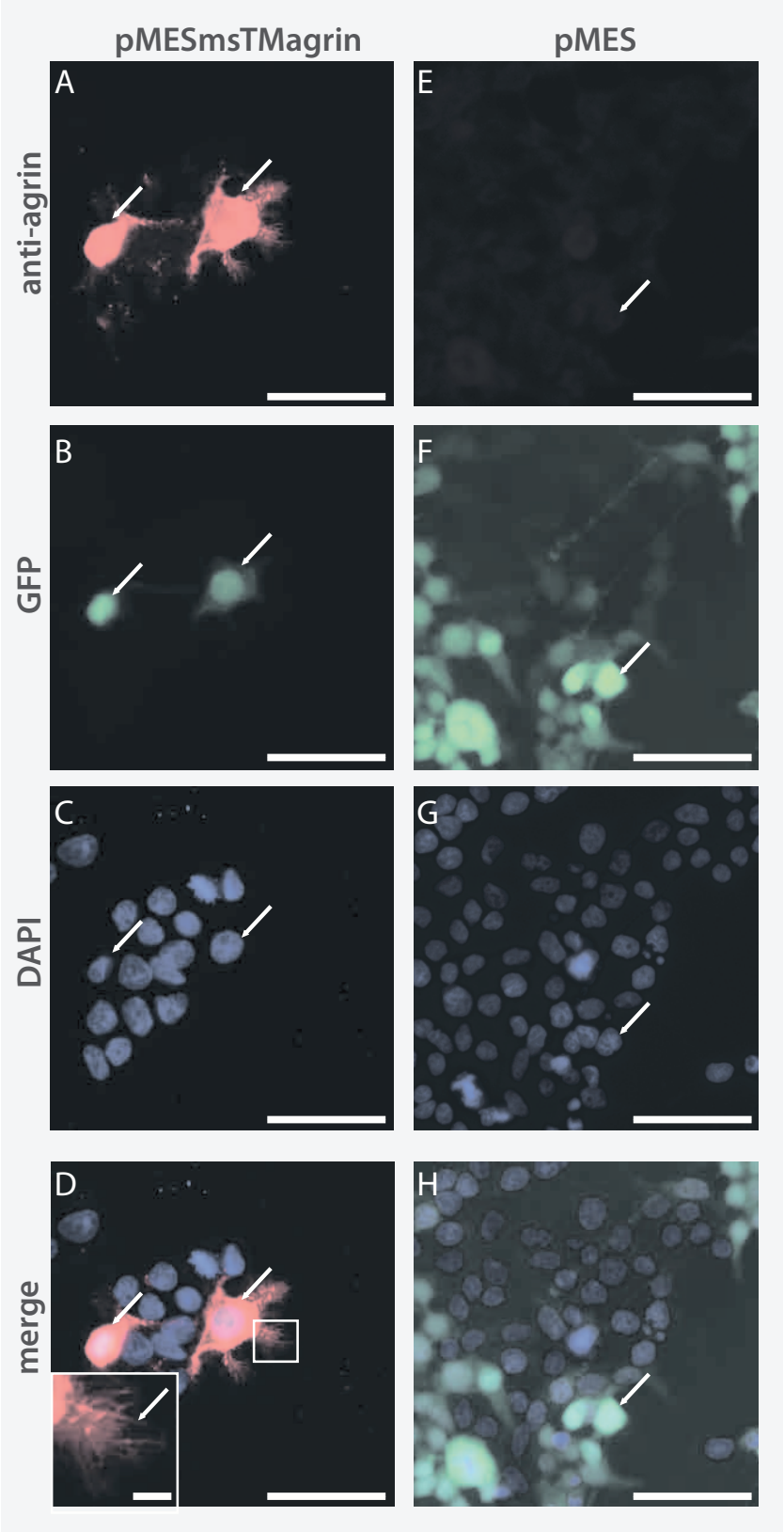

Figure 9: Immunostained HEK293T cells showing transmembrane agrin distribution and filopodia. (A–D): pMESmsTMagrin-transfected cells showed high agrin immunoreactivity (A) and numerous filopodia (D and inlet), compared to vector transfected control cells (E-H). Scale bar A-H: 50µm; scale bar inlet in D: 5µm

In addition, the Western blot analysis showed that mouse TM-agrin overexpressed in HEK293T cells is of the same molecular weight as its endogenous counterpart (

Figure 8).

After confirming the appropriate expression of TM-agrin in HEK293T cells, the msTM-agrin cDNA was transferred to a targeting vector backbone, which facilitates insertion of the construct into the ROSA26 locus. The ROSA26 locus has been used many times in the past for inserting expression constructs, since the locus shows high efficiency for homologous recombination and homozygous ROSA26 knock-out mice do not exhibit any detectable phenotype (Zambrowicz et al., 1997).

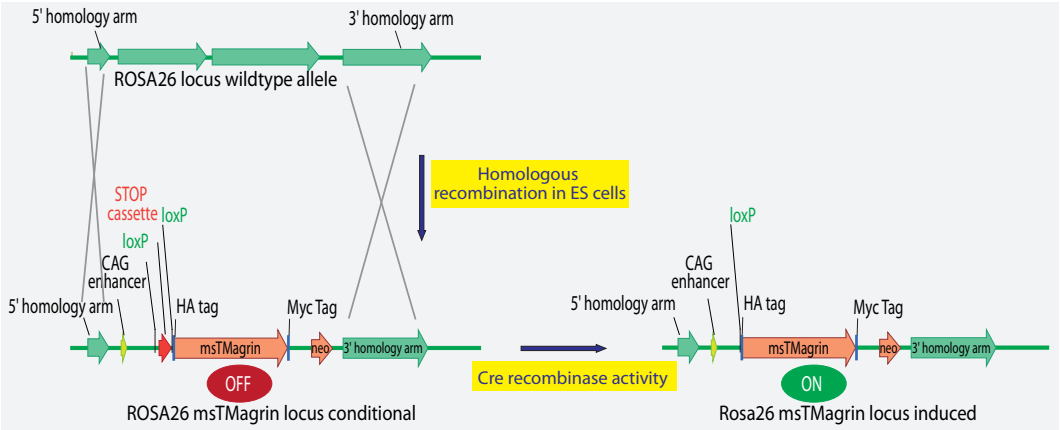

Figure 10: Insertion of the knock-in conditional msTMagrin construct and activation of expression by Cre-recombinase. The construct was inserted into the Rosa26 locus by homologous recombination in ES cells using two stretches of direct homology flanking the insertion cassette. Before Cre-recombinase exposure, expression is off due to a stop cassette (3 polyA sequences) flanked by loxP sites. After excision of the stop cassette, TM-agrin expression mediated by the CAG enhancer is turned on. Neo: Neomycin resistance for selection in ES cells.

The CreERT2-Tamoxifen inducible expression system was chosen for the generation of this TM-agrin overexpression mouse line, since the expression can be tightly controlled in time and space and since reproducibly high expression levels have been reported with many CreERT2 driver lines.

Since transmembrane agrin has been reported to be localized to glutamatergic synapses in the cortex and hippocampus (Ksiazek et al., 2007), I chose to cross to the CamKIICreERT2 mouse line as the CreERT2 driver allele, which shows high expression in excitatory neurons in these areas (Erdmann et al., 2007).

To test the baseline expression and the expression after Cre activity *in vivo*, the conditional targeting construct was co-transfected with and without a pNLSCre vector (expressing Cre recombinase with a nuclear localization signal, pPGK-Cre-bpA; Gu et al., 1993). Most important for proceeding with the generation of a conditionally expressing knock-in mouse line, overexpression from the targeting vector was shown to be dependent on Cre expression (Figure 11). In addition, I observed a large number of filopodia-like processes on the HEK293T cells that were transfected with the targeting vector and pNLSCre.

These results showed that the construct contains full-length murine TM-agrin and the cDNA expression is strictly Cre-dependent. Most importantly, mouse TM-agrin cDNA overexpression induces similar filopodia-like processes as chick TM-agrin. In summary, my results demonstrate that the vector I designed is suitable to investigate the function TM-agrin overexpression in vivo.

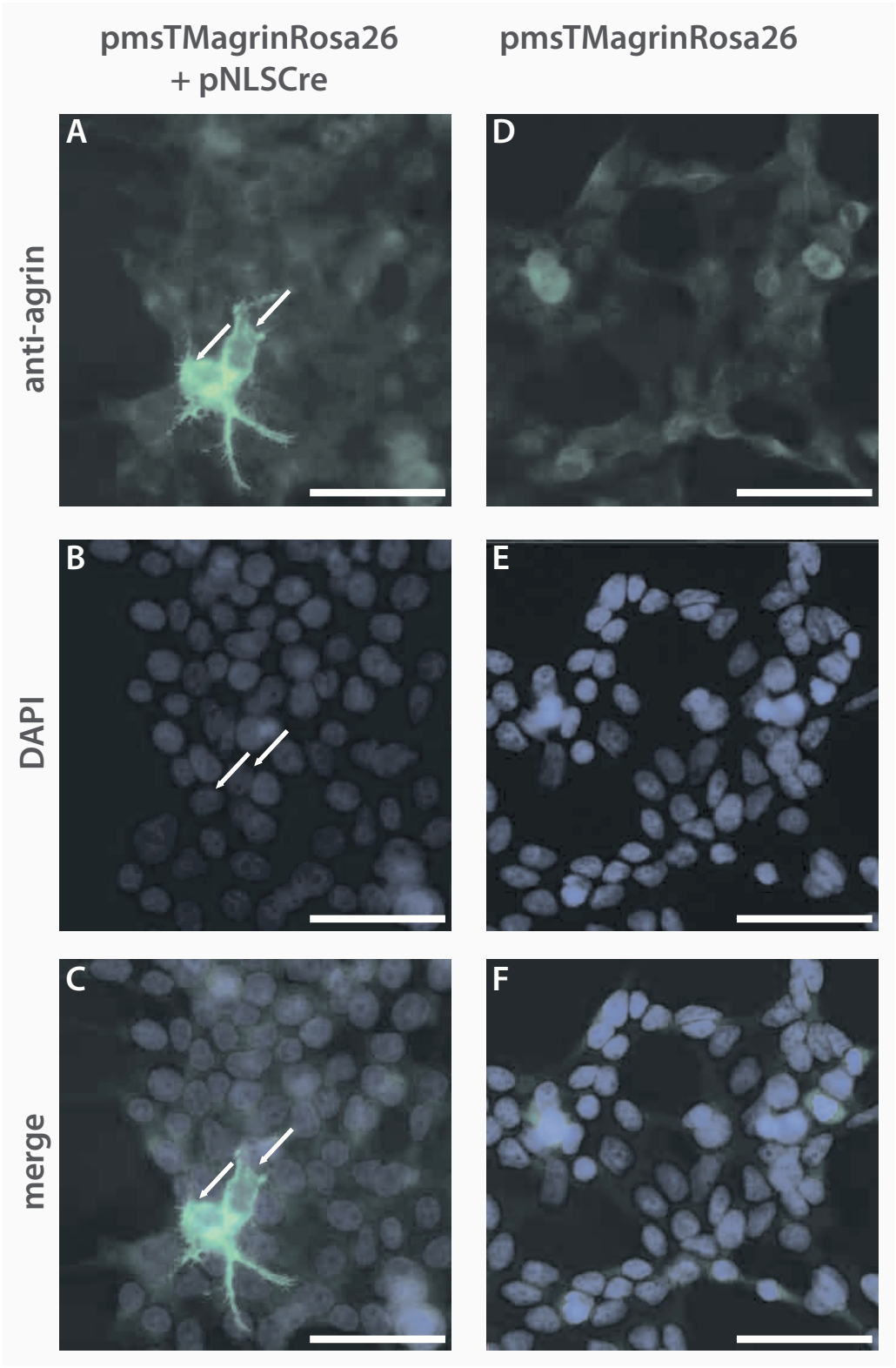

Figure 11: Immunostained HEK293T cells expressing the pAS20 targeting construct alone (D-F) and the targeting construct co-transfected with pNLSCre (A- C). Without NLSCre, the cells showed little agrin immunoreactivity (D). Transfected cells expressing msTMagrin under Cre-control showed high agrin immunoreactivity. In the absence of pNLSCre, no cells expressing the msTMagrin construct were found, demonstrating that Cre-mediated expression was tightly controlled.

3.2. Levels of Cre induction and levels of agrin protein expression

Transient expression of recombinant proteins in cell culture usually results in high protein levels, as seen in Western blotting and by immunocytochemistry. We expected that high levels of TM-agrin *in vivo* might be needed to see an effect caused by TM-agrin. The first available mouse litters were used to assess the level of agrin protein level in total mouse brain by quantitative Western blotting. As shown in Figure 12, the overexpression levels differed between control and TM-agrin overexpressing mice about three-fold depending on the method of tamoxifen administration. When mice were injected with tamoxifen three times during week 5 and whole brain membrane extracts prepared in week 9, I achieved agrin levels in Agrn/Cre mice almost 11-fold higher than in the WT/Cre control mice (Figure 12). Notably, the agrin protein levels in Agrn/WT mice were as low as in the WT/Cre mice, showing that the TM-agrin overexpression cassette in the Rosa26 locus resulted in tight control over expression in the absence of Cre. When tamoxifen was administered by feeding for two weeks, the agrin protein levels increased with the time given for recovery on regular food after the tamoxifen containing food. This might be explained by agrin protein accumulating over time after the start of expression. After three weeks of recovery, I achieved an approximately 7-fold increase in agrin protein levels in the brain when compared to WT/Cre control.

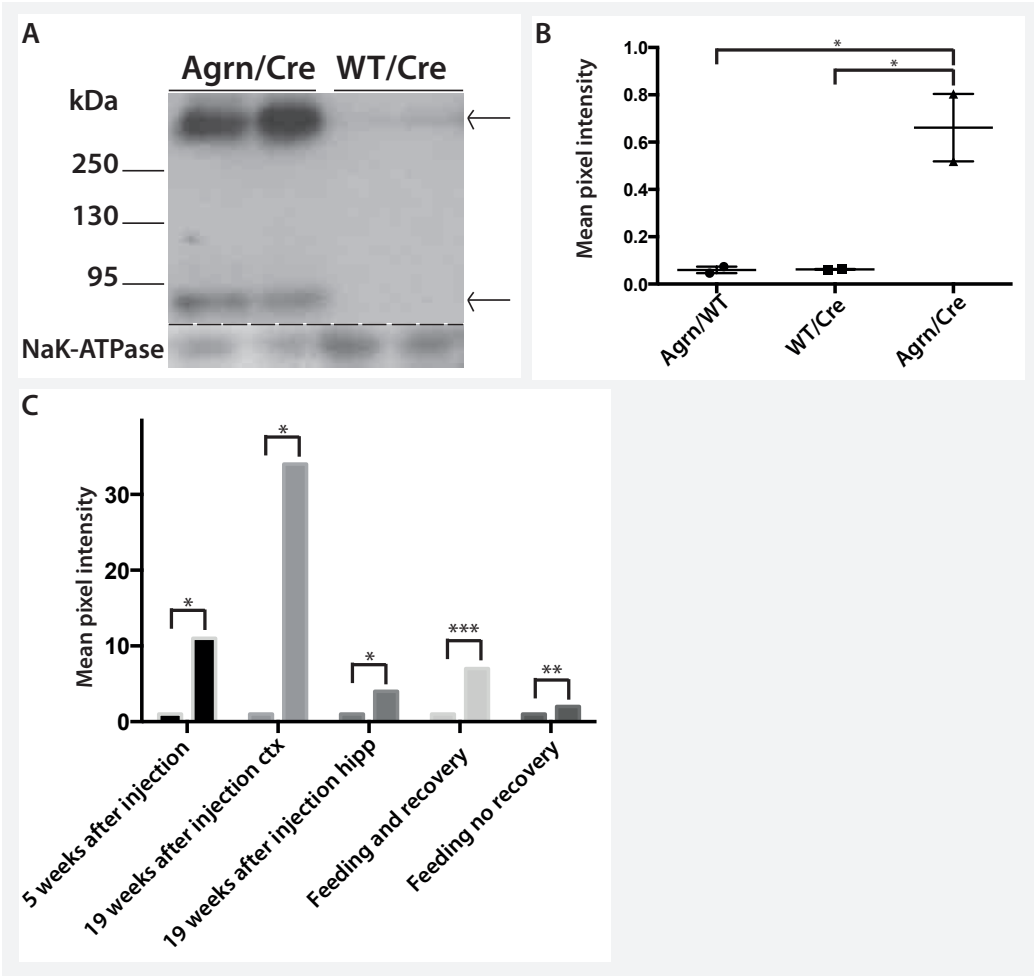

Figure 12: Western blot analysis of whole brain membrane fractions of WT/Cre and Agrn/Cre mice. A) Arrows point to full-length agrin protein and a lower molecular weight band with a size to be expected for the Neurotrypsin cleavage product of agrin. B) Quantification of the mean pixel intensity of agrin immunoreactivity determined by infrared signal detected in Western blots by Licor Odyssey scanner. Error bars of the scatter plots depict standard error of the mean (SEM). Statistical analysis on the Gaussian distributed values was performed by one-way ANOVA ($p < 0.022$). C) Combined Western blot analysis of normalized Tamoxifen administration protocols. From left to right: Animals were injected 3 times in week 5 (Monday-Wednesday-Friday) with 2mg tamoxifen (Sigma-Aldrich) in 100µl Mygliol (Caelo) and Western blot analysis of whole brain membrane extracts was performed in week 10, showing the mean pixel intensity of agrin immunoreactivity to be increased 10-fold in the Agrn/Cre mutants compared to WT/Cre control animals (Student's t-test $p = 0.022$). On average, 19 weeks after injection the animals showed a 34-fold increase in the cortex membrane preparations ($p = 0.0291$) and a 4.4-fold increase in the hippocampus ($p = 0.012$). When Tamoxifen was given in food pellets, the animals showed a 2-fold increase in agrin immunoreactivity after 2 weeks of tamoxifen containing diet ($p = 0.0045$). This yield could be improved by recovery on regular diet for 2 weeks, resulting in agrin protein levels 7.3-fold higher than in WT/Cre control animals ($p < 0.0001$). In subsequent Western blot and qPCR experiments, this feeding protocol was used to ensure high agrin protein yield. Ctx: cortex; hipp: hippocampus.

This Agrn/Cre mouse model was generated to investigate how neurons in their natural network *in vivo* react to TM-agrin overexpression. When

analysing individual neurons as well as entire neuronal networks, it is important to have an estimate of how many neurons in the network express the knock-in construct. Therefore, I examined the percentage of cells expressing the recombinant TM-agrin protein compared to non-expressing cells. Since TM-agrin localizes to synapses and these are very numerous in the brain, it was not possible to estimate the rate of induction by agrin staining. Instead, I made use of the fact that CreERT2 translocates to the nucleus after tamoxifen administration and analysed nuclear localized Cre staining in cortex layer 3 and in the hippocampal CA1 region (Figure 13). In the hippocampus CA1 region, the nuclei of glutamatergic cells are located in the nuclear layer and therefore are easily distinguishable from other cells. In this region, the percentage of cells positive for nuclear Cre immunoreactivity was around 72% (Figure 13). In contrast, in the cortex it was not possible to differentiate between glutamatergic neurons and other cell types within layer 2-3. The percentage of all cells positive for nuclear Cre immunoreactivity was determined around 40% (Figure 13). It is reasonable to assume that 72% is the better estimate of the true ratio of CreERT2 induction in glutamatergic neurons. These results showed that 72% of the pyramidal cell somata in the CA1 region of the hippocampus as well as 40% of cell somata in cortex layer 2-3 expressed Cre recombinase.

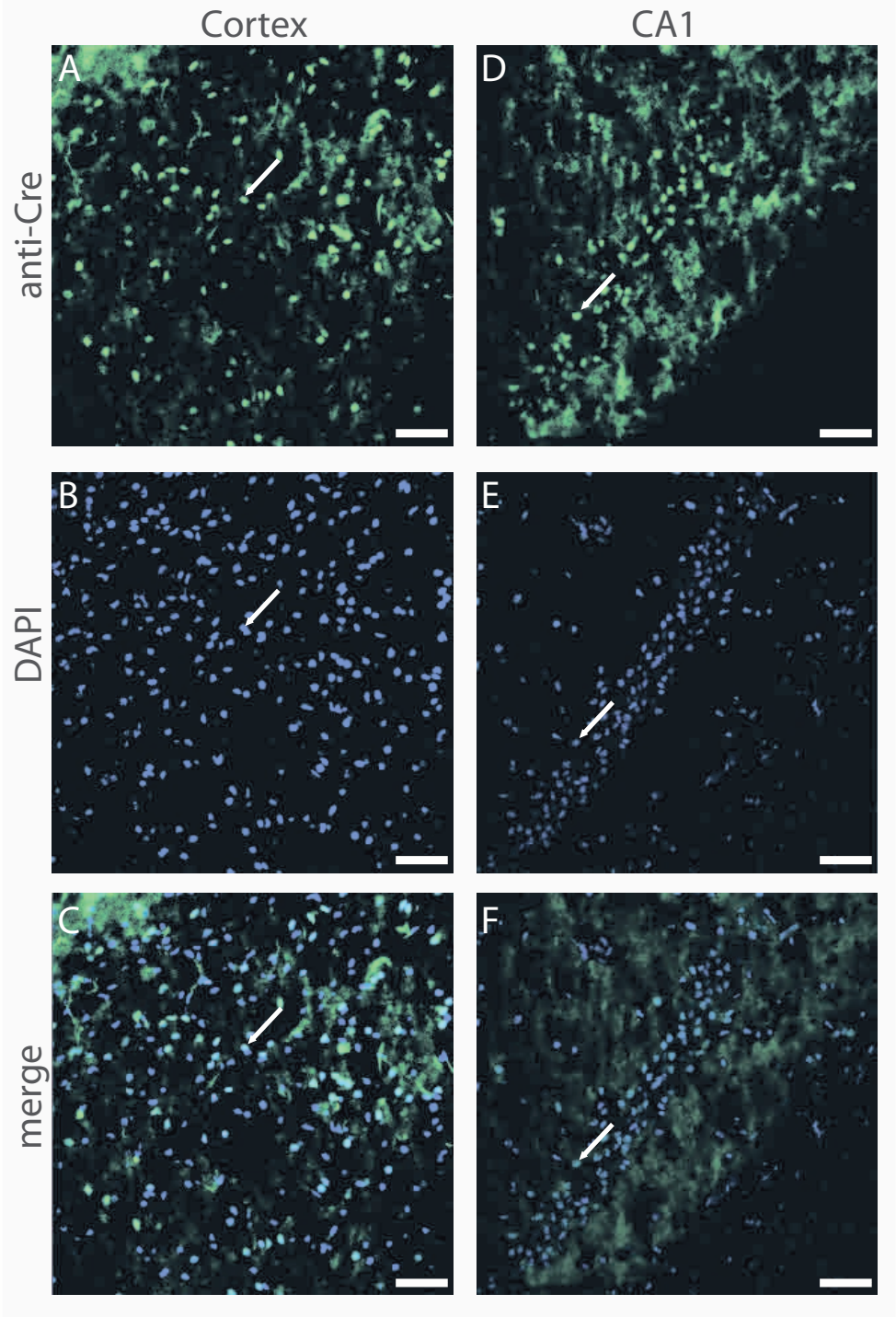

	Nuclei total	Cre-positive nuclei	Cre induction
Cortex	842	333	40%
CA1 nuclear layer	95	68	72%

Figure 13: Estimation of Cre induction in cortex (A-C) and hippocampus CA1 nuclear layer (D-F) of Agrn/Cre mice. Note that in hippocampus CA1, all the nuclei examined belong to glutamatergic pyramidal cells, whereas in the cortex, DAPI staining of all cells was assessed. Scale bar: 50µm.

Next, I tested whether the subcellular localization of recombinant agrin is the same as endogenous agrin. Figure 14 shows that anti-agrin immunoreactivity in both genotypes was punctate, consistent with the concentration of agrin at synapses. Moreover, as expected, the intensity was higher in the Agrn/Cre mice compared to the WT/Cre littermates. NtA-agrin is part of blood vessel endothelial cells. The antibody used in this study detects NtA-agrin as well as TM-agrin and hence blood vessel staining can be used as internal control of antibody specificity. The intensity of the blood vessel staining was similar in both groups. These results show that the recombinant TM-agrin exhibited a punctate localization comparable to endogenous agrin.

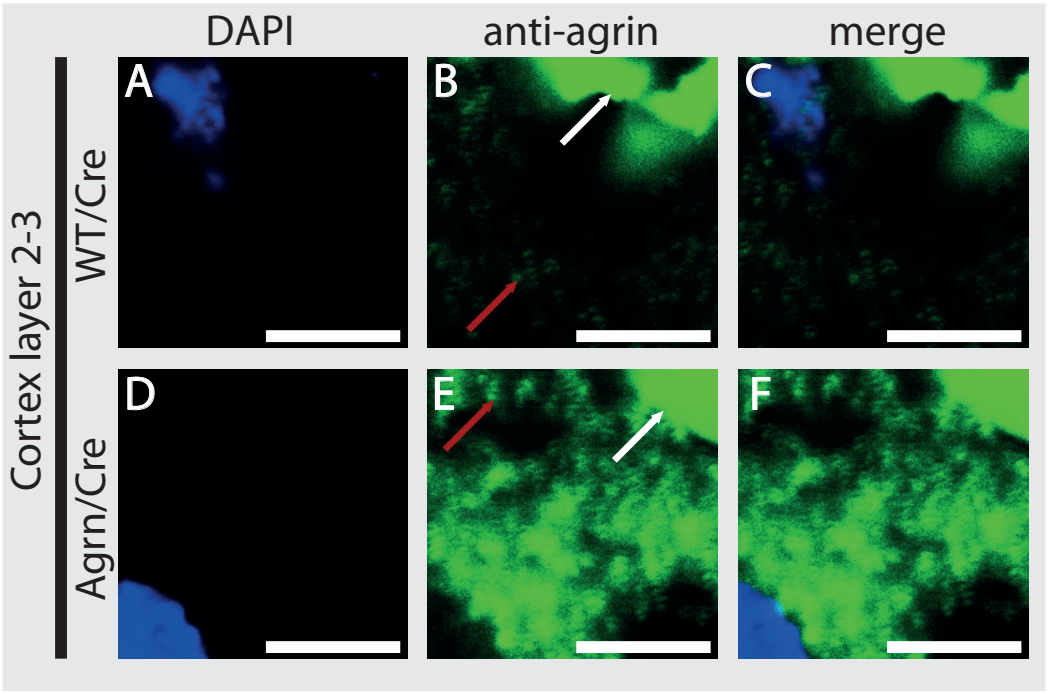

Figure 14: Distribution and intensity of anti-agrin immunoreactivity in WT/Cre (A-C) and Agrn/Cre (D-F) mice. WT/Cre and Agrn/Cre mice were injected with tamoxifen in week 5 and perfused with 4% PFA in week 8. 20µm Cryosections were immunostained with antibodies raised against the C-terminal of agrin. A-C: WT/Cre mouse brain sections showing cortex layer 2-3. D-F: Agrn/Cre mouse brain sections showing cortex layer 2-3. White arrows: Agrin immunoreactivity in the basal lamina of blood vessels showed comparable intensity between Agrn/Cre and WT/Cre mice. Red arrows: Synapse-like staining of agrin was more intense in Agrn/Cre mice than in WT/Cre mice. Scale bar: 5µm.

3.3. Initial characterization of TM-agrin overexpressing mice

To investigate if TM-agrin overexpression affects non-neuronal organs or the peripheral nervous system, a primary phenotypic screen of the TM-agrin mice was performed in collaboration with the German mouse clinic (Helmholtz Zentrum Neuherberg, Munich). The following aspects were analysed: Nociception, bone and cartilage, metabolism, cardiovascular system, eye function, clinical chemistry and haematology, immunology, lungs, pathology, neurology and general behaviour (overview of tests: Fuchs et al., 2009). The screen revealed no apparent behavioural or physiological phenotype (results not shown). The weight of the mice did not differ in males and in females to control animals (Figure 15).

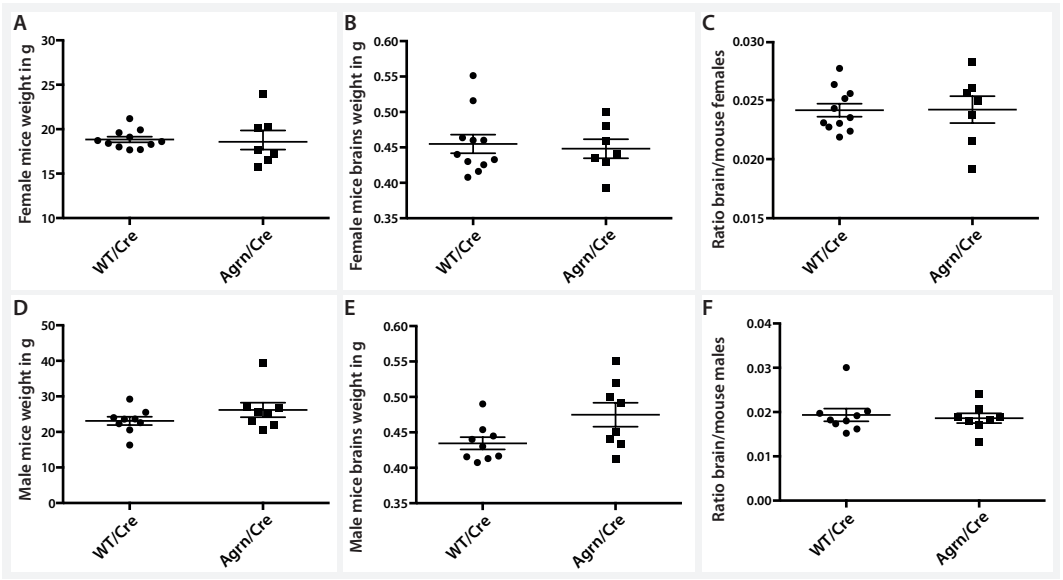

Figure 15: Weight of whole animals and brains of WT/Cre and Agrn/Cre mice. The animals were injected at 5 weeks and sacrificed between 8 and 10 weeks. The weights of whole animals (A and D), whole brains (B and E) and the ratio between animal and brain weights (C and F) do not differ significantly in males or females. Error bars of the scatter plots depict standard error of the mean (SEM).

Induction of TM-agrin overexpression in the CNS did not affect mortality or fertility in long-term observations. To conclude, TM-agrin overexpression did not result in any apparent gross morphological changes.

Previous studies of agrin knock-out mice, whose perinatal death was rescued by motoneuron-specific agrin expression, showed a significant reduction in brain size, although the number of cells was unchanged (Ksiazek et al., 2007). To test whether agrin overexpression also had an effect on brain size I weighed the mouse brains and analysed the forebrain volume in MRI images. The weight of the mouse brains did not differ significantly between the Agrn/Cre and Agrn/WT groups in males and females (Figure 15). Likewise, the volume of cortex and hippocampus showed no significant difference when analysed by MRI (Figure 16). MRI studies were done in collaboration with Dr. Luciana Afonso (Helmholtz Zentrum Neuherberg, Munich). Moreover, the general layering of the cortex and the hippocampus was unaltered, demonstrating no excessive cell death and cellular rearrangements in the CNS. Collectively, these results demonstrate that TM-agrin does not cause substantial degeneration or proliferation in these areas of the CNS.

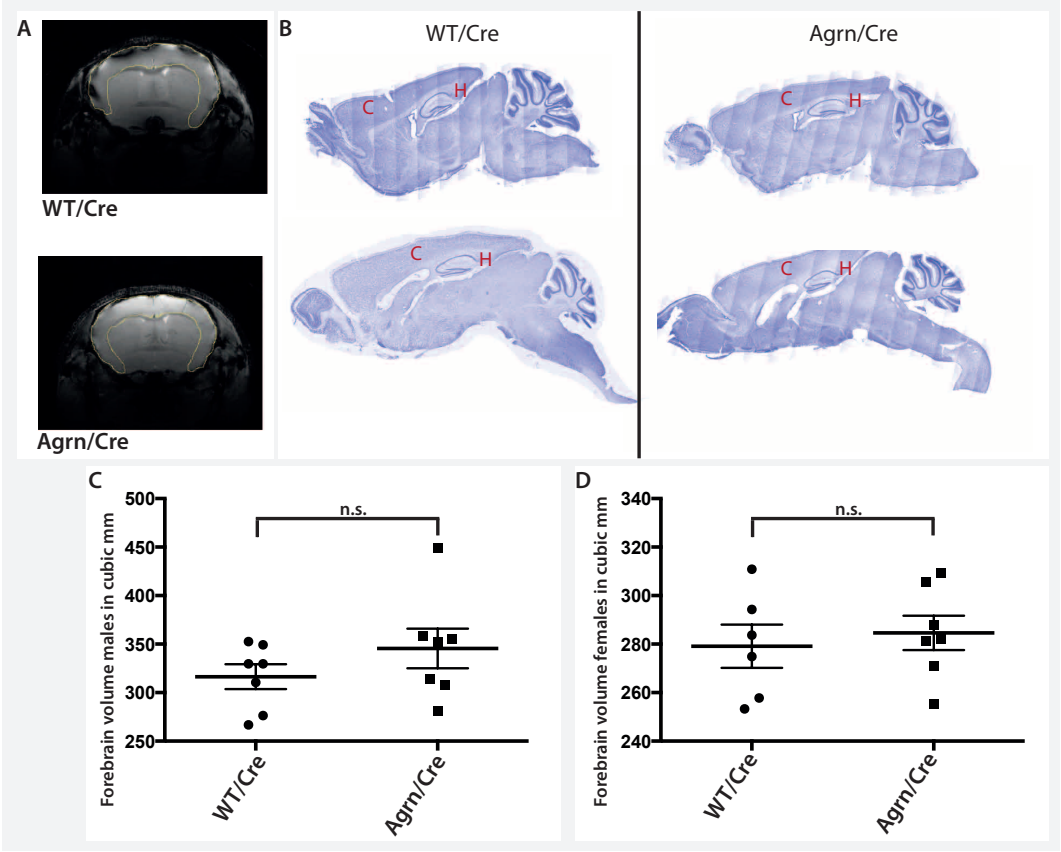

Figure 16: Volume of mouse cortex and hippocampus determined by visual analysis of Nissl stainings (B) and quantifications of MRI images (A). Analysis of 6-7 mice per group, 20 MRI optical sections each, showed no statistical difference in forebrain volume in males and females (C and D).

3.4. Expression levels of synapse-associated candidate genes

Overexpression of a synaptogenic or synapse-modifying gene can have an effect not only on the maturation, formation and morphology of a synapse, but also on the function and transmission efficiency. To investigate if TM-agrin overexpression affects the regulation of synapse-associated proteins we performed expression profiling of mRNA extracted from cortices of Agrn/CamKIICreERT2 (Agrn/Cre) mice and their WT/CamKIICreERT2 (WT/Cre) littermates. Both mouse lines were fed with tamoxifen-containing food during week 5 and sacrificed during week 10. After 5 weeks of

expressing the TM-agrin allele, the mice showed a significant regulation of several of the analysed mRNAs (Table 6).

Primers specific for the transmembrane isoform of agrin showed the expected increase in TM-agrin mRNA in the overexpressing animals. The increase in TM-agrin mRNA was on average 17-fold. This correlates well with the 7-fold increase in agrin protein levels observed in whole brain membrane preparations of mice fed with tamoxifen and sacrificed after 5 weeks of induction (Figure 12).

Among the members of the active zone of both inhibitory and excitatory synapses, whose expression was tested with qPCR, Munc13-1 (mouse unc13 homologue A, *C. elegans*) and Munc13-2 (mouse unc13 homologue B, *C. elegans*) were significantly downregulated. In contrast, several postsynaptic proteins of glutamatergic synapses were significantly upregulated, including the Grin1 cDNA, coding for the NMDA-receptor subunit NR1. The Dlg4 gene, coding for the glutamatergic postsynapse scaffolding protein PSD95, showed a trend towards upregulation, which was however not significant due to variation between the animals.

	WT/Cre	Agrn/Cre	Fold regulation	p-value	R^2
Agrin	0,49± 0,02	8,4 ± 1,83	17	0,05	
		Presynaptic			
Munc13-1	0,004 ± 0,0006	0,001 ± 0,0007	0,17	0,03	0,86
Munc13-2	0,0007 ± 0,0002	0,0001 ± 9,6e-005	0,27	0,03	0,84
Munc13-3	0,052 ± 0,021	0,021 ± 0,007	0,40	0,17	0,64
Synaptotagmin-1	0,9 ± 0,06	1,7 ± 0,56	1,89	0,28	0,98
Bassoon	12 ± 3,7	10 ± 7,4	0,23	0,85	0,98
Synaptophysin	27 ± 6,4	24 ± 24	0,9	0,91	0,27
Synaptobrevin	7,1 ± 0,80	6,01 ± 2,96	0,85	0,77	0,57
		Postsynaptic			
PSD-95	73 ± 31	170 ± 61	2,3	0,28	0,91
SAP-102	1,40 ± 0,62	1,40 ± 0,28	1	0,99	0,04
Dystroglycan	0,08 ± 0,01	0,48 ± 0,11	6,29	0,02	0,17
Gephyrin	0,07 ± 0,002	0,002 ± 0,0003	0,04	< 0,0001	0,14
Neuroligin-2	2,7 ± 0,25	1,1 ± 0,42	0,41	0,03	0,68
		Neurotransmitter Receptors			
NMDAR1	26 ± 5,6	70 ± 5,6	2,7	0,005	0,86
AMPAR1	12 ± 1,6	11 ± 2,3	0,95	0,84	0,73
GABA1	36 ± 3,0	5,7 ± 3,1	0,24	0,001	0,62

Table 6: qPCR analysis of different candidate genes showing regulation of several genes involved in inhibitory and excitatory synapse formation and function. The qPCR experiments and analysis were performed by Gerry Handara. All qPCR experiments were done in technical triplicates with HPRT as housekeeping control gene, and at least 3 mice per genotype were tested. Results are given in mean value of cycle difference between housekeeping and gene of interest ± SEM. p-values are the results of student's t-test on the Gaussian distributed mean values performed in GraphPad prism. Linear regression analysis was performed using Excel (R^2 = coefficient of determination). Results with significant p-values (< 0.05) or significant correlation (R > 0.8) are highlighted red.

After correlation analysis, however, it was clear that PSD95 expression levels paralleled TM-agrin expression levels, meaning that the animals showing high agrin overexpression levels also showed high PSD95 mRNA levels (R^2 = 0.91).

Interestingly, most genes associated with inhibitory postsynapses were significantly downregulated: gephyrin, a scaffolding protein for GABA- and glycine receptor complexes (Kneussel and Betz, 2000; Yu et al., 2007), Neuroligin-2, an adhesion protein involved in inhibitory synapse maintenance (Reissner et al., 2008) and Gabra1, encoding the α1 subunit of

the $GABA_A$ receptor. The only exception to this was dystroglycan, which is an agrin binding protein at the neuromuscular junction and has been shown to be concentrated at GABAergic synapses (Levi et al., 2002; Pribiag et al., 2014). Dystroglycan expression was significantly upregulated more than 6-fold and, thus, behaved opposite to the other constituents of inhibitory synapses. In conclusion, TM-agrin overexpression in the murine cortex caused significant upregulation of several genes associated with glutamatergic synaptic transmission and a concomitant downregulation of several genes associated with GABAergic transmission. In addition, presynaptic proteins involved in vesicle exocytosis Munc12-1 and Munc13-2 were downregulated. Thus, TM-agrin overexpression in glutamatergic neurons also affects other neurons and changes the expression level of pre- as well as postsynaptic proteins.

3.5. Synapse density and size

Agrin knock-out mice, whose perinatal death was rescued by motoneuron-specific agrin expression, showed a 30% reduction in the number of synaptophysin positive puncta in the cortex, although the number of neurons was unchanged (Ksiazek et al., 2007). To determine if overexpression of TM-agrin similarly affects synapses in the CNS, the number and intensity of PSD95 (glutamatergic postsynaptic) and bassoon (general presynaptic) imunoreactive puncta were quantified in immunohistochemically stained cryosections of Agrn/Cre and WT/Cre brains.

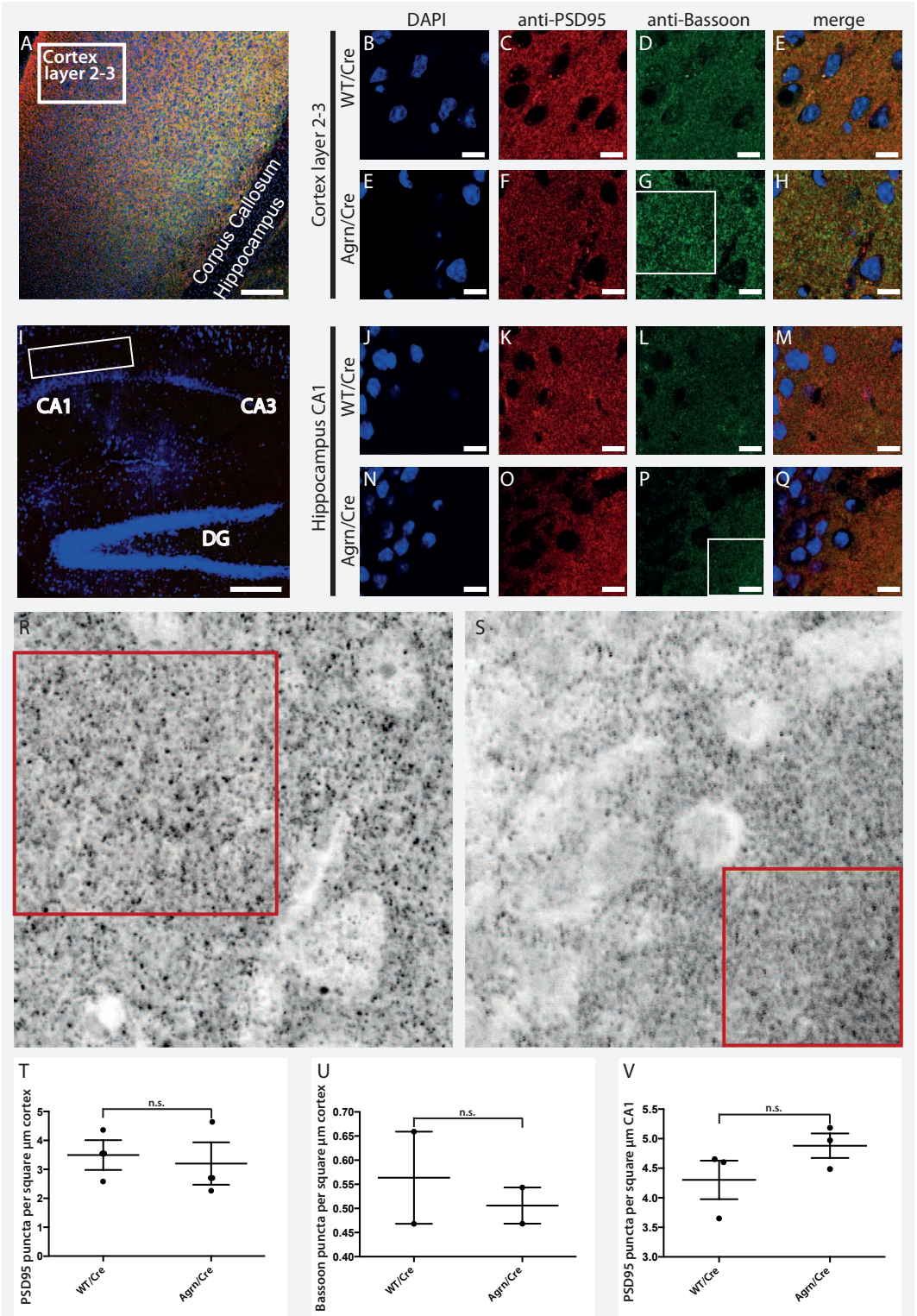

Figure 17: Density of synaptic marker immunoreactivity. Synaptic puncta staining in cortex and hippocampus of Agrn/Cre and WT/Cre mice injected with tamoxifen in week 5 and perfused with 4% PFA in week 8. Cryosections were immunostained with antibodies against bassoon and PSD95 to visualize pre- and postsynaptic puncta. A: Overview of Cortex sagittal section, boxed area indicates region of analysis. B-H: Magnification of cortex layer 2-3 region of analysis in WT/Cre mice and Agrn/Cre mice. I: Overview of hippocampus sagittal section, boxed area indicates region of analysis. J-Q: Magnification of hippocampus CA1 region of analysis in WT/Cre mice and Agrn/Cre mice. R-S: Original laser scanning confocal microscope images with

identical settings were greyscaled and analysed with ImageJ software (ICTN plugin, National Institute of Health); R: Bassoon cortex WT/Cre; S: Bassoon CA1 Agrn/Cre. T-V: The number of synaptic puncta does not differ significantly between the groups for neither synaptic marker. Error bars depict SEM of 3 mice per genotype in 12 to 38 individual images. Scale bar A and I: 200µm. Scale bar B-H and J-Q: 10µm.

Figure 17 shows the quantifications of anti-bassoon and anti-PSD95 positive puncta in the cortex and hippocampus CA1 region. No significant change in the number of synapses was detected (Figure 17 T-V).

After sorting of the individual results according to genotype and double-blind analysis it became evident that the area covered by above-threshold anti-PSD95 immunoreactivity and the staining intensity were significantly larger in the Agrn/Cre mice compared to the corresponding area in WT/Cre mice (Figure 18). Higher magnification revealed that most of the individual PSD95-immunopositive puncta were larger and more intensely stained in the cortex of Agrn/Cre mice than of WT/Cre control mice (Figure 18). The same observation was made in the hippocampal CA1 area of these mice (not shown).

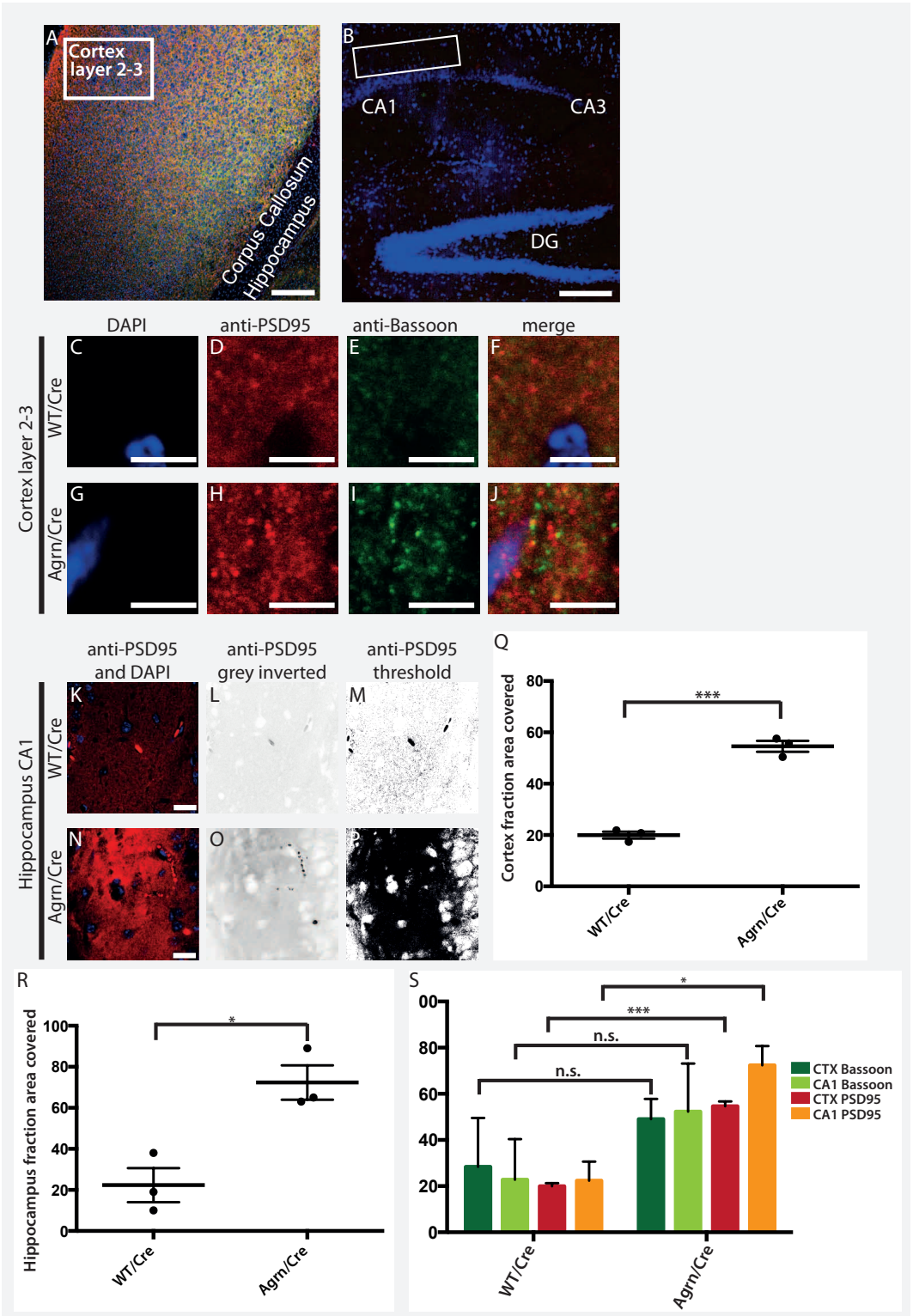

Figure 18: Fraction area covered by synaptic marker immunoreactivity. The fraction area covered by threshold PSD95 immunoreactivity (glutamatergic postsynapse) was significantly increased in Agrn/Cre mice hippocampus CA1 and cortex, indicating that PSD95 positive densities were denser and bigger. Bassoon immunoreactivity (general presynapse) was not significantly affected by TM-agrin overexpression. A) Overview of Cortex sagittal section, boxed area indicates region of analysis. B) Overview of hippocampus sagittal section, boxed area indicates region of analysis. C-J) Magnification of synaptic staining of cortex layer 2-3. K-P) Original images (K and N), greyscaled images (L and O) and threshold binary images (M and P). Q and R)

Quantifications of fraction area covered by anti-PSD95 immunoreactivity in cortex and hippocampus. Fraction area measurements were collected from three mice per genotype in 12 to 36 images per mouse. The PSD95 immunostaining showed an about 3-fold increase in the fraction of area covered in the Agrn/Cre mutant compared to the WT/Cre control (54.6% vs. 20%; p = 0.00017 for cortex and 72% vs. 22%, p = 0.0125 for hippocampus). S) Combined graph of bassoon and PSD95 immunoreactivity fraction area in cortex and hippocampus. The fraction area covered by bassoon staining did not differ significantly between Agrn/Cre and WT/Cre mice. Depicted are the mean values per mouse with standard error of the mean. Scale bar A and B: 200µm. Scale bar A-J: 5µm. Scale bar K and N: 20µm.

In conclusion, the overexpression of TM-agrin did not significantly affect synapse number in the cortex and hippocampus, but instead affected the size and density of the glutamatergic postsynaptic densities, as indicated by a 3-fold increase in the fraction area covered by PSD-95 immunoreactivity in Agrn/Cre mice compared to WT/Cre mice.

3.6. Dendritic spine density and morphology

Dendritic spines are postsynaptic specializations of excitatory synapses in the brain. To view them in detail using light microscopy I used the Golgi impregnation method, originally developed in 1873 by Camillo Golgi (Golgi, 1873). Even today this method remains a useful tool for analysing dendritic spine morphology, since only 1-5% of neurons are stained (Golgi, 1989). Golgi silver impregnation was performed on 10-week old Agrn/Cre and WT/Cre mice that had been injected with Tamoxifen in week 5. The results of an analysis of 4 to 6 mice per genotype and up to 102 measurements of individual spine head size as well as number and type is summarized in Figure 19.

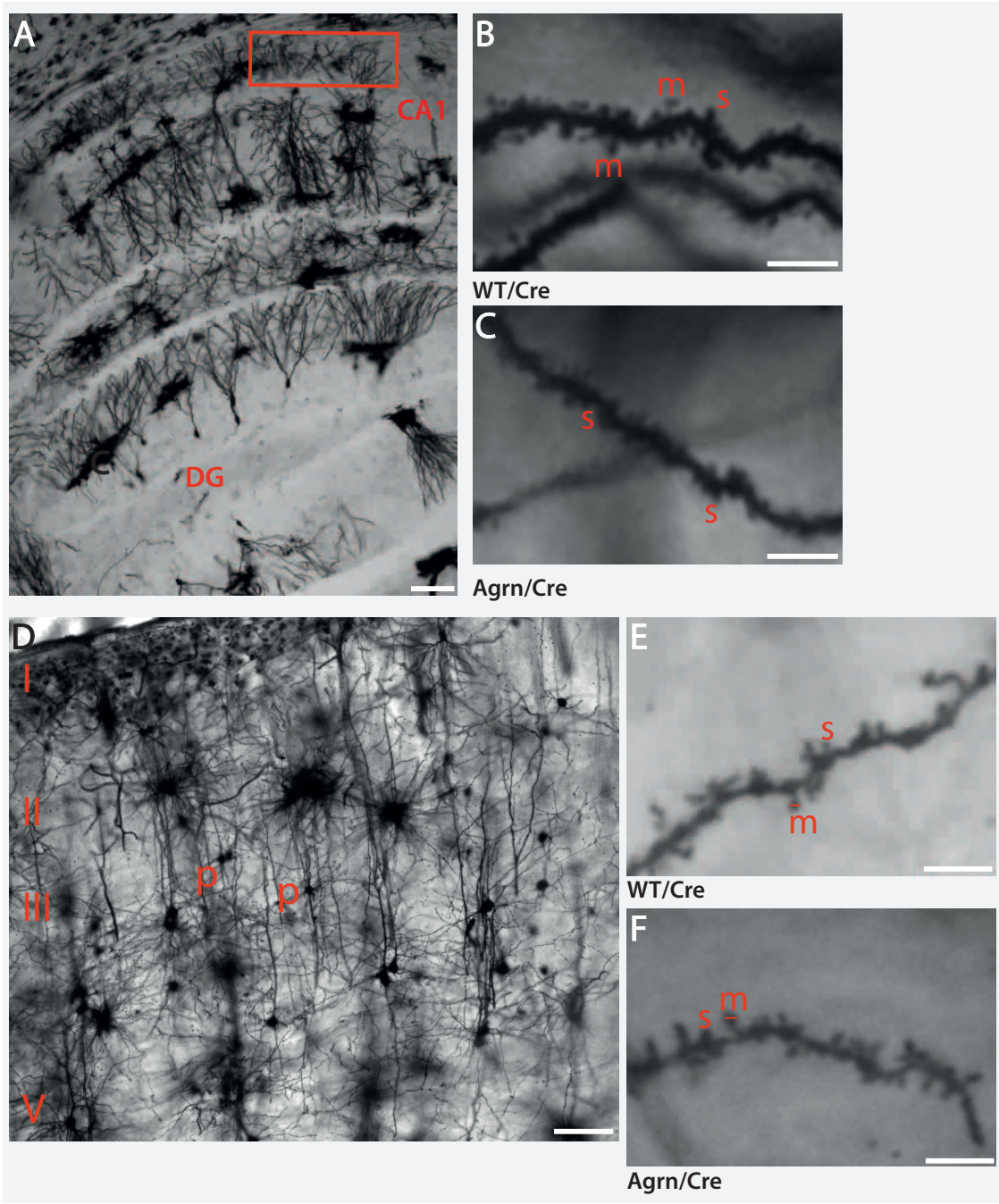
A
CA1
C
DG
B
m
s
m
WT/Cre
C
s
s
Agrn/Cre
D
I
II
III
V
p
p
E
s
m
WT/Cre
F
s
m
Agrn/Cre

	WT/Cre	Agrn/Cre	Significance	N	n
Cortex					
Spines per 100µm dendrite	77 ± 6.8	70 ± 13.9	n.s. (p = 0.69)	4	3
Stubby spines %	36 ± 6.9	47 ± 7.9	n.s. (p = 0.37)	4	3
Thin spines %	10 ± 4.3	14 ± 5.7	n.s. (p = 0.59)	4	3
Mushroom spines %	43 ± 8.9	49 ± 3.7	n.s. (p = 0.55)	3	3
Total spine head size in µm	0.67 ± 0.029	1.2 ± 1.18	* (p = 0.048)	4	52
Stubby spine head size in µm	0.61 ± 0.017	1.2 ± 0.22	n.s. (p = 0.063)	4	24
Thin spine head size in µm	0.50 ± 0.026	0.94 ± 0.14	* (p = 0.044)	4	5
Mushroom spine head size in µm	0.74 ± 0.026	1.2 ± 0.19	n.s. (p = 0.079)	4	25
Hippocampus CA1					
Spines per 100µm dendrite	110 ± 18	65 ± 2.7	n.s. (p = 0.094)	6	4
Stubby spines in %	42 ± 3.7	54 ± 2.9	* (p = 0.034)	6	4
Thin spines in %	8.8 ± 3.1	8.3 ± 2.8	n.s. (p = 0.92)	6	4
Mushroom spines in %	44 ± 1.5	33 ± 2.9	* (p = 0.044)	6	4
Total spine head size in µm	1.1 ± 0.22	1.4 ± 0.18	n.s. (p = 0.43)	4	102
Stubby spine head size in µm	1.1 ± 0.20	1.2 ± 0.20	n.s. (p = 0.27)	4	52
Thin spine head size in µm	0.76 ± 0.17	1.0 ± 0.11	n.s. (p = 0.20)	4	8
Mushroom spine head size in µm	1.3 ± 0.24	1.3 ± 0.20	n.s. (p = 0.96)	4	27

Figure 19: Morphology and density of dendritic spines in the hippocampus CA1 and cortex: Golgi stainings of hippocampus (A-C) and cortex (D-F) of Agrn/Cre and WT/Cre heterozygous mice. The mice were injected with tamoxifen in week 5 and sacrificed in week 10. 150µm cryosections were analysed by light microscopy and blinded images with identical settings were quantified in regard to dendritic spine density on basal dendrites of pyramidal cells, the portion of the dendrite after the third branching point from the soma. A) Overview of hippocampus area, box indicates the area of analysis (DG: dentate gyrus). B and C) Magnifications of basal dendrites (m: mushroom spine, s: stubby spine). B) Overview of cortical layers 2-5. E and F) Magnifications of layer 3 pyramidal neurons basal dendrites. Table: Summary of dendritic spine quantifications including SEM, Student's t-test p-values, mice per genotype (N) and average measurements per mouse (n). Scale bar A and D: 50µm; scale bar B, D, E and F: 5µm.

The total spine head size and the thin spine head size was increased in the cortex. The number of stubby spines was increased in Agrn/Cre mice versus WT/Cre mice, whereas the number of mushroom-like spines was decreased. In conclusion, the results of the detailed analysis of the synapse structure revealed changes in spine morphology, i.e. a shift from mushroom spines to stubby spines and an increase in the dendritic spine head size.

4. Discussion

The heparan sulfate proteoglycan agrin is essential for the formation, maintenance and regeneration of the synapse between a motoneuron terminal and its target muscle fiber (Samuel et al., 2012; Werle and VanSaun, 2003; Gautam et al., 1996; for review see Tintignac et al., 2015). However, agrin's role in the developing and adult CNS is much less clear. Previous studies from our laboratory have shown that TM-agrin overexpression in various cell culture systems including neurons, causes the cells to extend filopodia-like processes. It was hypothesized that these processes might be precursors for dendritic spine synapses (McCroskery et al., 2006; Ramseger et al., 2009; Porten et al., 2010; Fiala et al., 1998). In agreement with the hypothesis that TM-agrin is important for dendritic spine formation, mice depleted for agrin in the CNS show a reduction in the number of dendritic spines and a reduction in synaptic protein immunoreactivity (Ksiazek et al., 2007).

To investigate whether TM-agrin acts as a synapse-inducing factor or a synapse-strengthening factor in the CNS *in vivo* and to collect further evidence for a role of agrin during synaptogenesis and synapse maintenance, I generated and characterized a TM-agrin overexpressing mouse. Mice overexpressing a specific cDNA constitute a valuable addition to knock-out mice to understand fully the function of a protein of interest, especially in cases where the knock-out is lethal, restricting complete analysis of the knock-out phenotype.

Analysis of the mice showed that TM-agrin overexpression in adult glutamatergic neurons leads to larger postsynaptic densities of glutamatergic synapses and more intense immunofluorescense staining of the PSD95 scaffolding protein compared to those from littermate controls.

In addition, on basal dendrites of pyramidal neurons of cortex layer 2-3, the total spine head size and the thin spine head size showed an increase in TM-agrin overexpressing mice compared to control. Basal dendrites of hippocampus CA1 pyramidal neurons showed an increase in stubby spines accompanied with a decrease in mushroom spines on their basal dendrites. The gene expression profile also revealed that genes relating to glutamatergic synapse function were upregulated, while gene expression relating to GABAergic synapse function was downregulated. Thus, apparently TM-agrin affects excitatory and inhibitory synapses in a directly opposing manner.

4.1. The TM-agrin overexpressing mouse overall phenotype

What is the overall phenotype of the TM-agrin overexpressing mice?

The TM-agrin cDNA cloned from total mouse brain showed an increase in filopodia formation in HEK293T cells (see Figure 9). In addition, the targeting vector showed strict dependence on Cre expression and high agrin immunoreactivity (Figure 11). After the mice had been generated, I first confirmed that the double mutant mice (Agrn/Cre, WT/Cre as control) overexpressed the TM-agrin allele after tamoxifen administration. I observed up to 11-fold higher agrin protein levels compared to the WT/Cre control mice, depending on the method of tamoxifen administration. Approximately

70 % of the pyramidal neurons showed nuclear Cre immunoreactivity (Figure 13). The initial phenotyping of the mouse line confirmed that the mice were fertile and healthy, and the average survival rate was not apparently influenced by the TM-agrin overexpressing allele. Additionally, the mice did not show any difference in body weight, brain weight and forebrain volume (Figure 15, Figure 16). A large phenotypic screen performed in collaboration with the German Mouse Clinic did not result in any obvious phenotype connected to the vascular system, various organ systems, eye function, nociception and general behaviour (data not shown). Collectively, these data demonstrate that the mice represent a suitable model system to investigate the function of TM-agrin in the CNS by overexpression in a time- and spatially-controlled manner.

4.2. Changes in postsynaptic cluster morphology and dendritic spine morphology

Our initial hypothesis was that TM-agrin overexpression would promote filopodia formation and by this stimulate synapse formation and hence increase synapse and dendritic spine density. In contrast to this hypothesis, I did not observe a significant change in the number of PSD-positive clusters in the cortex or hippocampus of the TM-agrin CamKIICre mice compared to their control littermates (Figure 17). Likewise, the total number of dendritic spines did not apparently change in the cortex and hippocampus (Figure 19). Most importantly, I did not observe an increase in the number of filopodia extending from adult hippocampal or cortical neurons. A number of explanations for the lack of filopodia is possible:

a) The rapid turnover of the filopodia might preclude their detection.

b) The expression level of TM-agrin might not be sufficiently high *in vivo* to induce filopodia formation.

c) The filopodia only form on embryonic neurons but not on neurons of adult brains in response to TM-agrin overexpression.

However, when I analysed the anti-PSD95 positive synaptic puncta and the dendritic spine morphology in more detail I observed that individual postsynaptic puncta were more intensely stained and larger (Figure 18). In order to put this observation into a quantifiable format, I compared the fraction area of the image that is covered by above-threshold staining intensity (compare image analysis method: Pribiag et al., 2014). This combines the size and the staining intensity of the puncta simultaneously while at the same time applying a threshold over the whole experiment. This way it is possible to estimate the density and size of the individual puncta in many specimens of cortical and hippocampal sections. TM-agrin overexpressing mice showed a 3-fold increase in fraction area in the cortex and hippocampus compared to their control littermates. Presynaptic puncta visualized by anti-bassoon immunoreactivity showed a trend towards a similar increase, but due to high variability within the cohort of the same genotype, this trend was not significant (Figure 18). Another factor influencing significance is that bassoon is present at active zones of both inhibitory and excitatory synapses, whereas PSD95 antibodies only stain excitatory postsynaptic densities. As mentioned earlier, we assume agrin to have a more pronounced effect on excitatory synapses than on inhibitory synapses. Therefore, it can be expected that PSD95 immunoreactivity is more

significantly changed compared to bassoon and this might explain, why the values for bassoon immunoreactivity did not reach statistical significance.

To study dendritic spine morphology, I analysed hippocampal and cortical dendrites in more detail using the Golgi Silver impregnation technique (Golgi, 1873). The Golgi staining method has the advantage that only a small subset of neurons is stained, which allows tracing individual neurons and documenting their precise morphology. However, the technique requires brightfield microscopy and the sections cannot be analysed using confocal imaging. Therefore, the resolution is limited and it is not possible to simultaneously visualize Cre-positive neurons. In order to record a good estimate of dendritic spine morphology, I counted and measured a large number of individual dendritic spines. Dendrites of pyramidal neurons show less variable morphology in spines in distal compared to parts proximal to the soma. Therefore, for better reproducibility, I restricted the quantification of spine morphology on dendritic branches of basal dendrites after the third branching point. Most parameters (e.g. percentage of thin spines, stubby spine head size) on basal dendrites of pyramidal neurons of cortex layer 2-3 did not show significant differences in TM-agrin overexpressing compared to control animals (quantification table in Figure 19). However, the total spine head size and the thin spine head size showed an increase in diameter in TM-agrin overexpressing mice compared to littermate controls. Hippocampus CA1 pyramidal neurons showed an increase in the number of stubby spines compared to a decrease in the number of mushroom spines on their basal dendrites. As mentioned earlier, the development of spines proceeds from filopodia to stubby spines to mushroom spines. Since I analysed TM-agrin

overexpressing mice 5 weeks after Cre induction, the relative increase in the number of stubby spines results could indicate that TM-agrin overexpression halts the maturation of dendritic spines from stubby spines to mushroom spines. However, the distinction between stubby spines and mushroom spines is largely defined by estimating the thickness of the spine neck. Stubby spines have a thicker neck compared to the diameter of their head (Fiala et al., 1998). This visual analysis is difficult and might lead to errors. Therefore, another interpretation of these results could be that TM-agrin overexpression increases the thickness of the neck making thin spines look more like stubby spines. In any case, overexpression of TM-agrin influences the morphology of spines and, thus, influences excitatory synapse structure and should – as a consequence – influence its function.

4.3. Expression profile correlated to inhibitory and excitatory synapse function

The gene expression profile of cortical lysates of Agrn/Cre and WT/Cre was analysed in order to assess whether TM-agrin overexpression affects glutamatergic and GABAergic synaptic protein related gene expression in a similar manner. Together with the master's student Gerry Handara, I determined if TM-agrin overexpression had an influence on the expression of synapse-associated genes. We included genes that are associated with glutamatergic as well as GABAergic transmission, such as genes coding for scaffolding proteins and receptors. We used qRT-PCR to be able to distinguish even fine differences between the expression profiles. Our initial results confirmed the Western blot analysis and showed that TM-agrin mRNA

is significantly upregulated (on average 17-fold). In order to understand in detail how the expression profiles of the synapse-associated genes are linked to TM-agrin overexpression, and to investigate if the variation of the amount of TM-agrin overexpression is paralleled by a similar variation in the mRNA expression of synapse-associated proteins, we performed linear regression analysis determining the coefficient of determination (R^2, ranging from 0 to 1). For instance, a high coefficient of determination (R^2 = 0,98) between synaptotagmin expression and agrin overexpression shows that the variability of expression of the two genes is linearly linked. In this case, there is a statistical correlation between a high agrin level and the level of synaptotagmin upregulation in the individual mouse. The expression levels change significantly in parallel. As one increases, the other one increases too. This allowed us to observe the linear connection between the two expression profiles, even though the level of upregulation of synaptotagmin by itself compared to control (1.98-fold) is not statistically significant.

Our results showed that the expression of several genes associated with glutamatergic synaptic transmission were upregulated, while other genes associated with GABAergic transmission were downregulated. Specifically, the NR1 subunit of NMDA receptors was 2-fold upregulated and PSD95 showed a trend towards upregulation, which strongly correlated with the agrin level in the individual mouse (R^2=0.91). In contrast, the expression level of Gria1, encoding the AMPA receptor subunit 1, did not differ between TM-agrin overexpressing and littermate control mice. Gabra1, coding for the α1 subunit of the $GABA_A$ receptor, showed a 5-fold decrease in expression. Likewise, the GABA receptor-associated scaffolding protein gephyrin (Yu et

al., 2007) showed a 25-fold decrease in expression, and neuroligin-2, an adhesion protein specific for inhibitory synapses (Reissner et al., 2008), was 2.5-fold downregulated.

Another protein showing regulation on the expression level was dystroglycan, which was 6-fold increased in TM-agrin overexpressing mice compared to control. The increased expression of dystroglycan in the cortex of TM-agrin overexpressing mice constitutes the only exception to the general downregulation of GABAergic synapse-associated proteins in this mouse. Dystroglycan has been shown to bind agrin (Bowe et al., 1994; Campanelli et al., 1994) and agrin-immunoreactivity has been reported to colocalize with GABAergic postsynapses (Pribiag et al., 2014). Dystroglycan is a glycoprotein that is expressed as a precursor, which is cleaved into an extracellular protein (α-dystroglycan) and a transmembrane protein (β-dystroglycan) (Ibraghimov-Beskrovnaya et al., 1992). Within the dystrophin-associated glycoprotein complex dystroglycan links the cytoskeleton to the extracellular matrix. Dystroglycan is important for the stabilization of AChRs in the postsynaptic density of muscle fibers (Cote et al., 1999). It has been shown to bind to NtA-agrin at the NMJ via agrin's C-terminal LG1 and LG2 domains (Campanelli et al., 1994; Bowe et al., 1994) and it is also expressed in the retina and the brain, where is has been reported to colocalize with $GABA_A$-receptors (Blank et al., 1997; Levi et al., 2002; Pribiag et al., 2014). Additionally, the LG-domain-containing synaptic adhesion proteins α- and β-neurexins were identified as presynaptic binding partners of α-dystroglycan by affinity chromatography of brain homogenates (Sugita et al., 2001). Prolonged elevation of excitatory neuronal activity increases dystroglycan

expression, which restores homeostasis (Pribiag et al., 2014). It will be interesting to see whether neuronal activity is indeed increased in the TM-agrin overexpressing mouse brains.

4.4. Effect of TM-agrin overexpression in the adult on existing synapses

Returning to the initial questions I posed earlier, the results obtained answer them as follows:

1. Does the overexpression of TM-agrin induce filopodia-like processes *in vivo*?

No, TM-agrin overexpression does not induce filopodia-like processes *in vivo* as it does *in vitro*.

2. Does overexpression of TM-agrin in glutamatergic neurons affect their existing synapses in the adult?

Yes, rather than resulting in the formation of more synapses, TM-agrin overexpression in adult glutamatergic synapses *in vivo* results in a change in the existing synapses, specifically in more intensely stained PSD95 clusters, increased head size of dendritic spines and upregulation of glutamatergic synapse associated gene expression. Additionally, the overall dendritic spine head size was increased and I observed an increase in stubby spines and a decrease in mushroom spines. Also, expression of genes associated with glutamatergic synapses was observed to be upregulated, while the expression of genes related to GABAergic synapses was shown to be downregulated.

How does TM-agrin mediate these changes in adult synapses? Specifically:

1. Could the changes in dendritic spine head size and morphology, the increase in glutamatergic postsynapse staining intensity and regulation of expression profiles of synapse associated genes be the result of synapse strengthening? What would be the mechanism underlying the synapse strengthening?

2. Does TM-agrin overexpression only affect the neuron that is expressing the allele (*cis*-effect or purely postsynaptic effects) or the neighbouring wildtype cells as well (*trans*-effect or presynaptic effects)?

These questions will be addressed in the following paragraphs.

Ksiazek et al. demonstrated a decrease in excitatory synapse formation and a reduced mEPSP number in the murine cortex resulting from CNS-specific agrin depletion (Ksiazek et al., 2007). Since the developmental progression of the agrin-depletion was not analysed, the results can either be explained by endogenous agrin having a synapse-inducing or a synapse-strengthening effect. If TM-agrin has a synapse-inducing effect, we would predict an increase in the number of synapses after TM-agrin overexpression in a system that allows plasticity. If TM-agrin, however, has a synapse-strengthening effect, meaning allowing more neurotransmitter to be released or more receptors available in the same number of synapses, we expect no change in synapse number, but an increase in the spontaneous and the glutamate-evoked postsynaptic currents.

I did not observe a significant increase in the number of synapses visualized by anti-PSD95 and anti-bassoon immunoreactivity as a consequence of TM-agrin overexpression (Figure 17). However, the individual anti-PSD95 positive puncta were bigger and more intensely

stained (Figure 18). Likewise, in the Golgi-stained sections, the dendritic spine heads of cortical layer 2-3 pyramidal neurons were bigger on average (Figure 19). In previous studies, it was shown that the size of the dendritic spine directly correlates with the number of NMDA receptors incorporated into the PSD (Takumi et al., 1999). In agreement with this, our expression analysis showed that the mRNA levels of the NMDA receptor subunit NR1 were 2-fold higher in TM-agrin overexpressing mouse cortices compared to control mice. In addition, preliminary data comparing the intensity and size of NMDAR1 immunoreactivity-positive clusters showed a trend towards a similar increase in fraction area as the PSD95-immunoreactivity (data not shown). In summary, my results in adult CNS neurons would favour the idea of a synapse-strengthening effect of TM-agrin rather than a synapse-inducing effect, since the number of synapses seems to be unchanged.

Long-term memory formation involves both *de novo* synaptogenesis, structural plasticity (Leuner et al., 2003) and synapse strengthening, functional plasticity (reviewed in Bernardinelli et al., 2014). Structural plasticity results in increased spine number while functional plasticity results in an increase in spine size and synaptic activity, meaning higher frequency of individual EPSPs. The possibility that agrin might be involved in regulating synapse strength is not unprecedented: PSD95 upregulation has been implicated in synapse-strengthening after training (Radwanska et al., 2011). Nikonenko et al. observed a 8-fold increase in total PSD area and a 5-fold increase in the number of perforated PSDs in response to increased levels of PSD95 protein (Nikonenko et al., 2008). Interestingly, these processes were accompanied by an overall reduction in spine number. A larger postsynaptic

glutamatergic density with more clustered PSD95 and more PSD95-scaffold-associated NMDA-receptors would be expected to exhibit more excitatory activity, meaning higher frequency of individual EPSPs, as has been observed after induction of LTP. This will be interesting to test in the future, performing extensive electrophysiological profiling.

The results of the overexpression of TM-agrin in the CNS should be compared to a line of experiments involving neuroligin-1 overexpression in the mouse CNS. Overexpression of Neuroligin-1, a postsynaptic adhesion protein of glutamatergic synapses, leads to an increase in average spine head size, stabilisation of existing synapses in the adult in addition to formation of new synapses (Dahlhaus et al., 2010). This is in part consistent with our data in the cortex, where I observed an increase of overall dendritic spine head size (Figure 19). Later, it was shown that the cytoplasmic tail of neuroligin-1 can modulate this synaptogenic effect by activating intracellular signalling cascades in addition to an adhesive effect (Hoy et al., 2013). While full-length neuroligin-1 increases maturation of existing glutamatergic synapses, truncated neuroligin-1, missing the cytoplasmic tail, increased the number of postsynapses and flexibility in memory tasks. These studies show that changes in synaptic protein levels can lead to increased maturation of existing synapses as well as an increased number of new synapses. We can conclude that TM-agrin might act in a similar manner, possibly increasing maturation of existing synapses. What could be the mechanism of synapse strengthening by TM-agrin, meaning maturation of existing synapses?

Extensive *in vitro* studies of truncated forms of TM-agrin have been performed to map the domains responsible for the filopodia-inducing activity

(McCroskery et al., 2006; Porten et al., 2010; Lin et al., 2010). The filopodia-inducing phenotype of TM-agrin overexpressing cells was independent of the cytoplasmic part of the protein. Additionally, the intracellular part of TM-agrin shows little sequence conservation between mouse TM-agrin and chick TM-agrin (Neumann et al., 2001), but both induce the same *in vitro* phenotype in response to overexpression (Figure 9). Therefore, the cytoplasmic tail of agrin is likely not to be involved in the filopodia-inducing phenotype. Instead, agrin might be binding extracellularly to other proteins or dimerizing with itself.

One possible mechanism underlying the potential synapse-strengthening effect could be that TM-agrin is acting via trans-synaptic adhesion, by increasing binding between the synaptic membranes, thereby stabilizing synapses and by this favour particularly the stubby spine structure. Adhesion between the pre- and postsynaptic membrane plays an important role in synaptogenesis as well as in the strengthening of existing synapses. Rather than a signaling ligand binding to a receptor, adhesion molecules span the synaptic cleft and give the synapse stability and in some cases, specificity (for review on synaptic adhesion molecules see Yang et al., 2014). One example of adhesion molecules involved in synaptic organization is the interaction between neurexins on the presynaptic side and neuroligins on the postsynaptic side, which is important for synapse maturation and function but not essential for de novo synapse formation between an axonal growth cone and its target neuron (Varoqueaux et al., 2006, for review see Sudhof, 2008). Specificity for the synapse type is given by different isoforms

of neuroligin being localized only to either inhibitory or excitatory postsynapses (Varoqueaux et al., 2006).

Since agrin is expressed only as a transmembrane protein in the CNS, and concentrated at synapses, it can be assumed that a subpopulation of agrin spans the synaptic cleft acting as a trans-synaptic adhesion molecule, comparable to the HSPG syndecan (Ethell & Yamaguchi, 1999; Lin et al., 2007). Supporting this idea is the fact that agrin's precise localization within the synaptic cleft is not known. Ksiazek et al. found anti-agrin immunogold particles close to the pre- and the postsynaptic side in electron micrographs (Koulen et al., 1999; Ksiazek et al., 2007).

However, the agrin protein is approximately 95nm long (Denzer et al., 1997) and can hence span the synaptic cleft several times, which is usually only 20-30nm wide (Gray, 1959a). This makes the precise determination of localization difficult, and the possibility remains that it is distributed to both synaptic partners.

In addition, McCroskery et al. found that depletion of agrin by siRNA in hippocampal neuronal cultures results in a decrease in the number of synapses also in cells where only the presynaptic neuron is infected with agrin siRNA lentivirus. However, the decrease is not as pronounced as in cells that show suppression of agrin on the dendritic postsynaptic side (McCroskery et al., 2006).

Taken together, this suggests that TM-agrin is needed on both sides of the synapse for proper synapse formation and might act as an adhesion molecule across the synaptic cleft. If TM-agrin indeed acts as an adhesion molecule, it would be interesting to determine if it binds to itself across the

synaptic cleft or if other extracellular matrix proteins are involved in the trans-synaptic interaction.

4.5. *Cis*- versus *trans*-effects of TM-agrin overexpression

TM-agrin overexpression does not apparently have a synapse-inducing effect in the adult CNS, since we do not observe an increase in the number of synapses in the brain areas following TM-agrin overexpression. Instead, it is more likely that TM-agrin overexpression in adult neurons leads to synapse-strengthening specific to glutamatergic synapses, since the glutamatergic postsynaptic density clusters appeared significantly larger and more intense and NMDAR1 receptor mRNA shows upregulation in the TM-agrin overexpressing mice.

Most genes tested tested that are associated specifically with inhibitory synapses were significantly downregulated in the TM-agrin overexpressing mice. However, TM-agrin controlled by CamKIICre only shows overexpression in glutamatergic neurons. This leads to the next question, whether the observed phenotype is a result of *cis*-or *trans*-effects.

Our gene expression analysis results suggest a selective influence of TM-agrin overexpression on excitatory and inhibitory central nervous system synapses. If only excitatory synapses are strengthened by potential TM-agrin mediated adhesion, why do we observe a downregulation in inhibitory synapse associated gene expression? Is the TM-agrin-mediated effect on synapses due to a *ci-s* or a *trans*- activity?

Out of all cortical cells, only the glutamatergic pyramidal neurons express the CamKII gene and, thus, only pyramidal neurons should

overexpress CamKII promoter-driven TM-agrin (Erdmann et al., 2007, Burgin et al., 1990). In agreement with this, quantification of Cre positive neurons showed Cre immunoreactivity only in the pyramidal cell layer of the hippocampus CA1 region (Figure 13). However, the overexpression apparently affected GABAergic synapses as well, judging by the expression analysis showing downregulation of several genes associated with GABergic synapses. Four different synapse-types can be distinguished, if we assume that TM-agrin principally has the ability to locate to both the pre- and the postsynaptic membrane:

1. A glutamatergic synapse between two mutant pyramidal neurons, presumably exhibiting high levels of TM-agrin on both sides of the synaptic cleft (Figure 20, synapse 1).

2. A GABAergic synapse between a wildtype inhibitory interneuron and a mutant pyramidal neuron, exhibiting high levels of TM-agrin only on the postsynaptic side (Figure 20, synapse 2).

3. A glutamatergic synapse between a mutant pyramidal neuron and a wildtype inhibitory interneuron, exhibiting high levels of TM-agrin only on the presynaptic side (Figure 20, synapse 3).

4. A GABAergic synapse between two wildtype inhibitory interneurons, which only exhibits endogenous levels of TM-agrin on both sides of the synaptic cleft (Figure 20, synapse 4).

It is unclear at this stage, which of the four potential TM-agrin localizations causes the effects of TM-agrin overexpression. The most straightforward interpretation of the effect of TM-agrin overexpression on synapse structure is that TM-agrin affects only the postsynapses on TM-agrin

overexpressing pyramidal neurons. This would mean that the downregulation of genes associated with inhibitory synapse function at GABAergic synapses is caused by TM-agrin overexpression in the same cell (*cis*-effect, Figure 20, synapses 1 and 2), and that the changes in mRNA expression levels result exclusively from the pyramidal neuron population.

This would predict that TM-agrin is directly present at GABAergic postsynapses and has a downscaling effect on the expression levels of genes associated with GABAergic synapse function. Alternatively, the glutamatergic postsynapses negatively influence neighbouring GABAergic postsynapses via a secondary mechanism.

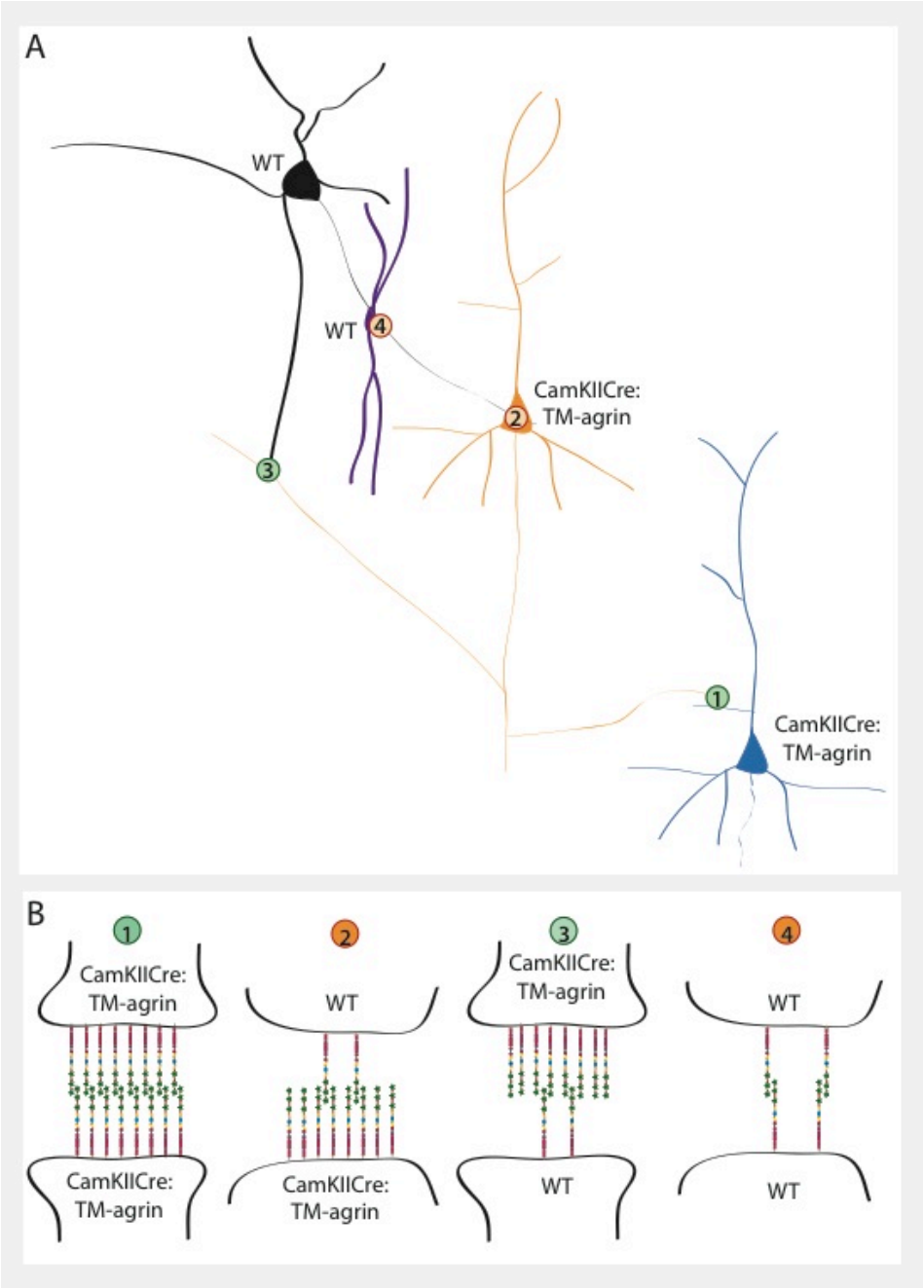

Figure 20: Four different synapse types that TM-overexpression can affect. A) Interaction modes between excitatory pyramidal neurons and inhibitory interneurons in the cerebral cortex. Excitatory synapses are highlighted by green dots, inhibitory synapses by red dots. TM-agrin is assumed to be able to distribute in the pre- and/or the postsynaptic partner of a synapse. This creates four different scenarios how TM-agrin overexpression can affect synapses (B). 1) A glutamatergic synapse between two pyramidal neurons, overexpressing TM-agrin on both synaptic membranes. 2) A GABAergic synapse on a pyramidal neuron, overexpressing TM-agrin only on the postsynaptic membrane. 3) A glutamatergic synapse on an inhibitory interneuron, overexpressing TM-agrin only on the presynaptic membrane. 4) A GABAergic synapse between two inhibitory interneurons, of which neither partner overexpresses TM-agrin. This type of synapse could only be affected by secondary circuit-ramifications.

4.6. Working model

We observed that the PSDs of glutamatergic synapses and dendritic spine heads are larger and incorporate more PSD95 scaffolding protein in response to TM-agrin overexpression in the adult mice. Additionally, gene expression levels of proteins at glutamatergic synapses were upregulated, while gene expression relating to GABAergic synapses was downregulated. It appears that TM-agrin affects excitatory and inhibitory synapses in a directly opposite way. Three different scenarios might explain these results by making use of the model of the four synapse types described in Figure 20.

Scenario one: the synapses are strengthened by TM-agrin overexpression, resulting in more intensely stained PSD95 clusters and upregulation of NMDA receptor expression, if TM-agrin is present in high levels at both sides of the synaptic cleft (Figure 20, synapse type 1). Any other combination (Figure 20, synapse types 2, 3 and 4) results in a synapse-weakening effect accompanied by downregulation of receptor genes. GABAergic inhibitory synapses in this model never have high levels of TM-agrin on both sides, while there are glutamatergic synapses with and without high levels of TM-agrin on both sides (Figure 20, synapse 1 and 3 respectively). If we assume that agrin only strengthens the synapse if it is present at a stoichiometric ratio on both sides, this would explain why only glutamatergic synapses are strengthened. On the molecular level, one could interpret the downregulation of GABAergic synapse associated genes by the adhesion molecule disturbing the pre- or postsynaptic membrane organization when left without sufficient amounts of a binding partner. I

favour this scenario because it explains why only glutamatergic synapses are strengthened by TM-agrin overexpression.

Scenario two: the TM-agrin I cloned (y4/z0) affects GABAergic synapses only on the postsynaptic side, and only in a manner which results in downregulation of postsynapse-associated genes (such as genes coding for the $GABA_A$ α1 subunit, Neuroligin-2 and gephyrin). Considering the intricate organization of the cerebral cortex, it is plausible that a lack of inhibition in the circuit would result in a shift in the excitation to inhibition balance (as shown in neuronal cultures for example in: Marchenkova et al., 2016). On the molecular level, one interpretation could be that TM-agrin overexpression on one side of the synaptic cleft blocks other synaptogenic proteins from strengthening the GABAergic synapse. One candidate protein would be pleiotrophin. Pleiotrophin strengthens GABAergic synapses as shown by the appearance of higher frequency of spontaneous postsynaptic inhibitory currents in pleiotrophin overexpressing mice (Pavlov et al., 2006). Since agrin binds pleiotrophin at the NMJ (Daggett et al., 1996), it is conceivable that TM-agrin counteracts this inhibitory synapse strengthening effect. Alternatively, TM-agrin could be scavenging soluble synapse-strengthening factors.

A third, entirely different scenario to explain why TM-agrin overexpression does not lead to an increase in synapse numbers but instead to larger, denser PSDs in response to adult onset of overexpression, would be the reduced plasticity in adult networks. Agrin overexpression was induced in postnatal week five, which is two weeks after the developmental phase of synaptogenesis is finished (Li et al., 1997; O'Connor et al., 1994). If the

neurons cannot accommodate more synapses, the overexpression of a synaptogenic protein might be expected to act as a synapse-strengthener. Precedence for synapse inducers having different effects on synapses depending on the maturity of the neurons is the overexpression of neuroligin-1 in immature hippocampus dentate gyrus granule neurons (Schnell et al., 2012). In contrast to the overexpression in adult neurons, which mainly leads to an increase in average spine head size and stabilization of existing synapses, new-born neurons infected with neuroligin-1 overexpressing retrovirus form a larger amount of filopodia and exhibit a higher density of dendritic spines on growing dendrites than their wildtype neighbours (Dahlhaus et al., 2010). Since new-born granule neurons need to integrate and form new connections in the existing hippocampal network, this study suggests that the effect of Neuroligin-1 is dependent on the plasticity of the network. TM-agrin could act in a similar manner, inducing new filopodia in an immature network but stabilizing existing mature synapses in the adult network. However, this scenario does not explain why glutamatergic and GABAergic synapses are affected in an opposing manner by TM-agrin overexpression.

4.7. Future experiments

How do we distinguish the three different scenarios mentioned above from each other? Additional experiments are needed to accurately dissect whether TM-agrin acts as a synapse-strengthener when present on both synaptic partners, whether it only negatively regulates GABAergic synapses, or whether its endogenous function during development is in fact synaptogenic.

First and most obvious, the functional analyses of GABAergic versus glutamatergic synapses needs to be completed by Western blotting to test whether the candidate proteins show regulation on the protein level, as well as by analysing the distribution of $GABA_A$ receptor and gephyrin in cortical sections and determining if their distribution changes in response to higher levels of TM-agrin.

To test whether the effects of increased size of dendritic spine heads, larger and more intensely stained postsynaptic densities in the cortex and hippocampus, and the regulation of excitatory and inhibitory synapse associated genes truly translate into functional plasticity, we need to electrophysiologically characterize neurons which overexpress TM agrin and their pre- and postsynaptic partners. By comparing the frequency of spontaneous postsynaptic activity, or the threshold to induce epileptic seizures, one could test whether the basal activity is indeed higher in pyramidal neurons overexpressing TM-agrin. One way to conclusively determine whether GABAergic interneurons are affected in *trans* by neighbouring TM-agrin overexpressing pyramidal cells would be by selectively patch-clamping inhibitory interneurons in the cortex in order to test whether they show decreased inhibition in the TM-agrin overexpressing mice.

Additionally, testing for behavioural effects, such as shorter translation of newly acquired abilities into long-term-memories, using for example a water maze test (D'Hooge and De Deyn, 2001) is a prerequisite to analyse the relationship between functional plasticity and facilitation of long-term-memory formation after TM-agrin overexpression.

The Golgi impregnation method has one obvious disadvantage: One cannot co-stain for cell-specific markers. Since the Cre-induction rate can be estimated to be around 70%, it would be interesting to confirm the results of dendritic spine morphology and extend the analysis to neuronal morphology by analysing Thy1-YFP-H mice (Feng et al., 2000). These mice express YFP in only a small subset of neurons. This would make it possible to analyse the dendritic spines in detail using confocal microscopy and restrict the analysis to confirmed Cre-positive, TM-agrin overexpressing cells.

In addition, a more detailed analysis of single cells would be possible in cultures of embryonic neurons. Primary neuronal cultures are very useful tools to study neuronal circuits because individual synapses can be traced back via the dendrites to their neuron. In contrast, the 3-dimensional *in vivo* system makes tracing of individual synapses difficult. By visualizing the different neuronal populations with specific markers and staining their dendrites *in vitro*, one could analyse the individual effects on synapses of glutamatergic and GABAergic cells. This would be another approach to determine whether the GABAergic synapse-associated gene expression profile should be interpreted as a *cis*-effect or a *trans*-effect.

There is a possibility that the different TM-agrin isoforms expressed during the synaptogenic period (Li et al., 1997) in the mouse exert different functions. Therefore, another interesting set of *in vitro* experiments would be to clone and express the different isoforms in culture and test if the effects on PSD95 and gephyrin clustering differ between them.

The third scenario implies that agrin is in fact acting synaptogenic, but the system we are using is not plastic enough to accommodate more

synapses. One way to test this alternative model would be to overexpress TM-agrin in a more plastic system, i.e. to perform early postnatal induction of expression. Neurogenesis in the mouse starts around embryonic day 10 to 12 (Molyneaux et al., 2007), but the CamKIIα promoter only drives gene expression from around postnatal day 3 (Casanova et al., 2001). However, it would be interesting to determine whether the overexpression effect differs from the adult and if we could observe an increase in synapse numbers.

Taken together, in addition to raising new questions opening the door to further experiments, the new evidence provided here of TM-agrin overexpression resulting in an increased size of dendritic spine heads, larger and more intensely stained postsynaptic densities in the cortex and hippocampus, together with the regulation of excitatory and inhibitory synapse associated genes in response to TM-agrin overexpression, added significantly to the understanding of TM-agrin function in the CNS.

5. Bibliography

Alfonso, J., Fernandez, M. E., Cooper, B., Flugge, G., & Frasch, A. C. (2005). The stress-regulated protein M6a is a key modulator for neurite outgrowth and filopodium/spine formation. *Proc Natl Acad Sci U S A, 102*(47), 17196-17201.

Allen, N. J., Bennett, M. L., Foo, L. C., Wang, G. X., Chakraborty, C., Smith, S. J., & Barres, B. A. (2012). Astrocyte glypicans 4 and 6 promote formation of excitatory synapses via GluA1 AMPA receptors. *Nature, 486*(7403), 410-414.

Altman, J. (1969). Autoradiographic and histological studies of postnatal neurogenesis. IV. Cell proliferation and migration in the anterior forebrain, with special reference to persisting neurogenesis in the olfactory bulb. *J Comp Neurol, 137*(4), 433-457.

Annies, M., Bittcher, G., Ramseger, R., Loschinger, J., Woll, S., Porten, E., Abraham, C., Ruegg, M. A., & Kröger, S. (2006). Clustering transmembrane-agrin induces filopodia-like processes on axons and dendrites. *Mol Cell Neurosci, 31*(3), 515-524.

Benson, D. L., & Tanaka, H. (1998). N-cadherin redistribution during synaptogenesis in hippocampal neurons. *J Neurosci, 18*(17), 6892-6904.

Bernardinelli, Y., Nikonenko, I., & Muller, D. (2014). Structural plasticity: mechanisms and contribution to developmental psychiatric disorders. *Front Neuroanat, 8*, 123.

Blank, M., Koulen, P., & Kröger, S. (1997). Subcellular concentration of beta-dystroglycan in photoreceptors and glial cells of the chick retina. *J Comp Neurol, 389*(4), 668-678.

Bliss, T. V., & Lomo, T. (1973). Long-lasting potentiation of synaptic transmission in the dentate area of the anaesthetized rabbit following stimulation of the perforant path. *J Physiol, 232*(2), 331-356.

Blundon, J. A., & Zakharenko, S. S. (2008). Dissecting the components of long-term potentiation. *Neuroscientist, 14*(6), 598-608.

Bourne, J. N., & Harris, K. M. (2008). Balancing structure and function at hippocampal dendritic spines. *Annu Rev Neurosci, 31*, 47-67.

Bowe, M. A., Deyst, K. A., Leszyk, J. D., & Fallon, J. R. (1994). Identification and purification of an agrin receptor from Torpedo postsynaptic membranes: a heteromeric complex related to the dystroglycans. *Neuron, 12*(5), 1173-1180.

Burgess, R. W., Skarnes, W. C., & Sanes, J. R. (2000). Agrin isoforms with distinct amino termini: differential expression, localization, and function. *J Cell Biol, 151*(1), 41-52.

Burgin, K. E., Waxham, M. N., Rickling, S., Westgate, S. A., Mobley, W. C., & Kelly, P. T. (1990). In situ hybridization histochemistry of Ca2+/calmodulin-dependent protein kinase in developing rat brain. *J Neurosci, 10*(6), 1788-1798.

Burk, K., Desoeuvre, A., Boutin, C., Smith, M. A., Kröger, S., Bosio, A., Tiveron, M. C., & Cremer, H. (2012). Agrin-signalling is necessary for the integration of newly generated neurons in the adult olfactory bulb. *J Neurosci, 32*(11), 3759-3764.

Campagna, J. A., Ruegg, M. A., & Bixby, J. L. (1995). Agrin is a differentiation-inducing "stop signal" for motoneurons in vitro. *Neuron, 15*(6), 1365-1374.

Campanelli, J. T., Roberds, S. L., Campbell, K. P., & Scheller, R. H. (1994). A role for dystrophin-associated glycoproteins and utrophin in agrin-induced AChR clustering. *Cell, 77*(5), 663-674.

Casanova, E., Fehsenfeld, S., Mantamadiotis, T., Lemberger, T., Greiner, E., Stewart, A. F., & Schutz, G. (2001). A CamKIIalpha iCre BAC allows brain-specific gene inactivation. *Genesis, 31*(1), 37-42.

Chase, T. N., Roberts, E., & Tower, D. B. (1976). *GABA in nervous system function*. Paper presented at the Workshop on GABA in nervous system function, J & R Double Arch Ranch, Santa Ynez Valley, CA.

Christopherson, K. S., Ullian, E. M., Stokes, C. C., Mullowney, C. E., Hell, J. W., Agah, A., Lawler, J., Mosher, D. F., Bornstein, P., & Barres, B. A. (2005). Thrombospondins are astrocyte-secreted proteins that promote CNS synaptogenesis. *Cell, 120*(3), 421-433.

Clements, J. R., Magnusson, K. R., & Beitz, A. J. (1990). Ultrastructural description of glutamate-, aspartate-, taurine-, and glycine-like immunoreactive terminals from five rat brain regions. *J Electron Microsc Tech, 15*(1), 49-66.

Collins, M. O., Husi, H., Yu, L., Brandon, J. M., Anderson, C. N., Blackstock, W. P., Choudhary, J. S., & Grant, S. G. (2006). Molecular characterization and comparison of the components and multiprotein complexes in the postsynaptic proteome. *J Neurochem, 97 Suppl 1*, 16-23.

Cote, P. D., Moukhles, H., Lindenbaum, M., & Carbonetto, S. (1999). Chimaeric mice deficient in dystroglycans develop muscular dystrophy and have disrupted myoneural synapses. *Nat Genet, 23*(3), 338-342.

D'Hooge, R., & De Deyn, P. P. (2001). Applications of the Morris water maze in the study of learning and memory. *Brain Res Brain Res Rev, 36*(1), 60-90.

Daggett, D. F., Cohen, M. W., Stone, D., Nikolics, K., Rauvala, H., & Peng, H. B. (1996). The role of an agrin-growth factor interaction in ACh receptor clustering. *Mol Cell Neurosci, 8*(4), 272-285.

Dahlhaus, R., Hines, R. M., Eadie, B. D., Kannangara, T. S., Hines, D. J., Brown, C. E., Christie, B. R., & El-Husseini, A. (2010). Overexpression of the cell adhesion protein neuroligin-1 induces learning deficits and impairs synaptic plasticity by altering the ratio of excitation to inhibition in the hippocampus. *Hippocampus, 20*(2), 305-322.

Dailey, M. E., & Smith, S. J. (1996). The dynamics of dendritic structure in developing hippocampal slices. *J Neurosci, 16*(9), 2983-2994.

Dalva, M. B., Takasu, M. A., Lin, M. Z., Shamah, S. M., Hu, L., Gale, N. W., & Greenberg, M. E. (2000). EphB receptors interact with NMDA receptors and regulate excitatory synapse formation. *Cell, 103*(6), 945-956.

Daniels, M. P. (2012). The role of agrin in synaptic development, plasticity and signaling in the central nervous system. *Neurochem Int, 61*(6), 848-853.

de Wit, J., & Ghosh, A. (2016). Specification of synaptic connectivity by cell surface interactions. *Nat Rev Neurosci, 17*(1), 22-35.

de Wit, J., O'Sullivan, M. L., Savas, J. N., Condomitti, G., Caccese, M. C., Vennekens, K. M., Yates, J. R., 3rd, & Ghosh, A. (2013). Unbiased discovery of glypican as a receptor for LRRTM4 in regulating excitatory synapse development. *Neuron, 79*(4), 696-711.

de Wit, J., Sylwestrak, E., O'Sullivan, M. L., Otto, S., Tiglio, K., Savas, J. N., Yates, J. R., 3rd, Comoletti, D., Taylor, P., & Ghosh, A. (2009). LRRTM2 interacts with Neurexin1 and regulates excitatory synapse formation. *Neuron, 64*(6), 799-806.

DeChiara, T. M., Bowen, D. C., Valenzuela, D. M., Simmons, M. V., Poueymirou, W. T., Thomas, S., Kinetz, E., Compton, D. L., Rojas, E., Park, J. S., et al. (1996). The receptor tyrosine kinase MuSK is required for neuromuscular junction formation in vivo. *Cell, 85*(4), 501-512.

Deller, T., Korte, M., Chabanis, S., Drakew, A., Schwegler, H., Stefani, G. G., Zuniga, A., Schwarz, K., Bonhoeffer, T., Zeller, R., et al. (2003). Synaptopodin-deficient mice lack a spine apparatus and show deficits in synaptic plasticity. *Proc Natl Acad Sci U S A, 100*(18), 10494-10499.

Denzer, A. J., Brandenberger, R., Gesemann, M., Chiquet, M., & Ruegg, M. A. (1997). Agrin binds to the nerve-muscle basal lamina via laminin. *J Cell Biol, 137*(3), 671-683.

Dittgen, T., Nimmerjahn, A., Komai, S., Licznerski, P., Waters, J., Margrie, T. W., Helmchen, F., Denk, W., Brecht, M., & Osten, P. (2004). Lentivirus-based genetic manipulations of cortical neurons and their optical and electrophysiological monitoring in vivo. *Proc Natl Acad Sci U S A, 101*(52), 18206-18211.

Doyle, C. A., & Maxwell, D. J. (1991). Ultrastructural analysis of noradrenergic nerve terminals in the cat lumbosacral spinal dorsal horn: a dopamine-beta-hydroxylase immunocytochemical study. *Brain Res, 563*(1-2), 329-333.

Erdmann, G., Schutz, G., & Berger, S. (2007). Inducible gene inactivation in neurons of the adult mouse forebrain. *BMC Neurosci, 8*(63).

Ethell, I. M., Irie, F., Kalo, M. S., Couchman, J. R., Pasquale, E. B., & Yamaguchi, Y. (2001). EphB/syndecan-2 signaling in dendritic spine morphogenesis. *Neuron, 31*(6), 1001-1013.

Ethell, I. M., & Yamaguchi, Y. (1999). Cell surface heparan sulfate proteoglycan syndecan-2 induces the maturation of dendritic spines in rat hippocampal neurons. *J Cell Biol, 144*(3), 575-586.

Eusebio, A., Oliveri, F., Barzaghi, P., & Ruegg, M. A. (2003). Expression of mouse agrin in normal, denervated and dystrophic muscle. *Neuromuscul Disord, 13*(5), 408-415.

Falo, M. C., Reeves, T. M., & Phillips, L. L. (2008). Agrin expression during synaptogenesis induced by traumatic brain injury. *J Neurotrauma, 25*(7), 769-783.

Feng, G., Mellor, R. H., Bernstein, M., Keller-Peck, C., Nguyen, Q. T., Wallace, M., Nerbonne, J. M., Lichtman, J. W., & Sanes, J. R. (2000). Imaging neuronal subsets in transgenic mice expressing multiple spectral variants of GFP. *Neuron, 28*(1), 41-51.

Ferns, M. J., Campanelli, J. T., Hoch, W., Scheller, R. H., & Hall, Z. (1993). The ability of agrin to cluster AChRs depends on alternative splicing and on cell surface proteoglycans. *Neuron, 11*(3), 491-502.

Fiala, J. C., Feinberg, M., Popov, V., & Harris, K. M. (1998). Synaptogenesis via dendritic filopodia in developing hippocampal area CA1. *J Neurosci, 18*(21), 8900-8911.

Fiederling, A., Ewert, R., Andreyeva, A., Jungling, K., & Gottmann, K. (2011). E-cadherin is required at GABAergic synapses in cultured cortical neurons. *Neurosci Lett, 501*(3), 167-172.

Fuchs, H., Gailus-Durner, V., Adler, T., Pimentel, J. A., Becker, L., Bolle, I., Brielmeier, M., Calzada-Wack, J., Dalke, C., Ehrhardt, N., et al. (2009). The German Mouse Clinic: a platform for systemic phenotype analysis of mouse models. *Curr Pharm Biotechnol, 10*(2), 236-243.

Gautam, M., Noakes, P. G., Moscoso, L., Rupp, F., Scheller, R. H., Merlie, J. P., & Sanes, J. R. (1996). Defective neuromuscular synaptogenesis in agrin-deficient mutant mice. *Cell, 85*(4), 525-535.

Gietz, R. D., & Woods, R. A. (2002). Transformation of yeast by lithium acetate/single-stranded carrier DNA/polyethylene glycol method. *Methods Enzymol, 350*, 87-96.

Gingras, J., Rassadi, S., Cooper, E., & Ferns, M. (2002). Agrin plays an organizing role in the formation of sympathetic synapses. *J Cell Biol, 158*(6), 1109-1118.

Glass, D. J., Bowen, D. C., Stitt, T. N., Radziejewski, C., Bruno, J., Ryan, T. E., Gies, D. R., Shah, S., Mattsson, K., Burden, S. J., et al. (1996). Agrin acts via a MuSK receptor complex. *Cell, 85*(4), 513-523.

Golgi, C. (1873). Sulla struttura della sostanza grigia del cervelo. *Gazzetta Medica Italiana*(33), 244–246.

Golgi, C. (1989). On the structure of nerve cells. 1898. *J Microsc, 155*(1), 3-7.

Gomez, A. M., Froemke, R. C., & Burden, S. J. (2014). Synaptic plasticity and cognitive function are disrupted in the absence of Lrp4. *eLife, 3*, e04287.

Graham, F. L., Smiley, J., Russell, W. C., & Nairn, R. (1977). Characteristics of a human cell line transformed by DNA from human adenovirus type 5. *J Gen Virol, 36*(1), 59-74.

Granes, F., Garcia, R., Casaroli-Marano, R. P., Castel, S., Rocamora, N., Reina, M., Urena, J. M., & Vilaro, S. (1999). Syndecan-2 induces filopodia by active cdc42Hs. *Exp Cell Res, 248*(2), 439-456.

Gray, E. G. (1959a). Axo-somatic and axo-dendritic synapses of the cerebral cortex: an electron microscope study. *J Anat, 93*, 420-433.

Gray, E. G. (1959b). Electron microscopy of synaptic contacts on dendrite spines of the cerebral cortex. *Nature, 183*(4675), 1592-1593.

Groffen, A. J., Buskens, C. A., van Kuppevelt, T. H., Veerkamp, J. H., Monnens, L. A., & van den Heuvel, L. P. (1998). Primary structure and high expression of human agrin in basement membranes of adult lung and kidney. *Eur J Biochem, 254*(1), 123-128.

Groves, P. M., Linder, J. C., & Young, S. J. (1994). 5-hydroxydopamine-labeled dopaminergic axons: three-dimensional reconstructions of axons, synapses and postsynaptic targets in rat neostriatum. *Neuroscience, 58*(3), 593-604.

Grunwald, I. C., Korte, M., Adelmann, G., Plueck, A., Kullander, K., Adams, R. H., Frotscher, M., Bonhoeffer, T., & Klein, R. (2004). Hippocampal plasticity requires postsynaptic ephrinBs. *Nat Neurosci, 7*(1), 33-40.

Gu, H., Zou, Y. R., & Rajewsky, K. (1993). Independent control of immunoglobulin switch recombination at individual switch regions evidenced through Cre-loxP-mediated gene targeting. *Cell, 73*(6), 1155-1164.

Harris, K. M., Jensen, F. E., & Tsao, B. (1992). Three-dimensional structure of dendritic spines and synapses in rat hippocampus (CA1) at postnatal day 15 and adult ages: implications for the maturation of synaptic physiology and long-term potentiation. *J Neurosci, 12*(7), 2685-2705.

Harris, K. M., & Weinberg, R. J. (2012). Ultrastructure of synapses in the mammalian brain. *Cold Spring Harb Perspect Biol, 4*(5).

Houser, C. R. (1990). Cholinergic synapses in the central nervous system: studies of the immunocytochemical localization of choline acetyltransferase. *J Electron Microsc Tech, 15*(1), 2-19.

Howard, A., Tamas, G., & Soltesz, I. (2005). Lighting the chandelier: new vistas for axo-axonic cells. *Trends Neurosci, 28*(6), 310-316.

Hoy, J. L., Haeger, P. A., Constable, J. R. L., Arias, R. J., McCallum, R., Kyweriga, M., Davis, L., Schnell, E., Wehr, M., Castillo, P. E., & Washbourne, P. (2013). Neuroligin1 drives synaptic and behavioral maturation through intracellular interactions. *J Neurosci, 33*(22), 9364-9384.

Ibraghimov-Beskrovnaya, O., Ervasti, J. M., Leveille, C. J., Slaughter, C. A., Sernett, S. W., & Campbell, K. P. (1992). Primary structure of dystrophin-associated glycoproteins linking dystrophin to the extracellular matrix. *Nature, 355*(6362), 696-702.

Jastrow, H., Koulen, P., Altrock, W. D., & Kröger, S. (2006). Identification of a beta-dystroglycan immunoreactive subcompartment in photoreceptor terminals. *Invest Ophthalmol Vis Sci, 47*(1), 17-24.

Johnsson, A. K., & Karlsson, R. (2012). Synaptotagmin 1 causes phosphatidyl inositol lipid-dependent actin remodeling in cultured non-neuronal and neuronal cells. *Exp Cell Res, 318*(2), 114-126.

Jones, E. G., & Powell, T. P. (1969). Morphological variations in the dendritic spines of the neocortex. *J Cell Sci, 5*(2), 509-529.

Kammerer, R. A., Schulthess, T., Landwehr, R., Schumacher, B., Lustig, A., Yurchenco, P. D., Ruegg, M. A., Engel, J., & Denzer, A. J. (1999). Interaction of agrin with laminin requires a coiled-coil conformation of the agrin-binding site within the laminin gamma1 chain. *EMBO J, 18*(23), 6762-6770.

Karakatsani, A., Urban, S., Kalamakis, G., Schick, A., Ghanem, A., Zhang, Y., Conzelmann, K.-K., Rüegg, M. A., Ruiz de Almodovar, C., Gascon, S., & Kröger, S. (2016). *LRP4 regulates dendritic arborization and synapse formation in central nervous system neurons. Submitted manuscript.*

Kawaguchi, S. Y., & Hirano, T. (2006). Integrin alpha3beta1 suppresses long-term potentiation at inhibitory synapses on the cerebellar Purkinje neuron. *Mol Cell Neurosci, 31*(3), 416-426.

Kim, N., Stiegler, A. L., Cameron, T. O., Hallock, P. T., Gomez, A. M., Huang, J. H., Hubbard, S. R., Dustin, M. L., & Burden, S. J. (2008). Lrp4 is a receptor for Agrin and forms a complex with MuSK. *Cell, 135*(2), 334-342.

Kim, S., & Martin, K. C. (2015). Neuron-wide RNA transport combines with netrin-mediated local translation to spatially regulate the synaptic proteome. *eLife, 4*.

Klein, R. (2009). Bidirectional modulation of synaptic functions by Eph/ephrin signaling. *Nat Neurosci, 12*(1), 15-20.

Kneussel, M., & Betz, H. (2000). Receptors, gephyrin and gephyrin-associated proteins: novel insights into the assembly of inhibitory postsynaptic membrane specializations. *J Physiol, 525 Pt 1*, 1-9.

Koulen, P., Honig, L. S., Fletcher, E. L., & Kroger, S. (1999). Expression, distribution and ultrastructural localization of the synapse-organizing molecule agrin in the mature avian retina. *Eur J Neurosci, 11*(12), 4188-4196.

Kröger, S., Horton, S. E., & Honig, L. S. (1996). The developing avian retina expresses agrin isoforms during synaptogenesis. *J Neurobiol, 29*(2), 165-182.

Kroger, S., & Mann, S. (1996). Biochemical and functional characterization of basal lamina-bound agrin in the chick central nervous system. *Eur J Neurosci, 8*(3), 500-509.

Kröger, S., & Pfister, H. (2009). Agrin in the nervous system: Synaptogenesis and beyond. *Future Neurology, 4*(1), 67-86.

Kröger, S., & Schroder, J. E. (2002). Agrin in the developing CNS: new roles for a synapse organizer. *News Physiol Sci, 17*, 207-212.

Ksiazek, I., Burkhardt, C., Lin, S., Seddik, R., Maj, M., Bezakova, G., Jucker, M., Arber, S., Caroni, P., Sanes, J. R., et al. (2007). Synapse loss in cortex of agrin-deficient mice after genetic rescue of perinatal death. *J Neurosci, 27*(27), 7183-7195.

Kubota, Y., Hatada, S., Kondo, S., Karube, F., & Kawaguchi, Y. (2007). Neocortical inhibitory terminals innervate dendritic spines targeted by thalamocortical afferents. *J Neurosci, 27*(5), 1139-1150.

Kucukdereli, H., Allen, N. J., Lee, A. T., Feng, A., Ozlu, M. I., Conatser, L. M., Chakraborty, C., Workman, G., Weaver, M., Sage, E. H., et al. (2011). Control of excitatory CNS synaptogenesis by astrocyte-secreted proteins Hevin and SPARC. *Proc Natl Acad Sci U S A, 108*(32), E440-449.

Leuner, B., Falduto, J., & Shors, T. J. (2003). Associative memory formation increases the observation of dendritic spines in the hippocampus. *J Neurosci, 23*(2), 659-665.

Levi, S., Grady, R. M., Henry, M. D., Campbell, K. P., Sanes, J. R., & Craig, A. M. (2002). Dystroglycan is selectively associated with inhibitory GABAergic synapses but is dispensable for their differentiation. *J Neurosci, 22*(11), 4274-4285.

Li, L., Cao, Y., Wu, H., Ye, X., Zhu, Z., Xing, G., Shen, C., Barik, A., Zhang, B., Xie, X., et al. (2016). Enzymatic Activity of the Scaffold Protein Rapsyn for Synapse Formation. *Neuron, 92*(5), 1007-1019.

Li, Z., Massengill, J. L., O'Dowd, D. K., & Smith, M. A. (1997). Agrin gene expression in mouse somatosensory cortical neurons during development in vivo and in cell culture. *Neuroscience, 79*(1), 191-201.

Lin, L., McCroskery, S., Ross, J. M., Chak, Y., Neuhuber, B., & Daniels, M. P. (2010). Induction of filopodia-like protrusions by transmembrane agrin: role of agrin glycosaminoglycan chains and Rho-family GTPases. *Exp Cell Res, 316*(14), 2260-2277.

Lin, Y. L., Lei, Y. T., Hong, C. J., & Hsueh, Y. P. (2007). Syndecan-2 induces filopodia and dendritic spine formation via the neurofibromin-PKA-Ena/VASP pathway. *J Cell Biol, 177*(5), 829-841.

Lopez-Munoz, F., Boya, J., & Alamo, C. (2006). Neuron theory, the cornerstone of neuroscience, on the centenary of the Nobel Prize award to Santiago Ramon y Cajal. *Brain Res Bull, 70*(4-6), 391-405.

Madisen, L., Zwingman, T. A., Sunkin, S. M., Oh, S. W., Zariwala, H. A., Gu, H., Ng, L. L., Palmiter, R. D., Hawrylycz, M. J., Jones, A. R., et al. (2010). A robust

and high-throughput Cre reporting and characterization system for the whole mouse brain. *Nat Neurosci, 13*(1), 133-140.

Marchenkova, A., van den Maagdenberg, A. M., & Nistri, A. (2016). Loss of inhibition by brain natriuretic peptide over P2X3 receptors contributes to enhanced spike firing of trigeminal ganglion neurons in a mouse model of familial hemiplegic migraine type-1. *Neuroscience, 331*, 197-205.

Mascarenhas, J. B., Ruegg, M. A., Sasaki, T., Eble, J. A., Engel, J., & Stetefeld, J. (2005). Structure and laminin-binding specificity of the NtA domain expressed in eukaryotic cells. *Matrix Biol, 23*(8), 507-513.

Matsuo, N., Reijmers, L., & Mayford, M. (2008). Spine-type-specific recruitment of newly synthesized AMPA receptors with learning. *Science, 319*(5866), 1104-1107.

McCroskery, S., Chaudhry, A., Lin, L., & Daniels, M. P. (2006). Transmembrane agrin regulates filopodia in rat hippocampal neurons in culture. *Mol Cell Neurosci, 33*(1), 15-28.

McMahan, U. J. (1990). The agrin hypothesis. *Cold Spring Harb Symp Quant Biol, 55*, 407-418.

Ming, G. L., & Song, H. (2011). Adult neurogenesis in the mammalian brain: significant answers and significant questions. *Neuron, 70*(4), 687-702.

Molyneaux, B. J., Arlotta, P., Menezes, J. R., & Macklis, J. D. (2007). Neuronal subtype specification in the cerebral cortex. *Nat Rev Neurosci, 8*(6), 427-437.

Neill, T., Schaefer, L., & Iozzo, R. V. (2015). Decoding the Matrix: Instructive Roles of Proteoglycan Receptors. *Biochemistry, 54*(30), 4583-4598.

Neumann, F. R., Bittcher, G., Annies, M., Schumacher, B., Kröger, S., & Ruegg, M. A. (2001). An alternative amino-terminus expressed in the central nervous system converts agrin to a type II transmembrane protein. *Mol Cell Neurosci, 17*(1), 208-225.

Nikonenko, I., Boda, B., Steen, S., Knott, G., Welker, E., & Muller, D. (2008). PSD-95 promotes synaptogenesis and multiinnervated spine formation through nitric oxide signaling. *J Cell Biol, 183*(6), 1115-1127.

Nitkin, R. M., Smith, M. A., Magill, C., Fallon, J. R., Yao, Y. M., Wallace, B. G., & McMahan, U. J. (1987). Identification of agrin, a synaptic organizing protein from Torpedo electric organ. *J Cell Biol, 105*(6 Pt 1), 2471-2478.

O'Connor, L. T., Lauterborn, J. C., Gall, C. M., & Smith, M. A. (1994). Localization and alternative splicing of agrin mRNA in adult rat brain: transcripts encoding isoforms that aggregate acetylcholine receptors are not restricted to cholinergic regions. *J Neurosci, 14*(3 Pt 1), 1141-1152.

O'Connor, L. T., Lauterborn, J. C., Smith, M. A., & Gall, C. M. (1995). Expression of agrin mRNA is altered following seizures in adult rat brain. *Brain Res Mol Brain Res, 33*(2), 277-287.

Papa, M., Bundman, M. C., Greenberger, V., & Segal, M. (1995). Morphological analysis of dendritic spine development in primary cultures of hippocampal neurons. *J Neurosci, 15*(1 Pt 1), 1-11.

Paul, C. A., Beltz, B., & Berger-Sweeney, J. (2008). The nissl stain: a stain for cell bodies in brain sections. *CSH Protoc, 2008*, pdb prot4805.

Pavlov, I., Rauvala, H., & Taira, T. (2006). Enhanced hippocampal GABAergic inhibition in mice overexpressing heparin-binding growth-associated molecule. *Neuroscience, 139*(2), 505-511.

Pierce, J. P., van Leyen, K., & McCarthy, J. B. (2000). Translocation machinery for synthesis of integral membrane and secretory proteins in dendritic spines. *Nat Neurosci, 3*(4), 311-313.

Porten, E., Seliger, B., Schneider, V. A., Woll, S., Stangel, D., Ramseger, R., & Kröger, S. (2010). The process-inducing activity of transmembrane agrin requires follistatin-like domains. *J Biol Chem, 285*(5), 3114-3125.

Pribiag, H., Peng, H., Shah, W. A., Stellwagen, D., & Carbonetto, S. (2014). Dystroglycan mediates homeostatic synaptic plasticity at GABAergic synapses. *Proc Natl Acad Sci U S A, 111*(18), 6810-6815.

Radwanska, K., Medvedev, N. I., Pereira, G. S., Engmann, O., Thiede, N., Moraes, M. F. D., Villers, A., Irvine, E. E., Maunganidze, N. S., Pyza Eż, M., et al. (2011). Mechanism for long-term memory formation when synaptic strengthening is impaired. *Proc Natl Acad Sci U S A, 108*(45), 18471-18475.

Ramon Y Cajal, S. (1995). Cajal's Histology of the Nervous System of Man and Vertebrates (N. Swanson & L. Swanson, Trans.). Oxford: Oxford University Press.

Ramseger, R., White, R., & Kröger, S. (2009). Transmembrane form agrin-induced process formation requires lipid rafts and the activation of Fyn and MAPK. *J Biol Chem, 284*(12), 7697-7705.

Reissner, C., Klose, M., Fairless, R., & Missler, M. (2008). Mutational analysis of the neurexin/neuroligin complex reveals essential and regulatory components. *Proc Natl Acad Sci U S A, 105*(39), 15124-15129.

Reist, N. E., Werle, M. J., & McMahan, U. J. (1992). Agrin released by motoneurons induces the aggregation of acetylcholine receptors at neuromuscular junctions. *Neuron, 8*(5), 865-868.

Roche, & Diagnostics. (2009). *RealTime ready Universal ProbeLibrary*. Retrieved from Penzberg:

Ruegg, M. A., Tsim, K. W., Horton, S. E., Kröger, S., Escher, G., Gensch, E. M., & McMahan, U. J. (1992). The agrin gene codes for a family of basal lamina proteins that differ in function and distribution. *Neuron, 8*(4), 691-699.

Rupp, F., Payan, D. G., Magill-Solc, C., Cowan, D. M., & Scheller, R. H. (1991). Structure and expression of a rat agrin. *Neuron, 6*(5), 811-823.

Samuel, M. A., Valdez, G., Tapia, J. C., Lichtman, J. W., & Sanes, J. R. (2012). Agrin and Synaptic Laminin Are Required to Maintain Adult Neuromuscular Junctions. *PLoS One, 7*(10).

Sanes, J. R., & Lichtman, J. W. (2001). Induction, assembly, maturation and maintenance of a postsynaptic apparatus. *Nat Rev Neurosci, 2*(11), 791-805.

Sarrazin, S., Lamanna, W. C., & Esko, J. D. (2011). Heparan sulfate proteoglycans. *Cold Spring Harb Perspect Biol, 3*(7).

Schleyden, M. J., & Schwann, T. (1847). Microscopical researches into the accordance in the structure and growth of animals and plants. London: Sydenham Society.

Schnell, E., Bensen, A. S. L., Washburn, E. K., & Westbrook, G. L. (2012). Neuroligin-1 Overexpression in Newborn Granule Cells In Vivo. *PLoS One, 7*(10).

Siddiqui, T. J., Tari, P. K., Connor, S. A., Zhang, P., Dobie, F. A., She, K., Kawabe, H., Wang, Y. T., Brose, N., & Craig, A. M. (2013). An LRRTM4-HSPG complex mediates excitatory synapse development on dentate gyrus granule cells. *Neuron, 79*(4), 680-695.

Sudhof, T. C. (2008). Neuroligins and neurexins link synaptic function to cognitive disease. *Nature, 455*(7215), 903-911.

Sugita, S., Saito, F., Tang, J., Satz, J., Campbell, K., & Sudhof, T. C. (2001). A stoichiometric complex of neurexins and dystroglycan in brain. *J Cell Biol, 154*(2), 435-445.

Sugiyama, Y., Kawabata, I., Sobue, K., & Okabe, S. (2005). Determination of absolute protein numbers in single synapses by a GFP-based calibration technique. *Nat Methods, 2*(9), 677-684.

Sun, X. D., Li, L., Liu, F., Huang, Z. H., Bean, J. C., Jiao, H. F., Barik, A., Kim, S. M., Wu, H., Shen, C., et al. (2016). Lrp4 in astrocytes modulates glutamatergic transmission. *Nat Neurosci, 19*(8), 1010-1018.

Suzuki, K., Imai, Y., Yamashita, I., & Fukui, S. (1983). In vivo ligation of linear DNA molecules to circular forms in the yeast Saccharomyces cerevisiae. *J Bacteriol, 155*(2), 747-754.

Swartz, M. E., Eberhart, J., Pasquale, E. B., & Krull, C. E. (2001). EphA4/ephrin-A5 interactions in muscle precursor cell migration in the avian forelimb. *Development, 128*(23), 4669-4680.

Takumi, Y., Ramirez-Leon, V., Laake, P., Rinvik, E., & Ottersen, O. P. (1999). Different modes of expression of AMPA and NMDA receptors in hippocampal synapses. *Nat Neurosci, 2*(7), 618-624.

Tang, Y., Nyengaard, J. R., De Groot, D. M., & Gundersen, H. J. (2001). Total regional and global number of synapses in the human brain neocortex. *Synapse, 41*(3), 258-273.

Tian, Q. B., Suzuki, T., Yamauchi, T., Sakagami, H., Yoshimura, Y., Miyazawa, S., Nakayama, K., Saitoh, F., Zhang, J. P., Lu, Y., et al. (2006). Interaction of LDL receptor-related protein 4 (LRP4) with postsynaptic scaffold proteins via its C-terminal PDZ domain-binding motif, and its regulation by Ca/calmodulin-dependent protein kinase II. *Eur J Neurosci, 23*(11), 2864-2876.

Tintignac, L. A., Brenner, H. R., & Ruegg, M. A. (2015). Mechanisms Regulating Neuromuscular Junction Development and Function and Causes of Muscle Wasting. *Physiol Rev, 95*(3), 809-852.

Tsen, G., Halfter, W., Kröger, S., & Cole, G. J. (1995). Agrin is a heparan sulfate proteoglycan. *J Biol Chem, 270*(7), 3392-3399.

Tsim, K. W., Ruegg, M. A., Escher, G., Kröger, S., & McMahan, U. J. (1992). cDNA that encodes active agrin. *Neuron, 8*(4), 677-689.

Van Bockstaele, E. J., Cestari, D. M., & Pickel, V. M. (1994). Synaptic structure and connectivity of serotonin terminals in the ventral tegmental area: potential sites for modulation of mesolimbic dopamine neurons. *Brain Res, 647*(2), 307-322.

van Bommel, B., & Mikhaylova, M. (2016). Talking to the neighbours: The molecular and physiological mechanisms of clustered synaptic plasticity. *Neurosci Biobehav Rev, 71*, 352-361.

Varoqueaux, F., Aramuni, G., Rawson, R. L., Mohrmann, R., Missler, M., Gottmann, K., Zhang, W., Sudhof, T. C., & Brose, N. (2006). Neuroligins determine synapse maturation and function. *Neuron, 51*(6), 741-754.

Wallace, B. G. (1988). Regulation of agrin-induced acetylcholine receptor aggregation by Ca++ and phorbol ester. *J Cell Biol, 107*(1), 267-278.

Wallace, B. G. (1989). Agrin-induced specializations contain cytoplasmic, membrane, and extracellular matrix-associated components of the postsynaptic apparatus. *J Neurosci, 9*(4), 1294-1302.

Weatherbee, S. D., Anderson, K. V., & Niswander, L. A. (2006). LDL-receptor-related protein 4 is crucial for formation of the neuromuscular junction. *Development, 133*(24), 4993-5000.

Werle, M. J., & VanSaun, M. (2003). Activity dependent removal of agrin from synaptic basal lamina by matrix metalloproteinase 3. *J Neurocytol, 32*(5-8), 905-913.

Winzen, U., Cole, G. J., & Halfter, W. (2003). Agrin is a chimeric proteoglycan with the attachment sites for heparan sulfate/chondroitin sulfate located in two multiple serine-glycine clusters. *J Biol Chem, 278*(32), 30106-30114.

Wu, H., Xiong, W. C., & Mei, L. (2010). To build a synapse: signaling pathways in neuromuscular junction assembly. *Development, 137*(7), 1017-1033.

Yamagata, M., Herman, J. P., & Sanes, J. R. (1995). Lamina-specific expression of adhesion molecules in developing chick optic tectum. *J Neurosci, 15*(6), 4556-4571.

Yang, X., Hou, D., Jiang, W., & Zhang, C. (2014). Intercellular protein-protein interactions at synapses. *Protein Cell, 5*(6), 420-444.

Yu, W., Jiang, M., Miralles, C. P., Li, R. W., Chen, G., & de Blas, A. L. (2007). Gephyrin clustering is required for the stability of GABAergic synapses. *Mol Cell Neurosci, 36*(4), 484-500.

Zambrowicz, B. P., Imamoto, A., Fiering, S., Herzenberg, L. A., Kerr, W. G., & Soriano, P. (1997). Disruption of overlapping transcripts in the ROSA beta geo 26 gene trap strain leads to widespread expression of beta-galactosidase in mouse embryos and hematopoietic cells. *Proc Natl Acad Sci U S A, 94*(8), 3789-3794.

Zha, X., Wemmie, J. A., Green, S. H., & Welsh, M. J. (2006). Acid-sensing ion channel 1a is a postsynaptic proton receptor that affects the density of dendritic spines. *Proc Natl Acad Sci U S A, 103*(44), 16556-16561.

Zhang, B., Luo, S., Wang, Q., Suzuki, T., Xiong, W. C., & Mei, L. (2008). LRP4 serves as a coreceptor of agrin. *Neuron, 60*(2), 285-297.

6. Acknowledgements

I would like to thank everyone involved in this work for supporting me to get to the finish line: Stephan for his constructive comments, for his support and for lively discussions.

Johnny and Niklas for showing me that life is most fun when it does not go in a straight line. Joel for his love, support and scientific advice. My parents for always supporting me and my decisions, and especially my mother for giving me her time when I needed her.

Andromachi, Yina and Laura for fruitful discussions and emotional support, Katja and Martina and Susi for excellent technical assistance and Yvonne for being a fantastic caretaker of the mice.

Furthermore, I would like to thank Magdalena Götz and the SFB 870 for supporting my research position and Markus Rüegg and Wilko Altrock for antibodies.

Appendix

Abbreviations

AChR: acetylcholine receptor

bp: basepairs

BSA: bovine serum albumin

CASK: calcium/Calmodulin dependent serine kinase

CNS: central nervous system

E.coli: Escherichia coli

GABA: γ-aminobutyric acid

GFP: green fluorescent protein

HA: human influenza hemagglutinin

HRP: horseradish peroxidase

HSPG: heparan sulfate proteoglycan

ICC: immunocytochemistry

IF: immunoflurescence

IHC: immunohistochemistry

IRES: internal ribosome entry site

kb: kilo basepairs

LTP: long-term potentiation

NMJ: neuromuscular junction

NLS: nuclear localization signal

OB: olfactory bulb

ORF: open reading frame

PDL: poly-D-lysine

PNS: peripheral nervous system

qPCR: quantitative polymerase chain reaction

RT: room temperature

SEM: standard error of the mean

SVZ: subventricular zone

TM: transmembrane

WT: wildtype

Figure Index

Table Index

Permissions

The electron micrograph images in Figure 1 are reproduced from Gray, 1959b with the publisher's permission (Wiley Global Permissions). Permission is granted solely for use in conjunction with the thesis, and the material may not be posted online separately.

List of author contributions

Anna Schick generated all data and prepared all figures unless stated otherwise. **Gerry Handara** generated the expression profiling data summarized in Table 6 under **Anna Schick**'s supervision as part of his Master's thesis. **Martina Bürkle** performed most of the genotyping of the TM-agrin overexpressing mouse line. **Dr. Luciana Alfonso** performed the MRI exams of live mice at Helmholtz Zentrum, Neuherberg, as part of a collaboration agreement between Anna Schick and the German Mouse Clinic. **Dr. Joel Schick** and **Susanne Pfeiffer** electroporated the pAS20 targeting vector into mouse ES cells and generated a chimeric mouse line by blastocyst injection as part of a collaboration agreement between Anna Schick and the group of Dr. Joel Schick at Helmholtz Zentrum, Neuherberg. Susi Pfeiffer also purified the RNA used for cloning of TM-agrin from mouse heads.

Date Anna Schick